UNIVERSITY OF CAPE TOWN
IYUNIVESITHI YASEKAPA • UNIVERSITEIT VAN KAAPSTAD

EFFECT OF STRUCTURAL REPAIR AND STRENGTHENING ON STIFFNESS AND ULTIMATE CAPACITY OF CORROSION-DAMAGED RC BEAMS

MOJABENG TIGELI

THESIS SUBMITTED IN PARTIAL FULFILMENT OF THE REQUIREMENTS FOR THE DEGREE OF MASTER OF SCIENCE IN CIVIL ENGINEERING

SUPERVISORS: A/PROF. P. MOYO AND DR. H. BEUSHAUSEN

4th February 2010

DECLARATION

I declare that this thesis is my own work. It is being submitted for the Master of Science in Engineering at the University of Cape Town, South Africa. It has not been submitted before for any degree or examination in any other university.

_____

Signature

_____ day of _____ 2010

ABSTRACT

Over the years, the need for repair of reinforced concrete (RC) structures has increased significantly, both for old and new structures. The main cause of structural damage in RC structures is corrosion of reinforcement. Therefore there is a need to understand the effects of corrosion damage on the structural properties of RC members such as stiffness and ultimate capacity in order to develop improved and effective repair strategies that will minimise the risk of further damage and structural failure both in the short and long term. Corrosion reduces the cross-sectional area of steel at the corrosion sites, leading to reduced stiffness and capacity of the structure to carry loading, which may result in structural failure if not detected and repaired or strengthened.

This study presents experimental results on the effectiveness of combined repair and strengthening of corrosion-damaged RC beams. Four RC beams 154 mm wide × 254 mm deep × 5000 mm long were tested. Three of the beams were subjected to different levels of accelerated corrosion (using 1000 mA impressed anodic current and 5% NaCl solution) under sustained service loads (2 kN) while one beam acted as a control. All four beams were monitored for deflections during the accelerated corrosion period. The beam dynamic characteristics were assessed at all stages; namely the undamaged stage, 10 % corroded, 15% corroded, exposed reinforcement, patch repaired and finally the CFRP strengthened stage. The three corrosion-damaged beams were patch repaired with a cementitious grout; two of them were strengthened with carbon fibre reinforced polymer (CFRP) laminates in addition to the repair. The effect of damage on the stiffness of the beams was inferred from strain measurements, deflections and dynamic properties (natural frequencies and modal shapes). The effect of patch repair and strengthening on corrosion damaged beams was deduced from the changes in their ultimate capacities.

From the deflection measurements measured during the corrosion process, stiffness decreased with the increase in corrosion level. Cracks develop and widen as the level of corrosion increases. The results obtained from dynamic testing consist of natural frequencies, mode shapes and damping ratios. The dynamic results show a drop in natural frequencies due to damage and not much change on the fundamental mode shapes is observed when comparing

the modes by the Modal Assurance Criterion (MAC) values. The MAC values did not prove useful in identifying damage or changes in RC beams.

The static results reveal that both the stiffness and the ultimate capacity are improved by about 25% and 50% respectively when both patch repair and FRP are applied on a damaged beam. Patch repair on its own improved the stiffness by approximately 5% but did not improve the ultimate capacity. As expected, it can be drawn from the results that the combined effect of both patch repair and CFRP strengthening improves the stiffness and ultimate capacity of the structure.

ACKNOWLEDGEMENTS

Special thanks to the CSIRG for the financial assistance throughout the duration of my studies. I would like to sincerely thank my two supervisors, A/Prof P. Moyo and Dr. H Beushausen for their guidance and support throughout the duration of this project. I have gained knowledge and skills from their professional characters and teaching. Their encouragement and positive criticism helped me to appreciate and improve my work and learn from my mistakes. Their assistance is highly appreciated.

Special gratitude to Prof M. Alexander for all the fatherly advice and encouragement, I definitely would not have carried through if it weren't for him. I would also like to extend my gratitude to Mrs. E. Yelverton, for her assistance in getting me all the materials I needed for my work and all the motherly love, sweet and cheering conversations all the time.

I would like to thank the lab and workshop staff of the Department of Civil Engineering, University of Cape Town; in particular Mr. Nicolas, Mr. Hassen, Mr. Moyana, Mr. May, and Mr. Witboi, for their technical assistance and patience throughout the labour intense experimental work. I would like to thank Mr. G. Malumbela for his time, guidance and patience; this would not have been easy without him. I'm very grateful to my officemate Ruks Beushausen, for being a wonderful friend and a big sister; I appreciate all her guidance and support during the period of my study.

Special thanks to wonderful friends; Dr. Alvin Masarira, Rethabile Melamu, Mike Otieno and Marc Gillmer, David Modise and Bokang Lethola who assisted with editing of the report. I would also like to thank my sister Malooele Tigeli and my boyfriend Nhlanhla Mdluli for all the encouragement and support throughout this period. Special thanks to my brother Lebakeng Tigeli for all the support and financial assistance during my period of study and lastly my parents, my sisters and my little princess for all the love and moral support throughout this study.

GLOSSARY OF TERMS

Accelerometer – An instrument for measuring ground acceleration as a function of time.

Adherent – A body that is bonded to another body with an adhesive.

Adhesive - Substance applied to matting surfaces to bond them together by surface attachment. An adhesive can be in a liquid, film or paste form.

Amplitude – Maximum value of a function as it varies with time. If the variation with time can be describes either by a sine or cosine function, it is said to vary harmonically.

Anisotropic – Fibre directionality where different properties are exhibited when tested along axes in different direction.

Aspect ratio – The ratio of length to diameter of fibre.

Block Size - The number of samples (time or frequency values) in all of the Traces of a Data Block or Acquisition window. The current Block Size is displayed in the File | Properties dialog box, and can be changed. Increasing the Block Size appends zeros to each Trace. Decreasing the Block Size removes samples from the right hand side (high frequencies or time values) of each Trace.

Boundary conditions – A constraint applied to a structure independent of time.

CFRP – Carbon Fibre Reinforcing Polymer

Corrosion – deterioration or disintegration of concrete and metal, by chemicals from external sources.

Critical damping – Minimum amount of viscous damping for which the system will not vibrate.

Cross Spectrum - The Cross Spectrum is a cross-channel measurement. It is calculated by multiplying the Fourier Spectrum of one signal by the complex conjugate of the Fourier Spectrum of another signal. A Cross Spectrum has magnitude & phase. For Operating Modal Analysis, Cross spectra are calculated between two or more Roving response signals and a (fixed) Reference response. Operating mode shapes can be obtained after DeConvolution windowing and FRF-based curve fitting of a set of Cross spectra.

Damped frequency – The frequency at which a viscous damped system oscillates in free vibration.

Damping – The property of the structure to absorb vibrating energy.

Damping ratio – Ratio of the viscous damping coefficient to critical damping.

Data Block file - One or more measurement Traces with a common time or frequency axis. Time domain measurements are real valued. Frequency domain measurements are complex

valued (real & imaginary or magnitude & phase). Each Trace contains values measured on the structure or acoustic surface, at a Point and in a direction (Scalar measurements have no direction.) Each Trace is numbered, starting from M#1. Measurement numbers (M#s) are used in the Animation Equations at each Point to display shape components in each direction.

Degrees of freedom –The number of independent coordinates required to completely define the position of the system at any time.

Delamination - Separation of layers in a laminate because of failure of the adhesive, either in the adhesive itself or at the interface between the adhesive and the adherent.

Diffusion – The movement of ions under a concentration gradient from a high concentration zone to a low concentration zone.

Durability – The long-term performance of the structure over the duration of the desired service life within a given exposure environment, without imposing excessive maintenance and repair expenses.

EMA - An acronym for Experimental Modal Analysis. During an EMA, the test article is artificially excited with either an impactor or a shaker. The excitation force and one or more responses caused by the force are simultaneously measured, and a set of FRF measurements is calculated The FRFs are then curve fit to obtain a set of experimental modal parameters for the structure.

Epoxy resin - A polymer resin characterised by epoxied molecule groups.

FFT- An acronym for Fast Fourier Transform. The FFT is a numerical algorithm that transforms a uniformly sampled time domain signal into it equivalent DFT (Digital Fourier Transform). The Inverse FFT transforms the DFT into its equivalent sampled time domain signal. The FFT in ME'scopeVES is a prime number FFT, which doesn't restrict the number of samples transformed to powers of 2.

Forced vibration – Vibration in which the response is due to external excitation of the system.

Fourier Spectrum- A Fourier Spectrum is the forward FFT of a uniformly sampled time waveform. Another name for the Fourier Spectrum is the DFT.

FRF- An acronym for Frequency Response Function. An FRF is a cross-channel frequency domain measurement that defines the dynamic properties of a machine or structure between a response DOF and an excitation force DOF. It is defined as the ratio (response Fourier spectrum / force Fourier spectrum). Excitation force is typically measured with a load cell.

Response motion is measured with an acceleration, velocity or displacement transducer. The FRF is a special case of a Transfer Function

FRP - Fibre Reinforcing Polymer

Free vibration – The vibration of a system in absence of external excitation.

Hydration – The chemical reaction between a substance, eg hydraulic cement and water.

Laminate – To unite layers of material with as adhesive. Also a structure resulting from bonding multiple plies of reinforcing fibre or fabric.

MAC - An Acronym for Modal Assurance Criterion. MAC indicates whether or not two shapes are the same or different. If MAC > 0.95 the shapes are the same. If MAC > 0.8, the shapes are similar. If MAC < 0.8 the shapes are different.

Migration – The movement of ions due to an external electrical field.

Mode Shape - Modes are used to characterize resonant vibration in structures. Each mode has natural frequency, damping value, and a mode shape. The mode shape is a standing wave deformation of the vibrating structure at its resonant (or modal) frequency.

Modal Peaks Function - One of the mode indicator choices available during the first step of curve fitting. It is used with the Count Peaks button for determining how many modes are in a set of measurements.

Natural frequency – The number of cycles per second at which a single degree of freedom system vibrates freely or a multidegree of freedom system vibrates in one of the normal modes.

Natural period – The time interval for a vibrating system in free vibration for one complete oscillation.

Power spectrum - Description of how signal is distributed with frequency.

PSD - An acronym for Power Spectral Density. A PSD is calculated by dividing an Auto Spectrum by its frequency resolution (the increment between frequency lines).

Resonance – The condition in which the frequency of the excitation equals the natural frequency of the vibrating system.

Response – The force or motion that results from external excitation of the structure.

Response spectrum – A plot of maximum response (displacement, velocity or acceleration) for a single degree of freedom system defined by its natural frequency (or period) subjected to a specific excitation.

Serviceability – the capacity of a material or structure to perform its function.

Spectral leakage - An effect in the frequency analysis of finite-length signal or finite-length segments of an infinite signal where it appears as if some energy has leaked out of the original signal spectrum into other frequencies.

Structure - An assemblage of framing members designed to support gravity loads and resist lateral forces. Structures may be categorized as buildings structures or non-building structures.

Viscous damping – Dissipation of energy such that the motion is resisted by a force proportional to the velocity but in the opposite direction.

Window function - It is a function that is zero valued outside of some chosen interval in signal processing.

TABLE OF CONTENTS

LIST OF FIGURES

LIST OF TABLES

Chapter 1

INTRODUCTION

1.1 Background to investigation

Owing to the rising need of repair of reinforced concrete (RC) structures, it is becoming increasingly important to understand the effect of damage on the structural properties of RC members, in order to develop improved and effective repair strategies that will minimise the risk of structural failure both in the short and long term.

The most common cause of deterioration in RC structures is corrosion of steel reinforcement. Corrosion results in cracking and staining of RC structures thus impairing their service limit state. Corrosion reduces the area of steel at the corrosion sites, which reduces the stiffness and capacity of the structure to carry loading (Bentur et al, 1997). The repairs of corrosion damaged structures require careful consideration of both durability and strength issues. Prior to repairing corrosion damaged members, a thorough performance assessment is required in order to establish the degree of damage and the appropriate repair materials and technique. Both durability and structural performance of the structure are considered when assessing damage. Here durability refers to the ability of concrete to resist the ingress of deleterious substances which may lead to corrosion of reinforcement while structural performance relates to the strength of the RC structure.

The usual approach used to restore durability is by use of patch repair mortars. For a repair to be successfully completed it must eliminate the cause of damage, repair the full extent of damage and ensure that the structure is protected from further damage or recurrence of the original cause for the projected lifespan. These require a careful consideration of material compatibilities between the repair and the substrate (Phaedonos, 2006).

There are a number of techniques for restoring the structural performance of RC structures. These techniques have evolved from concrete jacketing and external bonding of steel plates to the current use of patch repairs and fibre reinforced polymers (FRP) strengthening. In the past decade, there has been a growing interest on the use of FRP, as it has proved to be an excellent construction material because of its properties. FRP is corrosion resistant, light-weight, non-magnetic, exhibit high tensile strength, has low mechanical relaxation

qualities, good toughness and high fatigue resistance (Lau et al, 2001). In their study Cusson and Xi (2002) also demonstrated that FRP has low thermal conductivity, excellent resistance to corrosion and chemical attack and high strength to density ratio.

The assessment of the effectiveness of repair interventions requires a good understanding of the structural behaviour of the resulting composite member, particularly the behaviour of the individual materials involved in the multilayered repaired structure.

1.2 Scope of investigation

This research focuses on:

- Condition assessment of corrosion damaged and repaired RC beams. Modal testing is used for condition assessment of beams at different stages. The assessed condition stages involved are undamaged stage, corrosion damaged stage, repair preparation stage (exposed reinforcement), patch repaired stage and CFRP strengthened stage. Stiffness is inferred from deflections and strain measurements on repaired beams. All beams are assessed for ultimate capacity to investigate the effects of patch repair and CFRP strengthening as opposed to an undamaged beam.

- Assessment of the effectiveness of structural repair and strengthening interventions with the aim to draw attention to the procedure followed in selecting and implementing repairs on corrosion damaged structures.

- Understanding the combined effect of patch repairs and FRP strengthening of beams. Not much work on the integrated behaviour of the two has been reported in the literature.

1.3 Objective of investigation

The aim of the research is to design and conduct an experimental study to predict the effect of structural repair and strengthening on stiffness and ultimate capacity of corrosion damaged structures. Another objective is to understand the effect of corrosion damage on the modal properties of a RC beam.

1.4 Research overview

Following the introduction, the review will convey the work that was done to understand the effect of corrosion on the durability and structural performance of RC structures. The review entails the methods used to induce corrosion on RC elements and the effect of corrosion on RC elements as a basis of quantification. The review extents to the studies carried out on the types of repair and strengthening materials available and tests conducted for dynamic characterization of the structures in stiffness assessment.

Chapter 3 will cover the experimental procedures followed in the study. The experimental work ranges from building steel reinforcement cages, installing strain gauges on the cages, casting of concrete beams, inducing accelerated corrosion of steel reinforcement, testing at service state, repairing of corroded beams, strengthening with FRP and testing all beams to ultimate limit state.

Chapter 4 will convey the results on reinforcement corrosion obtained from the experimental work and the following *Chapter 5* discusses the dynamic testing results and *Chapter 6* will discuss the static testing results. This will thereafter be followed by the conclusions and recommendations.

Chapter 2

LITERATURE REVIEW

2.1 Reinforced concrete damage

Damage in RC structures refers to the deterioration of the structure from its original conditions. Deterioration of RC structures is caused among others by aging of structures, environmentally induced degradation, poor initial construction and lack of maintenance (Taljsten, 2006). Damage may lead to catastrophic structural failure if not detected and addressed through appropriate repair or strengthening interventions. Thus it is important to detect the existence of damage early and implement appropriate repair strategies. An important part of a repair strategy is the selection of appropriate repair material. There is a wide selection of materials for repairing and strengthening of structures new and innovative construction materials such as repair mortars and fibre reinforcement polymers (FRP) (Baghiee et al, 2008).

2.1.1 Corrosion damage

2.1.1.1 General considerations

While factors such as bad construction, extreme exposure and incorrect design of RC members may contribute to RC defects, corrosion damage is the *main cause* of RC structural failure. Corrosion damage is a common problem in new and old RC structures. The most direct damage resulting from steel corrosion in conventionally reinforced concrete is the reduction of steel diameter and cross-section (Bentur et al, 1997) as shown in Figure 2.1 and loss of bond between steel and concrete (El Maaddawy et al, 2005). Loss of steel section results in increase in stresses carried by the remaining steel, therefore reducing the load carrying capacity of the structure (Richardson, 1995).

Figure 2.1: Corrosion of steel reinforcement (http://irc.nrc-cnrc.gc.ca/ircpubs, 2004)

The properties of concrete cover to reinforcing steel play a significant role in the durability of RC structures. The most critical factors governing the commencement of corrosion are concrete permeability, cover thickness, environmental aggressiveness and availability of reactants, such as O_2, H_2O, Cl^- ions, as well as design errors (Capozucca, 1995).

In RC structures, steel is protected by a high pH (>12.5) of the concrete pore solution, which leads to the formation of a protective passive film on the surface of the reinforcement. This passive film passivates steel against corrosion. For corrosion to initiate, the film must be broken or depassivated. Depassivation may occur if the alkalinity of the pore water in the concrete pores decreases or due to penetration of the chloride ions (Richardson, 1995). Once the passive film is broken down, corrosion commences and corrosion products are produced. The volume of corrosion products produced in a corrosion reaction are at least twice the volume of steel that dissolved, thus, rust formation involves a substantial volume increase (Bentur et al, 1997). Most of the rust products remain confined within concrete surrounding the steel, generating expansive stresses, which causes high tensile forces within the concrete, leading to cracking of concrete cover, while some corrosion products leach to the concrete surface in the presence of moisture.

Corrosion cracks normally develop longitudinal to the direction of the reinforcement as shown in Figure 2.2. The compressed concrete around the corroded bars is consequently subjected to biaxial stresses and as a result of the transverse tensions, its longitudinal

strength to compressive stress decreases considerably (Capozucca, 1995). Damage to concrete cover accelerates the risk of further corrosion as there is free access of moisture and corrosion agents to reinforcing steel, as the ability of concrete cover to act as a protective layer to steel has been remarkably reduced.

Figure 2.2: Corrosion crack longitudinal to reinforcement direction (www.cement.org/tech/faq_cracking.asp, 2009)

2.1.1.2 Bond of corroded bars

Studies devoted to understanding the effect of corrosion on the bond between reinforcement bar and concrete have lead to the conclusion that there is a well defined relationship between the bond strength and corrosion level (Richardson, 1995; Capozucca, 1995; FIB, 2002, El Maaddawy et al, 2005). According to the FIB (2002), bond strength changes qualitatively as shown in Figure 2.3. El Maaddawy (2005) also illustrated that bond strength increases with the increase in corrosion prior to crack initiation, but a continuous loss of bond is observed after concrete cracks.

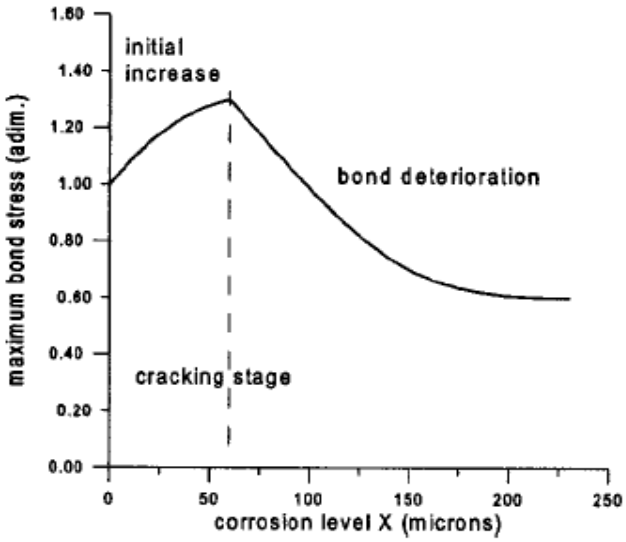

Figure 2.3: variation of bond strength with corrosion level (FIB 2002)

Maintaining composite action requires transfer of load between the concrete and steel. This load transfer is referred to as bond and is idealized as a continuous stress field that develops in the surrounding area of the steel-concrete interface. For RC structures subjected to loading, the bond stress capacity of the system should exceed the demand and there should be little movement between the reinforcing steel and the surrounding concrete. However, RC members lose stiffness when the bond between concrete and steel deteriorates.

2.1.1.3 Corrosion initiation

The degree of corrosion is defined as the mass loss of steel reinforcement due to corrosion (El Maaddawy and Soudki, 2003). The degree to which reinforcing steel corrodes depends on the duration and the rate at which the structure is corroding. In laboratory based studies, corrosion is often artificially induced and accelerated (Andrade, 1995 and El Maaddawy et al, 2005). The commonly used method for corrosion initiation in RC element is the impressing of a direct electrical current. Current is passed between the reinforcement and a stainless steel bar by connecting the positive terminal of the power supply to the reinforcement to act as an anode and the stainless steel to the negative terminal of the power supply to act as a cathode (El Maaddawy et al, 2005). After initiation, oxygen and moisture must be provided at the surface of the cathode to allow the corrosion process to proceed (Richardson, 1995). A number of techniques exist for detecting corrosion to

reinforcing steel in RC structures. They include the half-cell method, the DC polarization method and the AC Impendence method. A brief summary of the techniques follows.

2.1.1.4 Methods of estimating corrosion induced damage

i. Half-cell potential method

Half-cell potentials are a function of a concentration as well as the metal and solution. A more concentrated solution is generally more corrosive than a dilute one, so a current will flow in a cell made up of a single metal in two different concentrations of the same solution (Broomfield, 2003). A corrosion of steel is considered a concentration cell. This method can be used to obtain the potential contours and only indicates the corrosion probability of corrosion, not the corrosion rate (Haung and Yang, 2006).

ii. Direct Current (DC) Polarization method

This method does not consider the current drop effect; therefore, the corrosion rate is likely to be an underestimate (Haung and Yang, 2006). In this method, the polarization resistance is measured and corrosion current intensity is expressed as Equation 2.1.

$$I_{corr} = B\left[\frac{1}{R_p}\right] \quad \text{---------- (2.1)}$$

(Haung and Yang, 2006)

Where R_p is the polarization resistance and B is often taken as 26 mV[10] for steel in an alkaline environment.

iii. Alternating Current (AC) Impendence Method

This method is more theoretically precise in estimating the corrosion rate of RC, compared to other methods. It applies the electrochemical technique to detect corrosion in RC members (Haung and Yang, 2006). The electrochemical method is suitable for the determination of steel corrosion in concrete, following Faraday's law. The electrical current intensity used in the study is as follows:

$$I_{corr} = \Delta W F z \frac{D_{Fe}}{W_{Fe}} \quad \text{---------- (2.2)}$$

(Haung and Yang, 2006)

Where I_{corr} is the current intensity ($\mu A/cm^2$), F is Faraday's constant (96 500 coulombs), ΔW is mass loss due to corrosion (g), W_{Fe} is the atomic mass of steel (55.8 g/mole), D_{Fe} is the density of steel (7.86 g/cm^3) and z is valence (2) from the oxidation reaction of steel shown in Equation 2.3:

$$Fe^{2+} + 2e^{-} \rightarrow Fe \text{ ---------- (2.3)}$$

The AC impendence method is going to be adopted in the experimental work of this research. This method can be used in accelerated corrosion.

2.1.1.5 Accelerated corrosion production

The degree of corrosion is considered as one of the main parameters that can be useful in predicting the service life of corroding RC structure. The amount of dissolved steel, forming rust is governed by the electric current generated by the anodic oxidation reaction shown in Equation 2.2 and consumed by the cathodic reduction reaction shown in Equation 2.4:

$$H_2O + \frac{1}{2}O_2 + 2e^{-} \rightarrow 2OH^{-} \text{ ---------- (2.4)}$$

The mechanism of reinforcing steel corrosion is generally known to be electrochemical in nature (El Maaddawy and Soudki, 2007). The current flow is determined by Faraday's law and related to mass low by Equation 2.5.

$$I_{corr} = \frac{\Delta mFz}{Mt} \text{ ---------- (2.5)}$$

(Andrade, 1995)

Where Δm is the mass of steel consumed (g), M is the atomic mass of steel, I_{corr} is the current in amperes, t is the time in seconds, z is the ionic charge of steel and F is Faraday's constant. The atomic weight of steel is 56 g, the ionic charge is 2 and the Faraday's constant is 96 500 A/s

It is observed from Equations 2.5 that the amount of steel lost during accelerated corrosion is dependent on the amount of current supplied and the duration of the corrosion process.

Andrade (1995) described corrosion rate as the amount of corrosion produced by a unit surface area when referred to a specific period of time. One technique used in the study of corrosion rate is an electrochemical technique. The parameters of this technique are converted into the gravimetric parameters by means of Faraday's law. This method is extremely sensitive because of the high value of Faraday's constant, but can account for very low corrosion rates not reached with the same accuracy with other procedures, such as gravimetric procedure (Andrade, 1995). The maximum corrosion rate recommended by Andrade (1995) is 100 $\mu A/cm^{2;}$ in laboratory studies to avoid pitting corrosion. However, a higher current intensity of 500 $\mu A/cm^2$ has been reported in other studies (Haung and Yang, 2006).

The method used by Andrade (1995) for determining the current intensity is derived as a function of the steel density and the atomic weight of steel. The method compares well with the studies conducted by Haung and Yang (2006) and El Maaddawy and Soudki (2003), which determine the current intensity as a function of the steel molecular weight and time taken during corrosion. Although there is good correlation between different methods of inducing corrosion, there is no set standard procedure for inducing and measuring corrosion.

When relating the accelerated corrosion to in-situ corrosion due to carbonation or chloride contamination, the commonly recorded values of I_{corr} are less than 2 $\mu A/cm^2$. Values greater than 10 $\mu A/cm^2$ are never recorded (Andrade, 1995). Values less than 0.1 $\mu A/cm^2$ indicate life time longer than 100 years. Values giving cross-section losses of 5-25% during 20-50 years are those around 0.5-5 $\mu A/cm^2$, which are commonly measured onsite.

2.1.2 Structural performance indicators for corrosion-damaged structures

Corrosion of embedded reinforcement in RC structures impair the structural capacity through loss of bar section, loss of bond between reinforcement and concrete as a result of longitudinal cracks or loss of concrete cross section (Cairns et al, 2005). Corrosion damage therefore requires performance indicators to quantify damage. Structural performance assessment involves defining appropriate performance indicators and comparing the current state of a structure or structural component with these indicators. Examples of performance

indicators include ultimate capacity and stiffness which can be inferred from strain and deflection measurements and vibration characteristics. The structure may be considered to be unserviceable due to corrosion-induced cracking, but there is still some considerable remaining service life before the structure can become unsafe (Richardson, 1995).

2.1.2.1 Stiffness

Corrosion damage in RC structures reduces the structural stiffness of the structural elements. Torres-Acosta et al (2004) used flexural stiffness as the performance indicator and found that corrosion decreases the flexural stiffness of a RC structural element. They found that reduction in rebar radius results in decrease in flexural stiffness.

The stiffness of a RC member can be obtained from different parameters such as strain measurements for locating the position of the neutral axis, the use of dynamic characterization such as natural frequency and the deflection of the structure.

i. Natural frequency

With a change in the natural frequency of the system, it can be inferred that the system has undergone changes. The reduction in the natural frequency of the system presents a reduction in member stiffness. The relationship between the natural frequency and stiffness is governed by Equation 2.6.

$$\omega_i = \frac{\lambda_i^2}{2\pi L}\sqrt{\frac{EI}{m}} \quad \text{---------- (2.6)}$$

(Blevins, 2001)

Where ω_i is the natural frequency, λ_i is a dimensionless parameter which is a function of the boundary conditions, L is the span of beam span, E is the modulus of elasticity, I is the second moment of area and m is the mass of the beam. SI units are used throughout.

ii. Deflection capacity

Deflection capacity can be defined as the deflection of a member at failure (El Maaddawy et al, 2005). Loss of cross-sectional area of steel affects the stiffness of RC members. To determine the effect of the loss in area due to corrosion on stiffness, deflection relationships of tested RC members can be used. From the studies conducted by Haung and Yang (2006), to determine the beam stiffness from the load-deflection curve, the results reflected a large reduction in stiffness with an increase in corrosion. The relationship between deflections and stiffness is presented by Equation 2.7.

$$k = \frac{P}{\delta} \quad \text{----------} \quad (2.7)$$

(Blevins, 2001)

Where K is the stiffness, P is the applied load and δ is the deflection

2.1.2.2 Ultimate capacity

Although ultimate capacity cannot be used as a performance indicator in practice, it is a good measure of performance in research work. Corrosion damage reduces the area of reinforcing steel and reduces the ultimate capacity of the structure. Torres-Acosta (2004) found that an average reduction in rebar radius results in decrease in flexural load capacity. It is clear that, corrosion compromises the performance of the affected RC structures; therefore, there is a growing need for repairing and restoration of the service life of old and new structures before reaching the ultimate limit state. But, before any repairs or strengthening can take place, it is good practice to establish the level of deterioration and appropriate measures of redeeming the structure.

This research will adopt all the performance indicators mentioned above to investigate the changes that are brought about by the application of patch repair alone and both patch repair and FRP strengthening on damaged beams.

2.2 RC repair and strengthening

The crucial part of a successful repair of RC structures is to establish the primary cause and extent of deterioration. For a repair to be effectively completed it must eliminate the cause of damage, repair the full extent of damage and ensure that the structure is protected from further damage or recurrence of the original cause for its projected lifespan. Strengthening on the other hand has to alleviate the role of steel reinforcement in damaged structures to a significant degree. There are a number of existing repair techniques, some of which include both durability and structural repairs.

2.2.1 Durability repair

2.2.1.1 General considerations

Durability refers to the ability of concrete to resist the ingress of deleterious substances which may lead to corrosion of reinforcement while structural performance relates to the strength of the RC structure. Durability repair therefore refers to the repair of damaged structures to reduce further deterioration by blocking access to the aggressive corrosion agents. When repairing corrosion damaged RC structures, concrete is normally cut-out beyond the affected area and the reinforcing bars are cleaned before application of repair mortars. Durability repair involves replacing the deteriorated concrete to restore its durability by providing adequate cover to the reinforcement (Phaedonos, 2006).

The repair material should provide an alkaline protection to the reinforcing steel and a background for aesthetics. The repair material protects the reinforcing steel physically through its relatively impermeable structure and chemically through the high alkalinity (pH approximately 12.5 - 13.5) of the pore solution, allowing a protective film to be formed around the reinforcement. Cementitious repair mortars like concrete protect steel by providing a protective thin film of Fe_2O_3 that provides an electrochemical protection to the reinforcing steel (Dehwah et al, 2002). The study of passive film by Belaid et al (2000) shows that the presence of a $Ca(OH)_2$ rich layer provides protection by adhering to the steel and hindering the cathodic reaction. Sometimes coating is used on the steel reinforcement to act as a protective film before application of cementitious repair mortars.

There are several methods of application and materials in the repair of RC structures, examples of which are:

i. Patching with cementitious repair mortars

Cementitious mortars are designed for ease of application under a range of in-service conditions (i.e. horizontal, vertical, overhead etc). The mortars have suitable consistencies and adhesion for ease of application either by a trowel or by hand. These repair mortars are claimed to have low shrinkage by the manufacturers. The major requirement of cementitious repair mortars is that their properties be compatible with the parent concrete in terms of modulus of elasticity, coefficient of thermal expansion, shrinkage movement and permeability (Phaedonos, 2006).

ii. Patching with free-flowing grouts and fluid micro-concretes

These are useful for extensive and large repairs where access for hand/trowelled mortars is difficult. The grouts can be pumped or hand poured into formwork because their mixes are very workable and self-compacting.

iii. Pre-packing dry aggregates which are subsequently grouted

Single size coarse aggregate (10 - 20 mm) are packed into the repaired area, then grout is pumped from the furthest point to fill spaces between the aggregate within a simple formwork. The method does not require any vibration and it is suitable for underwater conditions.

2.2.1.2 Patch repairs

Based on the previously discussed materials and applications, the use of cementitious patch repair mortars will be adopted in the experimental work of this research based on the effect on load capacity and structural safety, serviceability and durability. A step-by-step patch repair procedure should address the concrete surface preparation, method of application, curing and surface finish.

The use of patch repair in concrete structures should reduce the rate of the prevailing mechanisms of deterioration. Patch repair should provide compatibility with the existing

structure so that the interaction with the substrate does not initiate another durability problem (Chidiac and Mailvagganam, 1997).

Several factors need to be considered to ensure compatibility between the repair material and the substrate during analysis of repair in a deteriorated concrete structure (Figure 2.4). Compatibility refers to the balance of dimensional (geometrical), chemical, permeability and electrochemical properties between the repair and substrate that ensures the system as a whole withstands forces induced by restrained volume changes, chemical and electrochemical effects without premature deterioration over a designed period of time (Vaysburd, 2006).

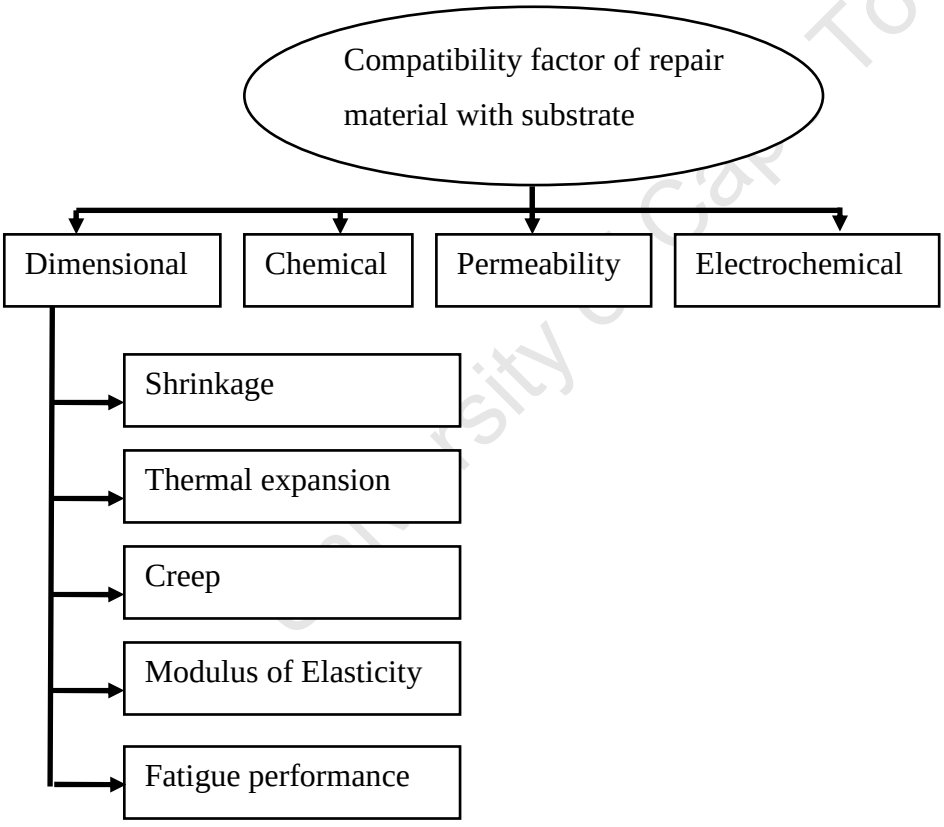

Figure 2.4: Compatibility factors (Vaysburd, 2006).

The chemical, permeability and electrochemical compatibilities of the repaired system are outside the scope of this research. The most crucial compatibility factor in this study is the *dimensional compatibility*. This compatibility covers a full spectrum of dimensional

changes possible in a concrete structure such as; drying shrinkage of the repair material restrained by the concrete substrate which causes cracking and delamination between the two materials, thermal expansion or contraction difference between the repair and the substrate materials, difference in modulus of elasticity causing unequal load sharing and strains resulting in interface stresses, creep properties and relative fatigue performance that cause stresses that can crack the repair material or cause debonding between the repair material and substrate interface (Vaysburd, 2006).

Debonding of the repair material is the most prominent failure mode in the repaired system resulting from incompatibility factors, therefore requires more attention (Vaysburd, 2006). Various researchers have developed models to understand the influence of the compatibility factors on the interfacial bond between the substrate and the patch repair. Most of the literature reported in the field of repair reveals that dimensional incompatibility, in particular drying shrinkage, is one of the major problems of concrete repair.

Cusson and Mailvaganam (1996) expressed that lack of compatibility in repaired structures results in spalling, cracking, scaling and subsequent loss of strength. The common modes of failure of concrete patch repair systems have been identified as tensile cracking through the thickness of the patch repair layer and peeling failure at the interface between repair layer and substrate concrete due to transverse tension (Rahman, et al, 2000).

Poor compatibility may result in shrinkage of the repair layer as a consequence of moisture loss. This results in build-up of stresses in both repair layer and concrete substrate as the repair layer is constrained by the substrate, and the drying shrinkage strains are not allowed to occur freely.

Application of patch repairs in corrosion damaged RC structures is associated with deterioration, delamination, cracking or spalling of concrete due to contamination by deleterious substances such as chlorides and carbon dioxide associated with the overall mechanism of corrosion of steel reinforcement (Phaedonos, 2006). Repair works in corrosion deteriorated RC structures must follow a sequential process.

The structural condition should be assessed and compared with the previous undamaged stage to establish the degree of deterioration. Possible causes of assessed damaged should be evaluated in order to come up with repair strategies that will ensure durability. The common repair process in corrosion damaged structures involves breaking damaged concrete back to sound and dense concrete by at least 20 mm behind the steel reinforcement, then cleaning off the corroded steel reinforcement and preparing the concrete substrate. Then an appropriate steel primer and substrate bonding coat can be applied before the patch repair mortar is applied to rebuild the cut member to the original surface profile.

2.2.2 Structural strengthening of RC

2.2.2.1 General considerations

Structural repair of RC structures deals with strengthening of the structural elements within the serviceability state or repairing the damaged structures to restore their strength. There are several techniques that can be used to strengthen RC structures, such as the external application of steel plates or FRP plates, concrete jacketing.

Externally bonding steel plates to RC members is one of the most common techniques used for upgrading RC members. This technique is cost-effective and efficient but has a number of drawbacks. It is prone to deterioration of the bond at the steel-concrete interface caused by the corrosion of steel (Banks et al, 2002). It has presented difficulty in manipulating the heavy steel plates at the construction site; especially in the case of flexural strengthening of long elements, therefore requiring scaffolding (Banks et al, 2002).

Figure 2.5 a: Concrete strengthened with steel plate (www-civ.eng.cam.ac.uk/cjb/cjbresearch1.html, 2008)

Another common conventional strengthening technique is the application of steel jackets. Jacketing is quite effective as far as strength, stiffness, and ductility are concerned, but it increases the cross-sectional dimensions and dead loads of the structure, is labor intensive, obstructs occupancy, and provides the RC element with a potentially undesirable stiffness increase (Banks et al, 2002). As an alternative, the conventional techniques can be replaced by FRP strips or sheets. FRP composites have gained widespread use as strengthening materials for RC structures in applications where conventional strengthening techniques have exhibited problems.

2.2.2.2 FRP Systems

There are three different types of Carbon Fibre Reinforcing Polymers (CFRP) systems; namely the sheet system, the laminate system and the Near Surface Mounted Reinforcement (NSMR) system. The systems can be used for various applications such as strengthening the existing structure such as change of cross section, external pre-stressing, and change of static system or design (Taljsten, 2006). The scope of this research covers only the application of CFRP in bending.

i. Laminate system

The laminate system consists of flat laminates, concrete primer and adhesive. The primer enhances the bond of the adhesive to the concrete (Taljsten, 2006). Laminate systems are

most suitable for flat surfaces such as beams, walls and slabs. Figure 2.5b shows the application of CFRP laminates to cater for increasing loads on a floor slab.

Figure 2.5 b: Concrete slab strengthened in bending (www.pulwellpultrusions.com/products5.htm)

ii. Sheet system

The sheet system consists of epoxy primer, putty, dry or pre-impregnated fibre and a resin system, which makes it a lengthier process than using the laminate system. This system often requires a post treatment such as painting, plastering or application of a thin layer polymer concrete (Taljsten, 2006). The sheet system is sensitive to irregularities on concrete surface and therefore requires pre-treatment. The sheet system is flexible and adapts to most surfaces as shown in Figure 2.5c where CFRP sheet is used to wrap columns. The system is most suitable for seismic retrofitting, strengthening of curved surfaces, strengthening of walls and slabs with openings.

Figure 2.5 c: CFRP sheet system for columns (www.fos-ta.com/FRP-projects.html)

iii. NSMR system

Near Surface Mounted Strengthening system is used mainly on surfaces that require protection from aggressive corrosion products. This system usually consists of circular or rectangular rods that are bonded in slots in the concrete cover of a structure, therefore requiring a concrete cover lager than 25 mm so that they can be fitted into the cover concrete. The pre-treatment of the surface consists of sawing slots in the concrete cover as shown in Figure 2.5d. The rods are then bonded in these slots with an epoxy adhesive or high quality cement grout (Taljsten, 2006).

Figure 2.5 d: NSMR strengthening. (www.hughesbros.com/aslan200/Aslan200_CFRP_bar)

2.2.2.3 Application of FRP

The main advantage of using FRP is its strength to weight ratio. FRP increases flexural load carrying capacity of concrete components. For tension face strengthening techniques, FRP presents better strengthening characteristics in terms of the ultimate flexural load capacity (Lau et al, 2001). It also increases ductility considerably without an excessive stiffness change (Banks et al, 2002).

The main disadvantages of externally strengthening structures with FRP materials are the risks of fire and accidental damage (Simonelli, 2005). Another disadvantage of FRP is that the long term performances are not established. Although FRP has presented a number of favourable characteristics, there are factors concerning the possible failure modes it exhibits.

The identified failure modes in a RC structure strengthened with FRP include the following; (i) yielding of steel followed by FRP fracture, yielding of steel followed by crushing of concrete while the FRP is still intact, (ii) FRP peel-off at the cutoff point due to shear failure of the concrete, (iii) FRP peel-off initiating far from the ends, due to inclined shear cracks in the concrete, (iv) FRP peel-off at the termination point or at a flexural crack due to high tensile stresses in the adhesive and (v) debonding at the FRP-concrete interface in areas of concrete surface unevenness or due to faulty bonding. Of all the listed failure modes, 'yielding of steel followed by crushing of concrete while FRP is still intact' is the most favorable failure mode.

Possible failure modes for RC members strengthened with FRP in flexure is the anchorage failure, which is due to the insufficient anchorage length of FRP laminates. For sheet bonded system, the most common failure mode is the mid-span debonding, which initiates from the tips of mid-span flexural cracks or flexure-shear cracks of RC concrete (Ueda and Dai, 2004).

The interfacial bond has proven to be relatively weak compared to the neighbouring material in the upgraded system, which lead to interest on clarifying the mechanisms of the bond between FRP and concrete substrate. In all repaired systems, the interfacial bond is responsible for transferring stresses from the concrete to the externally bonded FRP (Ueda and Dai, 2004).

2.3 Physical laboratory tests

The objectives of this research are to develop a comprehensive experimental study to calculate the effect of corrosion on stiffness and ultimate capacity of the structure and to assess the effectiveness of repair and strengthening measures to the system. Several tests

are required to determine the performance of the structural systems. Tests such as flexural tests, dynamic testing and modal testing can be used to determine the performance of the system in relation to the stiffness variation. To assess the overall performance of the repaired system, in this study; dynamic testing can be performed on undamaged beams, damaged beams and repaired beams.

2.3.1 Dynamic testing

2.3.1.1 General considerations

Dynamic testing started in the 19th century. Many of the early tests in dynamics were conducted as part of the safety inspection of bridges and involved monitoring bridge vibrations (Salawu and Williams, 1995). Over the years, these tests have evolved to the modern tests methods concerned with improving analysis and design procedures, assessment of structures and monitoring of in-service behaviour of structures.

Dynamic testing is considered as a procedure for determining the natural frequencies of a structure. The identified vibration mode shape for each natural frequency corresponds to the deflected shape when the structure is vibrating at that frequency (Salawu and Williams, 1995). Each vibration mode is associated with a damping value which is a measure of energy dissipation. The natural frequency, mode shape and damping value of a mode are referred to as modal parameters of a particular system. Dynamic tests for obtaining modal parameters are called modal tests.

Dynamic testing can be used for regular condition assessment of structures by monitoring the structure's dynamic responses. Change as a result of deterioration in the system (mass, stiffness and damping) leads to changes in the vibration response of the system. These can be measured using the standard dynamic testing techniques. In the work conducted by Tsai and Yang (1988), test results showed that the size of damage is proportional to the magnitude of observed changes in system parameters.

Damage causes changes in the physical properties of a structure which in turn alters its dynamic response characteristics. Monitoring the changes in the response parameters of a structure has been widely used for the assessment of structural integrity, performance and

safety (Bayissa and Harotos, 2005). There are variations in the dynamic response of the damaged structures due to cracks during vibrations.

The analysis of the dynamic response characteristics of a structure subjected to excitation and monitoring of the changes in the response parameters is an effective tool for the assessment of structural integrity (Dimarogonas, 1996; Brandon et al., 1999). These response parameters characterise the 'global' properties of the structure and have been widely used for in-service monitoring and evaluation of structural integrity after extreme events such as earthquakes (Bayissa and Harotos, 2005).

Changes in modal parameters differ throughout the modes, as the changes depend on the location and severity of damage. For this reason, data obtained from dynamic testing can be used to detect, locate and quantify damage. Dynamic based condition assessment is part of structural health monitoring (SHM). SHM involves monitoring of the natural frequency and modal analysis for damage detection.

The basic steps involved in dynamic testing are illustrated in Figure 2.6. The test structure is provided with an excitation force which is generated from a computer system for regulation. The force is amplified to reach the structure. The response transducers are connected to the structure to capture the response of the structure to the applied force. The signal conditioner filters the signal that is recorded and processed; all these are captured into a computer system and analysed.

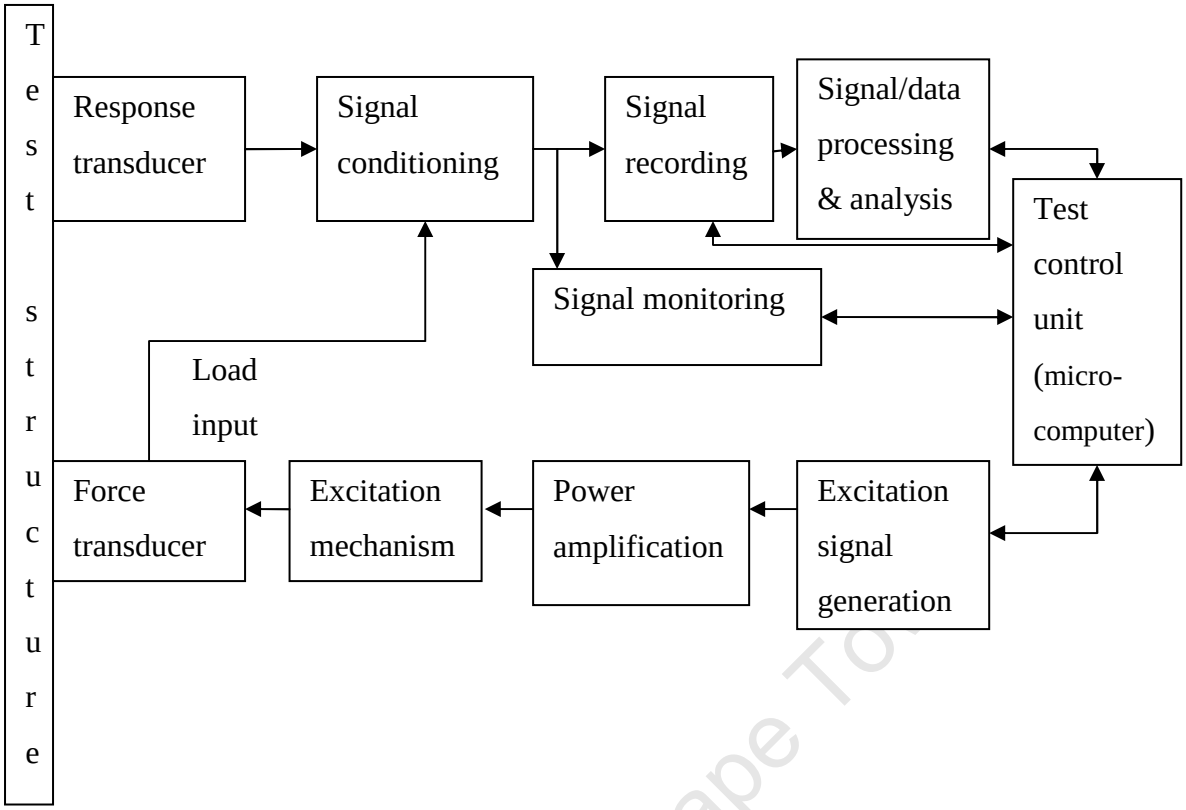

Figure 2.6: Stages involved in vibration testing (Salawu and Williams, 1995)

2.3.1.2 Changes to natural frequencies due to structural damage

Damage alters the natural frequencies of a structure. Loss of stiffness is inferred when measured natural frequencies are lower than expected. For damage to be detected with high confidence, natural frequency change of greater than 5% is expected. Researchers (Salane et al, Salane and Baldwin, 1990) found that dynamic tests on models and full scale structures indicate that changes in resonant frequency can occur due to support failure, crack propagation, shear failure and overloading causing internal damage. Detection of damage using frequency measurements might be unreliable when the damage is located at regions of low stresses, because the shift in the natural frequency might not provide sufficient information for integrity monitoring (Idichandy and Ganapathy, 1990). The existence of a crack at the section of a beam is equivalent to the reduction of the second moment of area, resulting in local bending stiffness at the cross-section. The reduction in frequency is more important when the crack occurs at the region of high curvature for the mode under consideration (Salawu, 1997).

2.3.1.3 Types of dynamic tests

The two main types of testing are ambient vibration testing, which does not have any control on the input and forced vibration testing in which vibration is artificially induced.

i. Ambient Vibration testing

In this method, the input excitation is not under the control of the test engineer. The vibration response is measured while the structure is under service load. The loading for this test could be from either wind, waves, vehicular or pedestrian traffic or other service loads. This requires assumptions about the nature of loading since the input is unknown.

ii. Forced vibration testing

This method involves application of input excitation of a known force level at a known frequency. The advantage of this method is that it suppresses the effect of noise in measured structural responses. Vibrations can be induced by means of a vibrator, vibrator exciter or shaker. These devices transmit the vibratory forces into the structure. Forced vibration testing is based on the fact that if loads on the structure are known and the resulting motion can be measured, it is then possible to estimate the properties of the structure (Salawu and Williams, 1995). Forced vibration method is to be adopted in this research on a beam tested in bending.

2.3.2 Vibration testing of beams in bending

The natural frequency of mode shapes can be determined using Equation 2.6 in page 10. The natural frequency can be related to static deflections. The natural frequency of a structure is the result of the exchange of kinetic and potential energy within the structure. Kinetic energy is associated with the motion of the structural mass, whilst potential energy is associated with the strain energy stored in the elastic structure during deformation.

One measure of the strain energy stored in a structure is the static deflection of the structure under the acceleration of gravity. There is a relationship between the static deflection of the structure under its own weight and the natural frequency of the structure.

Static deflection is given by Equation 2.8:

$$\delta_s = \frac{Mg}{k} \quad \text{---------- (2.8)}$$

Where M is the mass of the beam, g is the acceleration due to gravity and k is the stiffness.

Natural frequency (Hz) is given by Equation 2.9:

$$\omega_i = \frac{1}{2\pi}\left(\frac{k}{M}\right)^{\frac{1}{2}} \quad \text{---------- (2.9)}$$

(Blevins, 2001)

When substituting Equation 2.8 into Equation 2.9, Equation 2.10 results. This equation shows that the natural frequency can be estimated from the static deflection.

$$\omega_i = \frac{1}{2\pi}\left(\frac{g}{\delta_s}\right)^{\frac{1}{2}} \quad \text{---------- (2.10)}$$

Where δ_s is the deflection of a simply supported beam as shown in Figure 2.7.

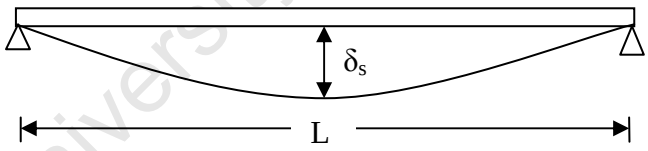

Figure 2.7: Static deflection diagram

The commonly used equation for estimating natural frequency is Equation 2.11 and it is said to underestimate the frequency of the system about 6.6% (Blevins, 2001), however it is mostly applicable to the first mode shape, not second or higher order mode shape of the system. The theoretical first, second and third modes are shown in Figure 2.8. The mode shapes (y_i) are calculated from Equation 2.12, where n is the mode shape number, x is the position along the beam and L is the span of the beam.

$$k = \omega^2 m \text{ ----------} \quad (2.11)$$

(He and Fu, 2001)

$$y_i = \sin\left(\frac{n\pi x}{L}\right) \text{ ----------} \quad (2.12)$$

(Blevins, 2001)

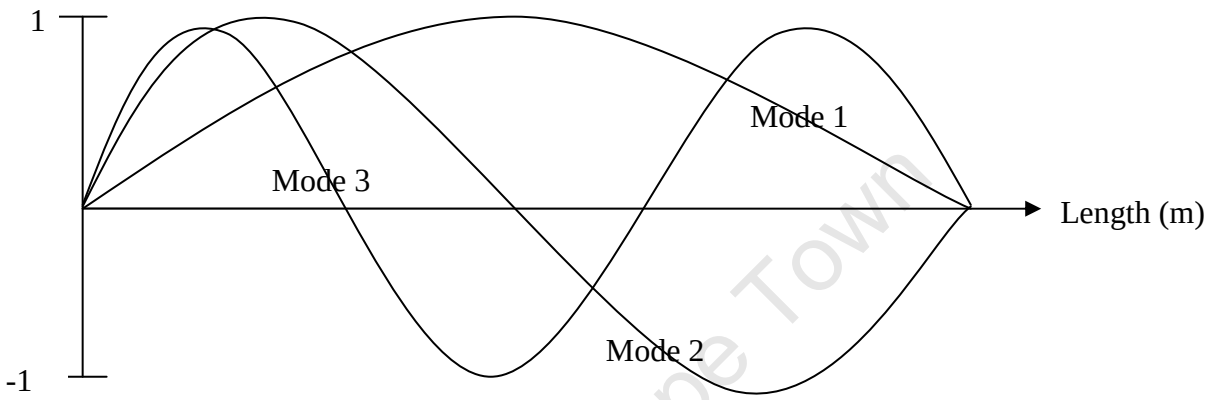

Figure 2.8: Different transverse mode shapes

2.4 Modal parameters

Modal analysis is the extraction of modal parameters using theoretical structural models or experimental data. There are two types of modal analysis namely Analytical Modal Analysis (AMA) and the Experimental Modal Analysis (EMA). The present work will focus on EMA. The EMA covers the data collection, signal processing and the modal parameter extraction.

2.4.1 Data collection

A series of dynamic tests were conducted on four beams using accelerometers while a shaker was used for the source of excitation. The modal analyses were performed on the response data to obtain Frequency Response Functions (FRF) and modal parameters in the frequency domain.

2.4.2 Signal processing

2.4.2.1 Signal sources for frequency response

The Fast Fourier Transform (FFT) and the power spectrum are powerful tools for analyzing and measuring signals from plug-in data acquisition (DAQ) devices. For example, one can effectively acquire time-domain signals, measure the frequency content, and convert the results to real-world units and displays (Cerna and Harvey, 2000).

To achieve a good frequency response measurement, significant stimulus energy must be present in the frequency range of interest. Two common signals used are the chirp signal and a broadband noise signal. The chirp signal is a sinusoid swept from a start frequency to a stop frequency, thus generating energy across a given frequency range. White and pseudorandom noise have flat broadband frequency spectra; that is, energy is present at all frequencies (Cerna and Harvey, 2000). It is best not to use windows when analyzing frequency response signals. If a chirp stimulus signal is generated at the same rate as the response is acquired, the acquisition frame size can be matched to the length of the chirp.

2.4.2.2 Choosing a window

There are several types of windows to chose from when analysing the frequency response date, such as rectangular (uniform) window, hanning window, hamming window, Blackman-Harris window, Exact Blackman and Flat Top window. Frequency characteristics of a window can describe how a window affects the frequency spectrum.

If the frequency of interest contains two or more signals very near to each other, spectral resolution is important. In this case, it is best to choose a window with a very narrow main lobe. If the amplitude accuracy of a single frequency component is more important than the exact location of the component in a given frequency bin, choose a window with a wide main lobe.

If the signal spectrum is rather flat or broadband in frequency content, use the Uniform/rectangular window. In general, the Hanning window is satisfactory in 95% of cases. It has good frequency resolution and reduced spectral leakage. The Flat Top window has good amplitude accuracy, but because it has a wide main lobe, it has poor frequency resolution and more spectral leakage. The Flat Top window has a lower maximum side lobe level than the Hanning window, but the Hanning window has a faster roll off-rate. If the

nature of the signal is unknown, the Hanning window is always the best option to start with. Although in this study, the chirp signal is used, the Hanning window is adopted.

2.4.2.3 Converting from a two-sided power spectrum to a single-sided power spectrum

Most real-world frequency analysis instruments display only the positive half of the frequency spectrum because the spectrum of a real-world signal is symmetrical around DC. Thus, the negative frequency information is redundant. The two-sided results from the analysis functions include the positive half of the spectrum followed by the negative half of the spectrum.

In a two-sided spectrum, half the energy is displayed at the positive frequency, and half the energy is displayed at the negative frequency. Therefore, to convert from a two-sided spectrum to a single-sided spectrum, discard the second half of the array and multiply every point except for DC by two.

In this study, the frequency points taken are 16384, but the data block size used is 8192, which is half of the total block size. The program used for acquiring data is LABVIEW Signal Express.

2.4.3 Modal parameters extraction

The three modal parameters that are acquired from the dynamic testing are natural frequency, mode shapes and the modal damping. These parameters are used in the study to analyse the performance of the beams before damage, after damage and after repair and strengthening of the damaged beams. These modal parameters are obtained from the Frequency Response Functions (FRF) produced when inducing vibrations to beams. These modal parameters can be obtained.

Chapter 3

EXPERIMENTAL INVESTIGATION

3.1 Introduction

Four full scale RC beams of dimensions 153 × 254 × 5000 mm were cast for the experimental study. Three of the beams were subjected to accelerated corrosion damage at different levels whilst under a sustained load and then tested under flexure. One of the beams was used as a control beam. The beams were corroded using a 5% NaCl solution.

3.1.1 Specimen details

The beam specimens had the following dimensions, 153 mm width, 254 mm depth and 5000 mm length. The reinforcing bars were placed symmetrical in the cross section, with the compression reinforcement at the top and the tension reinforcement at the bottom. The dimensions of the compression and tension reinforcement are 10 mm and 20 mm diameter respectively. Double-leg stirrups of 8 mm diameter mild steel were placed at 150 mm spacing centre to centre throughout the length of the beam. The stirrups around the centre of the beam where the corrosion pond was to be placed were covered with a shrink wrap to avoid access of the corrosion on the stirrups. Figure 3.1 shows a detailed beam specimen used in the study.

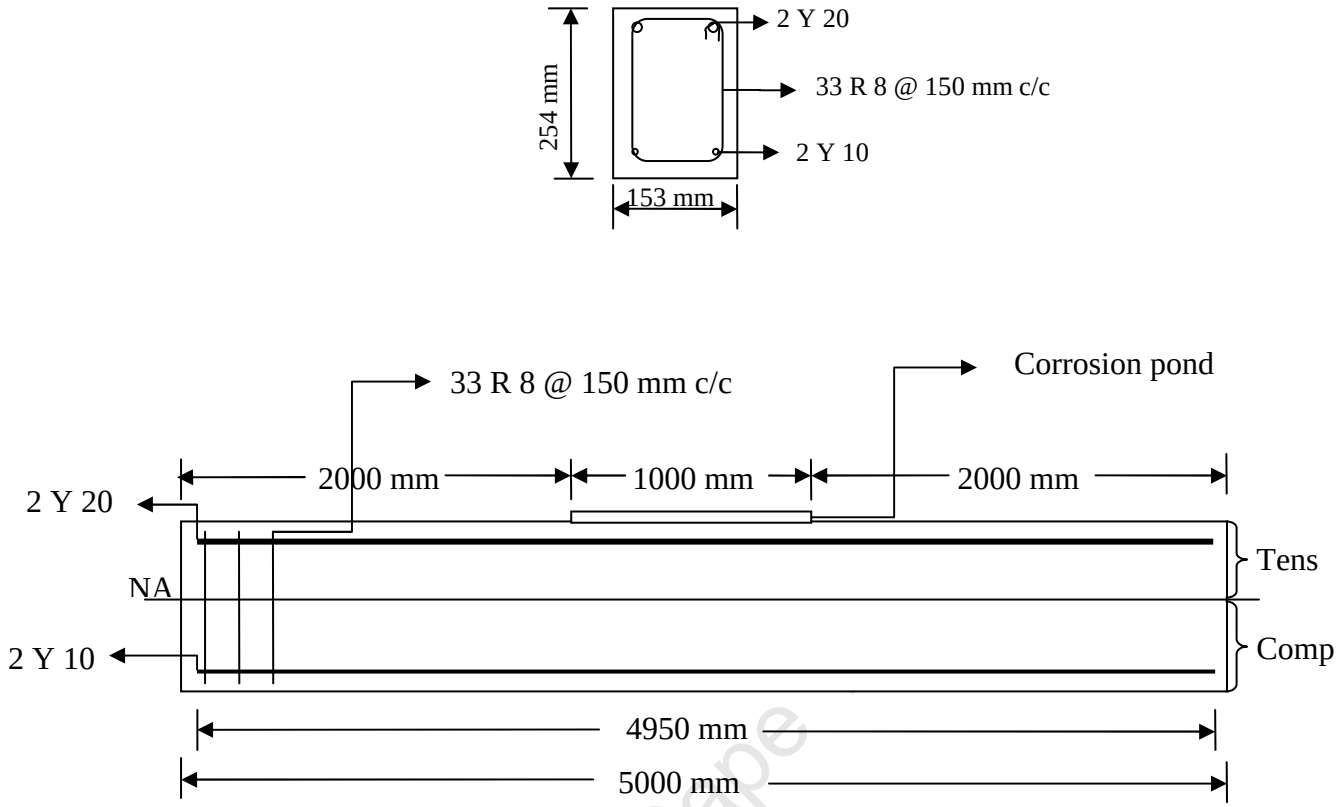

Figure 3.1: Inverted beam reinforcement detail (NOT TO SCALE)

3.1.2 Strain gauging

The reinforcement cages were fitted with the strain gauges for measuring the global strains in the beam during testing. Each beam is fitted with six strain gauges, three on both the tension and compression reinforcement. The strain gauges are very sensitive to dust, therefore require clean environment and skill. The reinforcement was ground for smoothing and cleaned before the gauges could be placed. The gauges were then glued to the smoothed surface and wires were soldered onto the gauges for connection to the data reading device as shown in Figure 3.2. The wires were extended such that they were long enough to connect after casting the beams.

Figure 3.2: strain gauges on the tension and compression reinforcement

Figure 3.3: Strain gauges protected with an impermeable membrane

The strain gauges on the tension and compression bars have a resistance of 120Ω and 350Ω respectively. The gauges were placed at 1600 mm from both the left and right sides of the reinforcement cages and one at mid-span of the cage. The left side of the beam was marked by the wires soldered on the tension reinforcement for corrosion. The strain gauges were covered with clear silicon to prevent water damage, then covered with putty to prevent any direct impact that might damage the sensitive gauges, then wrapped with an impermeable membrane shown in Figure 3.3. Concrete was then cast over the reinforcement cages with the gauges to construct the beams.

3.1.3 Materials and mixes

The beams were cast using ordinary Portland cement (OPC), with a w/b ratio of 0.55. 19 mm standard coarse aggregates were used as shown in Table 3.1. The average compressive strength of the concrete cubes after 28 days was 40 MPa, with a standard deviation of 2.8 MPa. Concrete was mixed in a concrete mixer and cast horizontally in the moulds, and then compacted with a poker vibrator and levelled with a trowel as shown in Figure 3.4. After casting, concrete was covered with plastic sheets for 48 hours, thereafter demoulded and cured by covering with a wet hessian cloth for 26 days as shown in Figure 3.5.

Table 3. 1: Mix proportions for 1m^3 mix for a 40 MPa concrete

Mix		Binder		Aggregates	
Binder type	w/b ratio	Quantity (kg/m^3)	Water (l/m^3)	Stone (Greywacke) (kg/m^3)	Sand (Klipheuwel) (kg/m^3)
CEM 1-42.5N	0.55	355	195	1007	840

Figure 3.4: Concrete after casting

Figure 3.5: Curing with a Hessian cloth

3.1.4 Accelerated corrosion

When preparing the beams for accelerated corrosion, wires were soldered on to the tension reinforcement and a piece of stainless steel rod. The reinforcement worked as an anode, whilst the stainless steel bar worked as a cathode. Beams 2, 3, and 4 were provided with a PVC pond of dimensions 150, 1000 and 30 mm for corrosion located at the mid-span of the beam as shown in Figure 3.6. A 5% NaCl solution was added into the pond and a 12 mm stainless steel bar of length 800 mm was immersed into the NaCl solution. To accelerate corrosion, the tensile steel bars and the stainless steel bar were connected to a power supply using electric copper wires. A silver brazing alloy with flux was used to connect the electric copper wires to the ends of the tensile reinforcing steel bars and to the stainless steel bar. The connections between the wires and the steel bars or stainless steel bar were covered

with shrink wrap to prevent moisture access. The tensile steel bars were connected to a positive terminal of the power supply to act as anode whilst the stainless steel bar was connected to the negative terminal of the power supply to act as a cathode. The stirrups around the tension reinforcement at the location of the pond were covered with an impermeable shrink wrap to avoid ingress of NaCl solution on the stirrups so as to prevent corrosion on them.

Figure 3.6: PVC corrosion ponds on concrete beams

The corrosion process consisted of wetting and drying cycles of 4 and 2 days respectively. For ease of monitoring, all corroded beam specimens were supplied with the same current intensity of 1000 $\mu A/cm^2$ which was divided equally between the two bars and the corrosion period was varied depending on the desired level of corrosion shown in Table 3.2. The relationship between corrosion current density and the steel mass loss due to corrosion was determined by applying Faraday's law using Equation 2.4 on page 11.

Table 3. 2: Corrosion programme

	Beam 1 (Control)	Beam 2	Beam 3	Beam 4
Corrosion	No	Yes	Yes	Yes
Estimated Corrosion level (%)	0	10	10	15
Corrosion duration (wetting days)	0	20	20	30

3.2 Repair process

3.2.1 Repair preparation

The corrosion damaged RC beams were prepared for repair by cutting-out the damaged area beyond the level of corroded steel, until sound concrete was reached. Damaged concrete was cut out with a grinder and broken out with a jack hammer to the level beyond the reinforcement to facilitate access to reinforcement when cleaning the corrosion products. The reinforcing bars were cleaned with a wire brush to remove the corrosion products before application of the patch repair mortars. Figures 3.7 and 3.8 show the section of the beam where damaged concrete was cut out and reinforcing bars after cleaning respectively. Durability repair in this work involves replacing the deteriorated concrete to restore its durability by providing adequate cover to the reinforcement.

Figure 3.7: Section through a beam where damaged concrete is cut out

Figure 3.8: Reinforcing steel after cleaning corrosion products

The beam was cut up to 25 mm beyond the tensile reinforcement. The surface was cleaned such that it is free of all contaminants and all weak concrete removed. The loose material was removed mechanically by sand blasting. The reinforcement bars were cleaned, after which the exposed part of the beam was wetted overnight to ensure full saturation for preparation of the patch repair application.

3.2.2 Patch repair

Beams 2, 3 and 4 were patch repaired with a patch repair mortar. The grout was used to replace the damaged concrete within the beam. Formwork was provided around the cut area shown in Figure 3.8 and the repair mortar was placed to replace the damaged concrete. Figure 3.9 shows the repaired section of the beam. The beams were covered with a polythene sheet over night and then covered with a wet hessian cloth after demoulding for 28 days.

Figure 3.9: Patch repair section through the beam

The repair mortar has compressive, tensile and flexural strengths of 75 MPa, 5.5 MPa and 7.5 MPa respectively. The repair mortar was bonded to the concrete substrate by an adhesive bonding agent.

3.2.3 Strengthening

The CFRP laminates were bonded on to the substrate using the special epoxy resin for the laminates. Before application of the CFRP laminates, the concrete surface was prepared by grinding off the top concrete to expose aggregates and air blowing it to remove loose dust. The CFRP laminates were cleaned with a cleansing agent to remove excess dirt before application. The epoxy adhesive is supplied in two components which were mechanically mixed as per supplier's instructions and then applied to the prepared concrete surface. The epoxy resin was placed on the concrete where the laminates were to be applied and the laminates were places on top of the epoxy, then pressed to the concrete with a roller to remove air bubbles between the laminates and the epoxy, then excess epoxy is removed.

Beams 2 and 4, with 10% and 15% corrosion respectively, were patch repaired and strengthened with CFRP laminates. The CFRP laminates used were 50 mm in width, 1.2 mm thick and 4900 mm long. Each beam was strengthened with two laminates running parallel throughout the length of the beam on the tensile face. The CFRP laminates were anchored at the end with a 300 mm thick CFRP wrap. The CFRP laminates had a tensile strength of 3100 MPa and a density of 1600 kg/m^{3}as specified by the supplier. Both beams were strengthened on the tension side where the patch repair was applied as shown on Figure 3.10. The strengthened beams were allowed to cure for 7 days after CFRP application before testing.

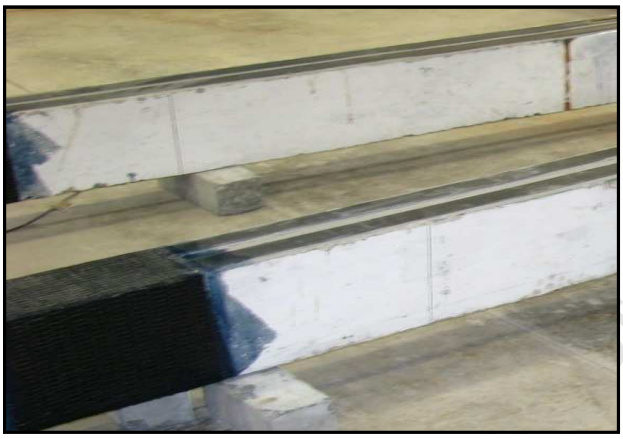

Figure 3.10: Externally bonded FRP laminates

3.3 Testing

Preliminary tests carried out before inducing corrosion involved loading all beams below their cracking moment under a four point loading set-up while measuring strains using strain gauges and deflections using LVDT's. Dynamic testing was conducted as part of the preliminary tests. The reason for conducting preliminary tests was to establish the control values for the beams as a basis of assessment. The main testing conducted in this study involved the following; corrosion, dynamic and static tests.

Beams 2, 3 and 4 were tested after 10 % corrosion was induced. Dynamic testing, strain measurements and deflection measurements were performed to assess the influence of

corrosion on the behaviour of concrete members before repair. The tests follow the same procedure as before corrosion. Beam 4 is corroded further after testing to achieve 15% corrosion level, while beams 2 and 3 were patch repaired. Beam 4 was also repaired after further corrosion was induced. Table 3.3 shows the experimental programme followed.

Table 3. 3: Experimental programme

	Beam 1 (Control)	Beam 2	Beam 3	Beam 4
Initial loading of undamaged beams(kN)	2.5	2.5	2.5	2.5
Deflections under load	Yes	Yes	Yes	Yes
Natural frequencies	Yes	Yes	Yes	Yes
Strain measurements	Yes	Yes	Yes	Yes
Corrosion	No	Yes	Yes	Yes
Patch repair	No	Yes	Yes	Yes
FRP strengthening	No	Yes	No	Yes
ULS	Yes	Yes	Yes	Yes

3.3.1 Dynamic testing

After 28 days of wet curing, the beams were mounted with anchor bolts on the tension side for dynamic testing. The anchor bolts were used to connect the stinger from the vibrator during dynamic testing. The beams were provided with square steel plates on the compression side for placement of the accelerometers during testing. The plates were glued onto the concrete surface and levelled using a spirit level.

The accelerometers were connected to magnetic disc connectors that fix the accelerometers to the steel plates on the beam as shown in Figure 3.11. Four accelerometers were used for every set of measurements. One accelerometer was used as a reference accelerometer, which is regarded as an input source while the other three were used as output sources. The reference accelerometer was not moved throughout the test. The shaker used as a source of excitation was also fitted with an accelerometer as another input source.

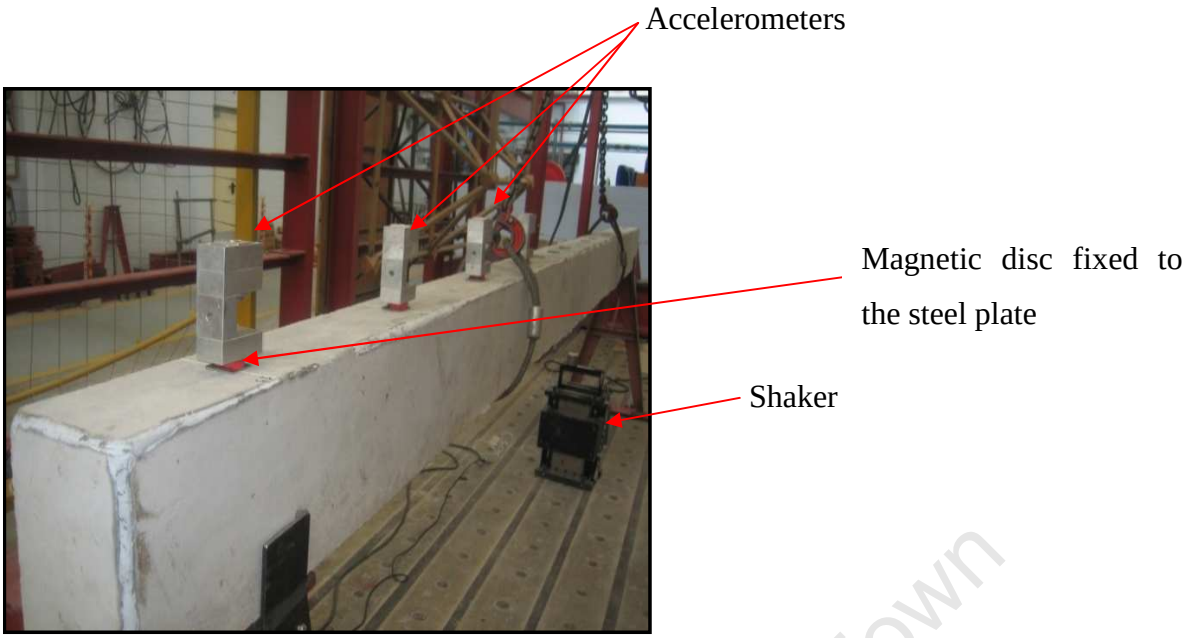

Figure 3.11: Position of accelerometers on the steel plates

The accelerometers used were colour coded to represent different channels. The system configuration showing all the system components and the system wiring are shown in Figures 3.12 and 3.13 respectively. The system components are CPU with a DAQ driver, amplifier and DC coupler. The DAQ card plugs into the CPU and connects to the BNC-2110.

The system uses a 24-bit data acquisition card, with a bit resolution of 2^{24}. The output voltage driving the shaker comes from the BNC-2110 through the amplifier and then to the shaker for excitation. Data was then collected from a PC, through a program called LABVIEW signal express. The signal used in the test was a y-chirp generated by the MATLAB programme.

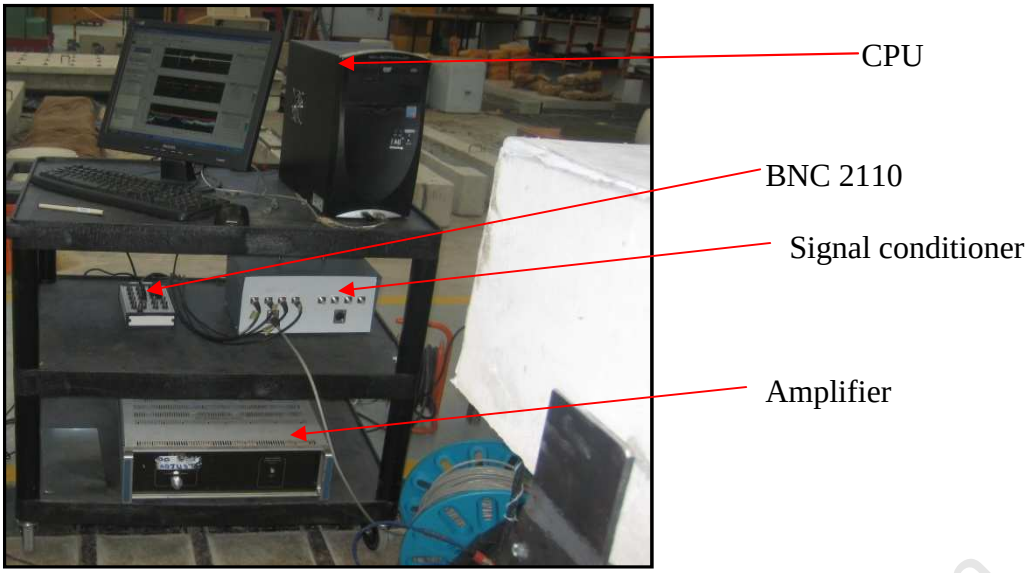

Figure 3.12: Dynamic test system configuration

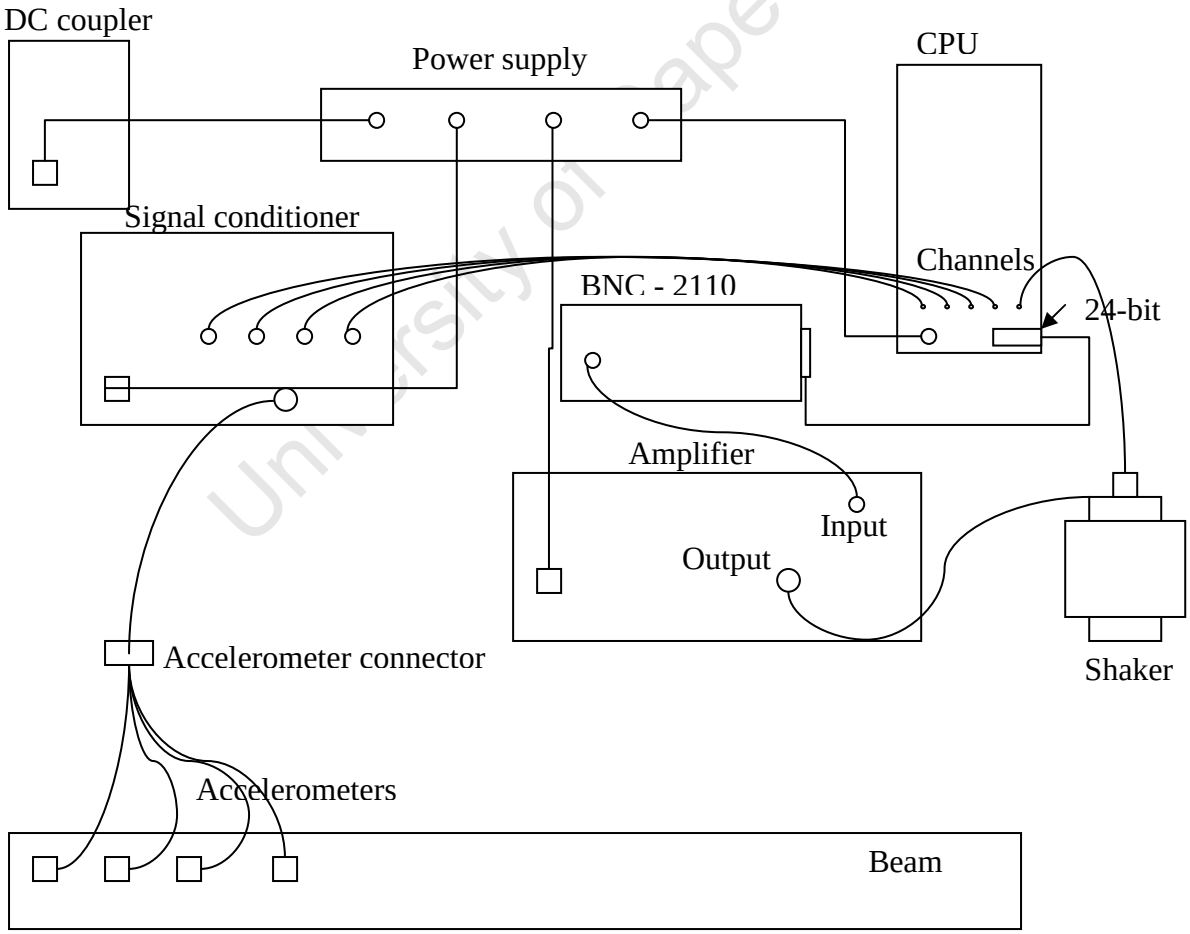

Figure 3.13: Instrument wiring diagram

The beam is tested by placing the accelerometers over the points marked with the steel plates. Each beam has 13 points spaced at 500 mm and 250 mm at the beam ends and around the beam's mid-span respectively. Four accelerometers were used per test set-up, one of which was used as a reference accelerometer and three of which were response measuring accelerometers. The reference accelerometer was fixed at point 1 and not moved while the other three accelerometers were shifted from point to point as a set to capture the beam response to excitation. Figure 3.14 shows the location of the steel plates on the beam.

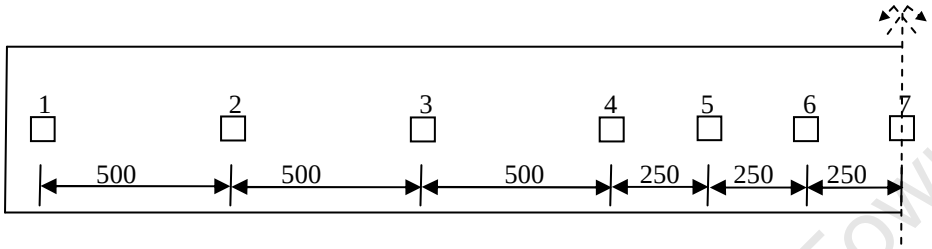

Figure 3.14: Testing points marked by steel plates on the beam

The main focus of this test is to investigate the dynamic characteristic behaviour of a RC beam element before and after corrosion damage and attempt to identify changes in the dynamic parameters due to corrosion which can be used for assessment of the structural condition.

The same test was performed on the beam after it was corroded and after the corrosion damaged area was cut out as shown in Figure 3.15. This is to assess the change in dynamic stiffness of the beam with exposed reinforcement before repair. This is done in order to assess whether or not the stiffness is affected when preparing for repair. Dynamic testing still continued after the beam was repaired and cured and strengthened with FRP laminates.

Figure 3.15: Dynamic testing of the beam after the damaged concrete was removed, before repairing

3.3.2 Static tests

3.3.2.1 Strain and deflection measurements

The strain and deflection measurements were taken under load. The initial load of 2.5 kN was applied by the four-point loading as shown in Figure 3.16. The strains were measured from the strain gauges that were cast into the beam, by connecting the strain gauge wiring to the resistors for measuring the resistance change when the beam was loaded. The resistance was then converted to strain measurements in (microstrain) when recording the reading. The same program as in dynamic testing (LABVIEW signal express) was used to record the strain measurements.

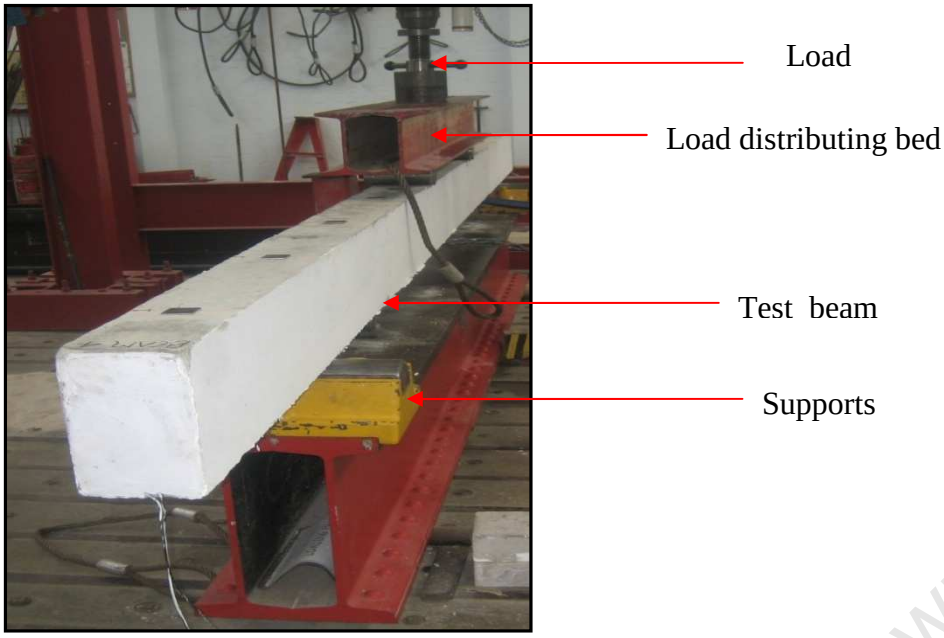

Figure 3.16: Four-point loading test bed

The deflections were measured using linear variable differential transformers (LVDTs). The LVDT converts a motion of an object to which it is coupled mechanically to a corresponding electrical signal. Deflections and strain measurements were measured simultaneously. The LVDT measures the deflection as voltage, which was converted to mm when recording the deflections. The LVDTs used had varying sensitivities of 65.25 and 1956.0 mV/mm.

Deflections were also monitored during the corrosion process. The beams were provided with dial gauges, two per beam. One gauge was placed at the beam end, where the load was applied and the second at the beam mid-span. The mid-span gauge was placed inside the corrosion pond but elevated to avoid corrosion damage on the dial gauge as shown in Figure 3.18. The deflections were measured per corrosion cycle to monitor deflections due to corrosion under load. The beam ends were measured with a dial gauge as shown in Figure 3.19.

The beams were corroded under constant sustained load and deflections were measured at positions shown in Figure 3.17. The load of 1 kN was applied at the ends of a simply supported beam 200 mm from the beam edges. The dial gauge measurements $\delta 1$ and $\delta 2$ represent the deflections at the mid-point and end-point respectively.

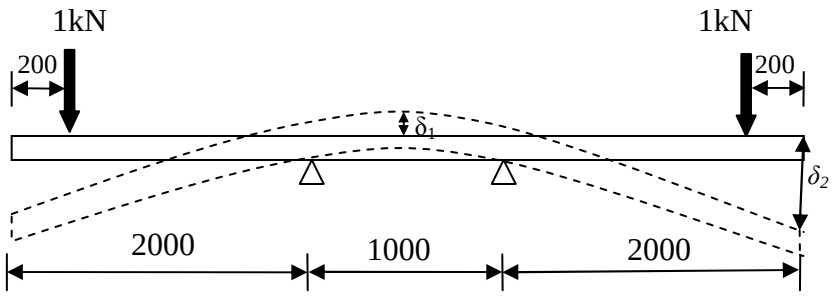

Figure 3.17: Location of deflection measurements during corrosion

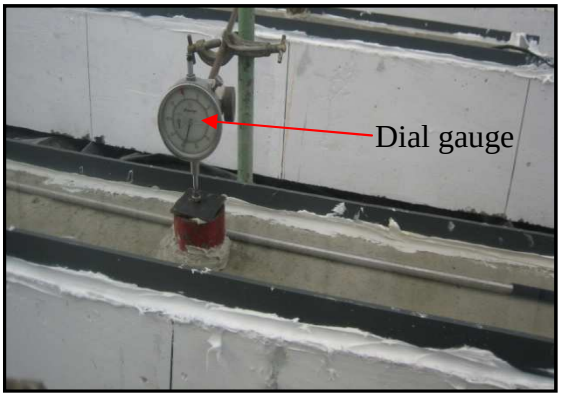

Figure 3.18: Dial gauge located inside the corrosion pond for mid-span deflection

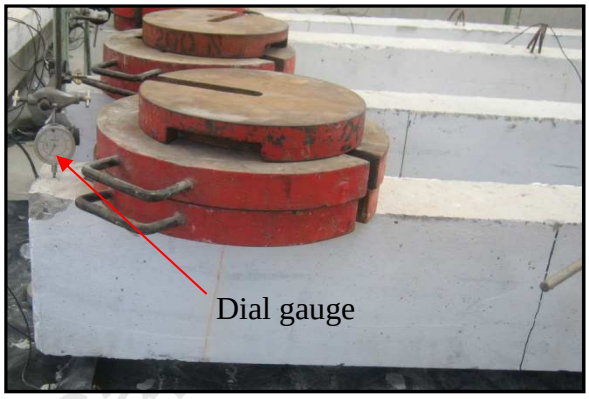

Figure 3.19: Dial gauge measuring the end-point deflection

3.3.2.2 Ultimate capacity

The ultimate capacity is associated with the load carrying capacity of the structure. Beyond the ultimate limit state, the structure cannot carry any more loads, and fails by the loss of stability, rupture of sections, loss of load carrying capacity due to excessive deformation. The beams were tested for ultimate load capacity under a four point loading configuration shown in Figure 3.20. Deflections and strains were monitored as the beams were loaded. Deflections were monitored at mid-span and 400 mm towards the supports on both sides. To measure strains, strain targets were mounted on the beam side 30 mm from the compression and tension surface as shown in Figure 3.20. Another set of targets was placed on the substrate beyond the patch repair to monitor debonding that might occur between the patch and the substrate during loading.

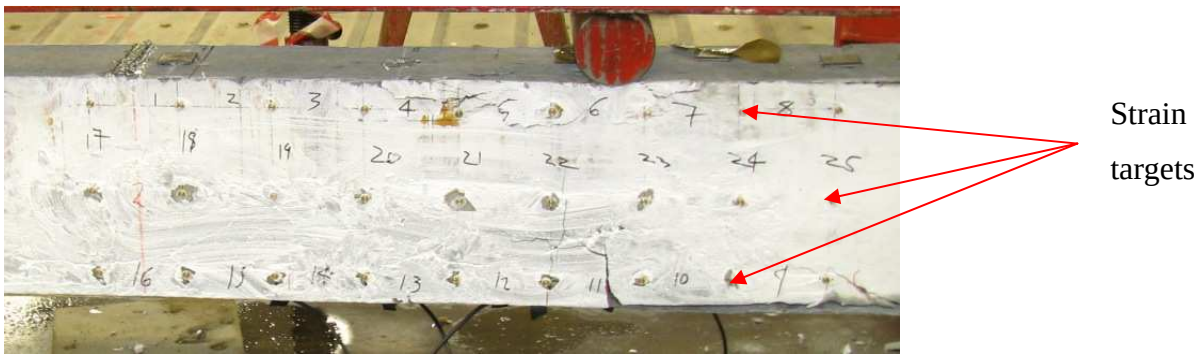

Figure 3.20: Strain targets on the beam

Another set of strains was measured using electronic strain gauges which were mounted on the FRP laminates and concrete on the tension side to detect debonding during loading. Three gauges were placed at mid-span of the beam, one on each laminate and one on the concrete between the FRP laminates. Two electronic gauges were placed on the FRP, one at the end of the patch repair and another one beyond the patch repair. Figure 3.22 shows the location of the strain targets and the strain gauges on the beam.

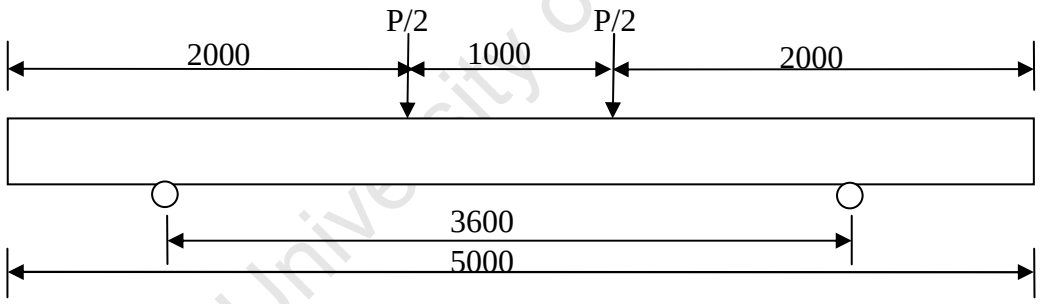

Figure 3.21: Loading configuration

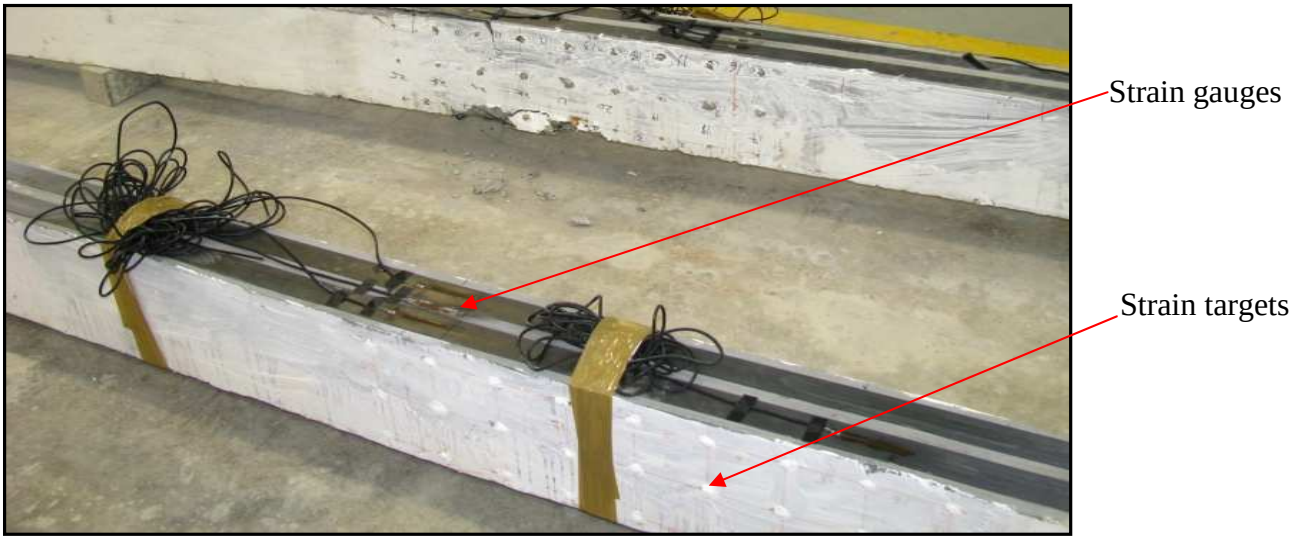

Figure 3.22: Strain gauges mounted on the FRP and strain targets placed on the side of the beam.

Subsequent to the experimental procedure, the results of all conducted tests are discussed. The results and discussions are divided into three Chapters; chapter 4 covers the results and discussions of the corrosion tests, Chapter 5 covers the results and discussions of the dynamic tests and Chapter 6 covers the results and discussions of the static tests conducted.

Chapter 4

BEAM CORROSION

4.1 Deflection under corrosion

The deflections measured during corrosion are shown in Table 4.1. Beam deflections were monitored throughout the duration of corrosion. Deflections were denoted positive (hogging) for mid-span deflections and negative (sagging) for end-point deflections as shown in Figure 3.17. The end-point deflections were measured on one side of the beam.

Table 4. 1: Deflection measurements in mm

Beam #	Deflection (cycle1)		Deflection (cycle 2)		Deflection (cycle 3)		Deflection (cycle 4)		Deflection (cycle 5)	
	δ_1	δ_2	δ_1	δ_2	δ_1	δ_2	δ_1	δ_2	δ_1	δ_2
1(Control)	0.1	-0.10	0.10	-0.10	0.12	-0.10	0.12	-0.10	0.125	-0.10
2(10% corrosion)	0.32	-2.40	0.41	-2.79	0.50	-3.01	0.59	-3.13	0.59	-3.13
3(10% corrosion)	0.54	-2.51	0.70	-3.81	0.91	-4.44	1.04	-4.87	1.04	-4.87
4(10% corrosion)	0.36	-2.13	0.56	-2.52	0.72	-3.00	0.85	-3.26	0.85	-3.28

The amplification of deflection with increase in corrosion period is presented in Figure 4.1a. Deflections presented in Figure 4.1a were up to an estimated 10 % steel mass loss due to corrosion. Beam 4 was corroded further to an estimated 15 % and the change in deflection is presented in Figure 4.1b. Mass loss of steel was estimated from Equation 2.1 in page 7.

The duration of corrosion is presented in cycles (4 days wetting and 2 days drying). Deflections were measured after each cycle. From the results presented, Beam 1 (control) had a constant deflection of 0.1 mm throughout the corrosion duration. Beams 2, 3 and 4 were corroded for duration of five cycles and had an average deflection of 0.83 mm with a standard deviation of 0.22 mm at mid-span and average deflection of 3.72 mm with standard deviation of 0.96 mm at beam end. The results showed increase in deflection as steel mass loss increases.

Loss of stiffness can be inferred from the increase in deflection. The results showed the beams lose stiffness due to corrosion. The loss of stiffness increases in a decreasing rate with time under

corrosion to the point where loss of stiffness does not change even though corrosion increases; this is observed from the constant deflection measurements after cycle 4 and cycle 5 for all beams. This can be further emphasized in Figure 4.1b where Beam 4 is corroded to an estimated 15% for duration of 8 cycles where deflections are constant after cycle 4. This shows that when the maximum loss of stiffness is attained, increase in corrosion duration (increase in steel mass loss), stiffness does not change.

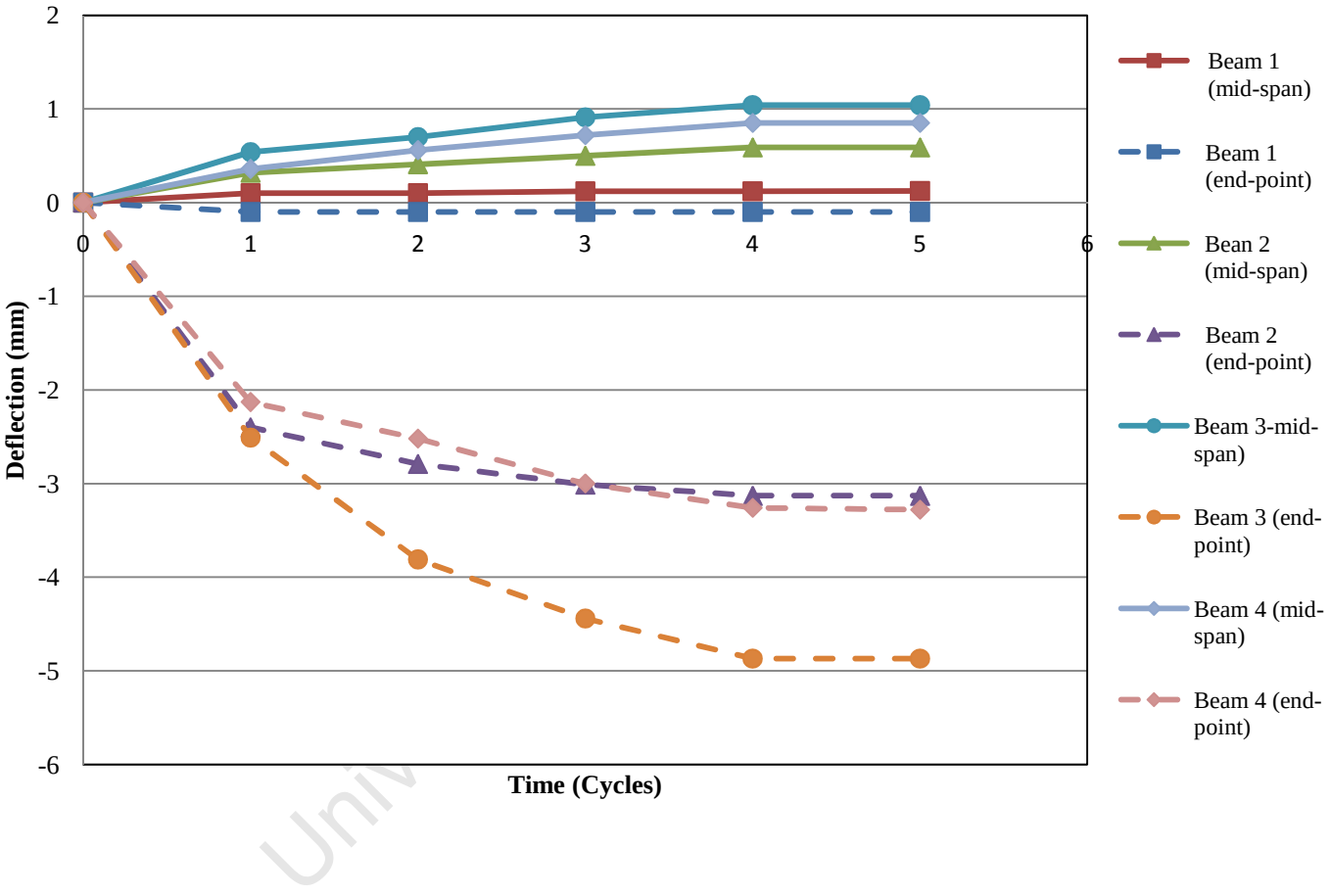

Figure 4.1a: Deflections during corrosion

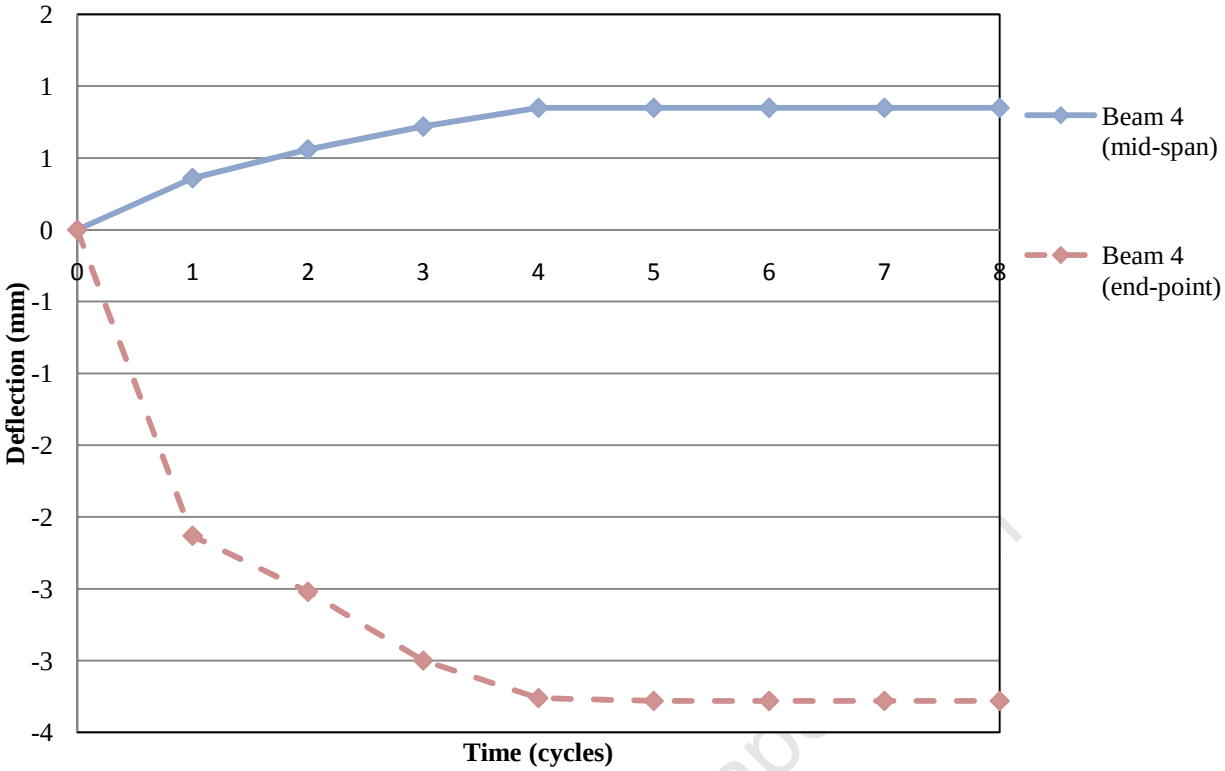

Figure 4.1b: Deflections of Beam 4 corroded up to 15% steel mass loss

4.2 Beam cracking

4.2.1 Crack widths

The crack widths were measured using a crack detection microscope. Beams 3 and 4 developed cracks on the extreme tensile face of the beam, where the corrosion pond was located as shown in Figures 4.2b and c, while beam 2 developed cracks on the side of the beam tensile zone as shown in Figure 4.2a. The cracks on all corroded beams extended beyond the corrosion pond by almost 70 mm. The crack width measurements were taken at 100 mm intervals along the length of the crack. The average crack widths measured on beams 2, 3 and 4 were 0.8 mm, 1.8 mm and 1.4 mm respectively; with the maximum cracks widths of 1.0 mm, 2.2 mm and 1.6 mm respectively for the estimated 10% corrosion. Beam 4 was further corroded to achieve an estimated 15% corrosion and the crack width increased to an average of 2.3 mm, with a maximum crack width of 2.7 mm.

4.2.2 Crack locations due to corrosion

The crack pattern due to expansion of corrosion products was monitored for each beam during corrosion. Three different types of crack patterns were observed (Figures 4.2a to c). Beam 2 had one surface crack on each side of the beam parallel to the corroded reinforcing bar. Beam 2 had corrosion products leaching out of the side cracks. Beam 3 had two surface cracks, both of them were located at the top surface directly above the reinforcing bars inside the corrosion pond, crack 1 extended along the length of the corrosion pond whilst crack 2 converged to crack 1 at the beam mid-spam, the corrosion products were leaching out of the cracks inside the pond. In Beam 4, two surface cracks were observed at the top surface directly above the reinforcing bars and both cracks extended along the length of the corrosion pond and the corrosion products were leaching out inside the pond. All the observed corrosion cracks were parallel to the steel reinforcement, yet all beams presented different crack locations. This shows that the crack locations are independent of the level of mass loss as all beams were corroded for the same duration. Beam 4 which was initially corroded to an estimated 10% mass loss maintained the same crack pattern when corroded further to an estimated 15% mass loss.

Figure 4.2a: Crack pattern for Beam 2.

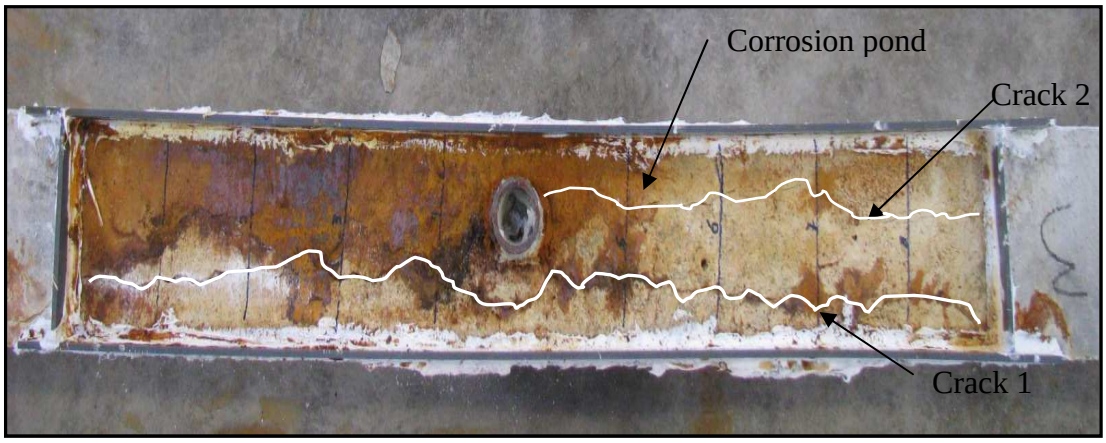

Figure 4.2b: Crack pattern for Beam 3.

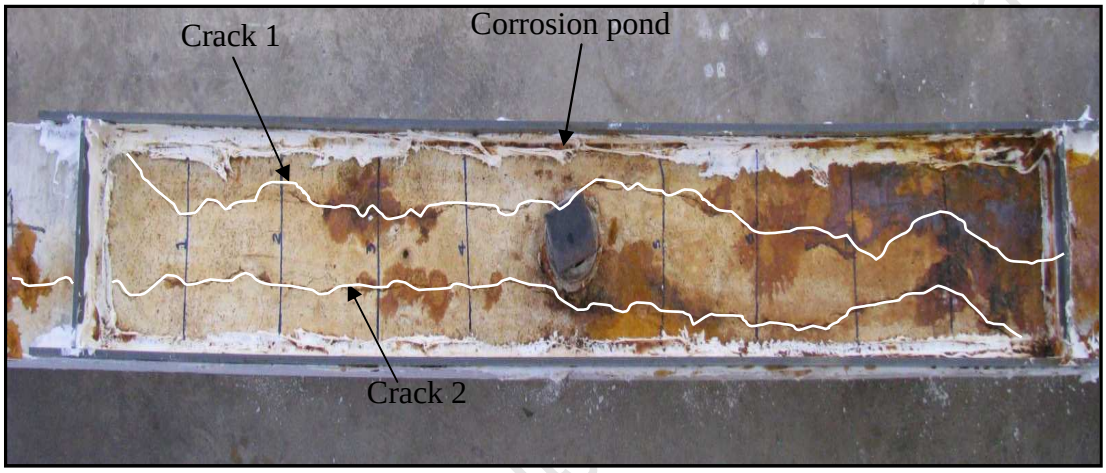

Figure 4.2c: Crack pattern for Beam 4.

4.3 Steel mass loss

Table 4.2 gives the measured results of steel mass loss based on the gravimetric mass loss. The corroded steel bars were cut to approximately 200 mm pieces and then weighed to find their mass; the mass loss was calculated using equation 4.1. Figure 4.3 shows the location of bars extracted to determine mass losses. Mass loss was measured 300 mm beyond the corroded region on both sides of the bar.

$$M_{loss} = \left(\frac{2.47L_i - m_i}{2.47L_i} \right) \times 100 \quad \text{---------- (4.1)}$$

Where M_{loss} is the percentage mass loss, L_i is the length of bar in meters, m_i is the mass of bar in kilograms and 2.47 is the nominal mass per length of 20 mm high tensile steel bar in kg/m.

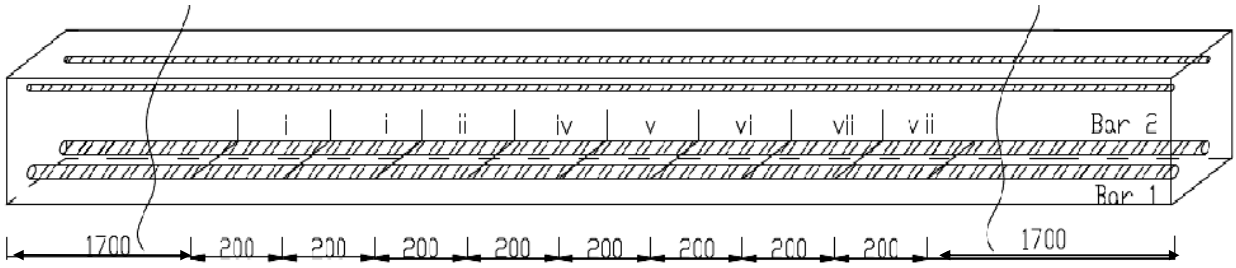

Figure 4.3: Location of bars extracted to determine steel mass losss

According to Table 4.2, the bars were corroded 300 mm beyond the corrosion region on both sites. The bars around mid-span (iv and v in Figure 4.3) showed a comparable mass loss to the estimated. Mass loss beyond the corrosion region (i and viii in Figure 4.3) showed the least mass loss as mass loss seemed to decrease when moving away from the centre of the corrosion region. Figure 4.4 shows the corroded bars extracted from the beam. The bars showed pitting corrosion mainly concentrated around the centre of the corrosion region. The bars are arranged in the same order as in Table 4.2. Bars iv and v are the bars at the centre of the corroded region.

Table 4. 2: Mass loss of steel for the extracted bars

Beam #	Mass loss per bar																
	Bar 1								Bar 2								Aver age
	I	ii	iii	iv	v	vi	vii	viii	i	ii	iii	iv	v	vi	vii	viii	
2	2.9	3.2	5.9	6.8	8.3	7.2	5.7	4.1	4.0	5.2	8.7	10.4	15.5	16.6	10.0	4.3	6.5
3	2.9	5.9	7.5	8.9	12.4	11.9	6.3	3.5	4.9	8.3	6.4	5.9	6.5	6.1	4.3	2.7	7.5
4	4.4	6.7	10.6	18.9	15.9	8.3	7.5	2.5	0.5	7.5	13.1	11.9	14.1	16.7	12.8	0.2	10.1

Figure 4.4: Corroded steel bars

The measured average mass losses of steel on both bars for the three corroded beams are shown in Figure 4.5. Beam 4 which was corroded to an estimated 15 % mass loss had a maximum mass loss of 18.9 %; while beams 2 and 3 with an estimated mass loss of 10 % had maximum mass losses of 16.6 % and 12.4 % respectively. The maximum mass loss on all the beams occurred around the centre of the corroded bar. The mass loss of steel was different on the two bars at the same length along the beam as observed from Table 4.2.

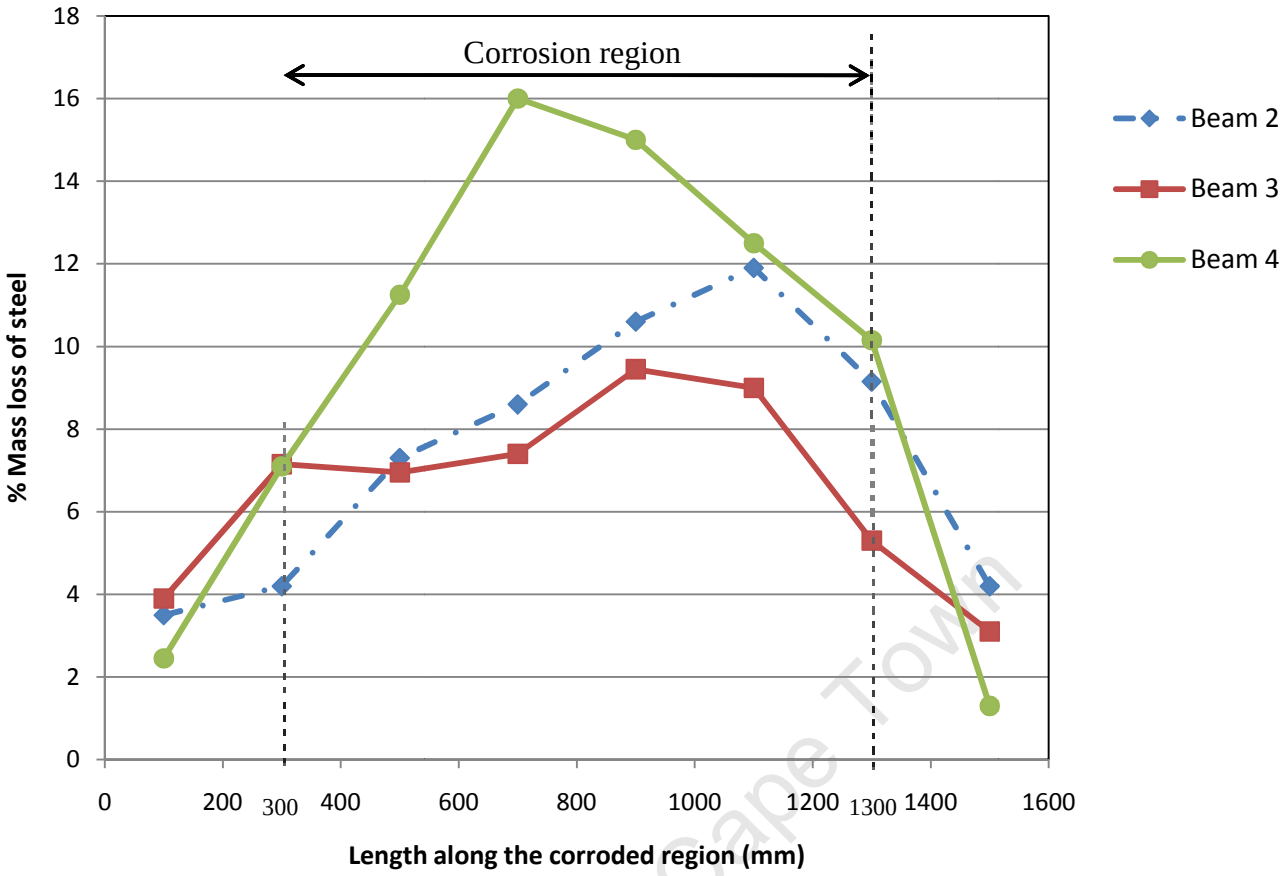

Figure 4.5: Mass loss of steel along the corroded region

Figure 4.5 showed the average mass loss of steel for both bars in each beam. Beam 4 with the maximum corrosion period showed the highest mass loss of steel as expected. Beams 2 and 3 which were corroded for the same period showed comparable mass losses of steel as they were expected to have approximately the same mass loss of steel.

The results of mass loss of steel corresponding to the crack widths are plotted in Figures 4.6a to c. The mass loss of steel and the crack widths are recorded against the bar length along the corroded region. Zero to 1000 mm represents the position of the corrosion pond.

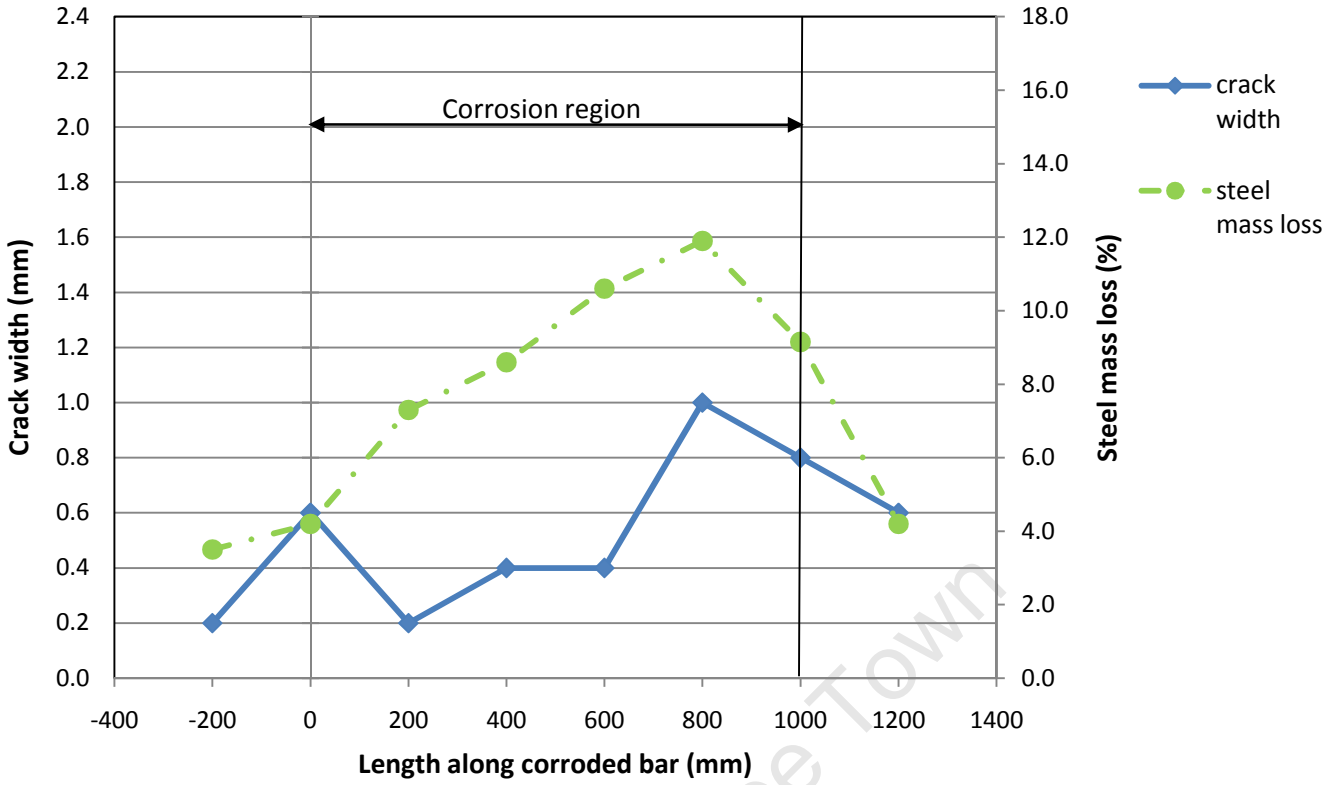

Figure 4.6a: Beam 2 crack widths corresponding to steel mass loss along beam length

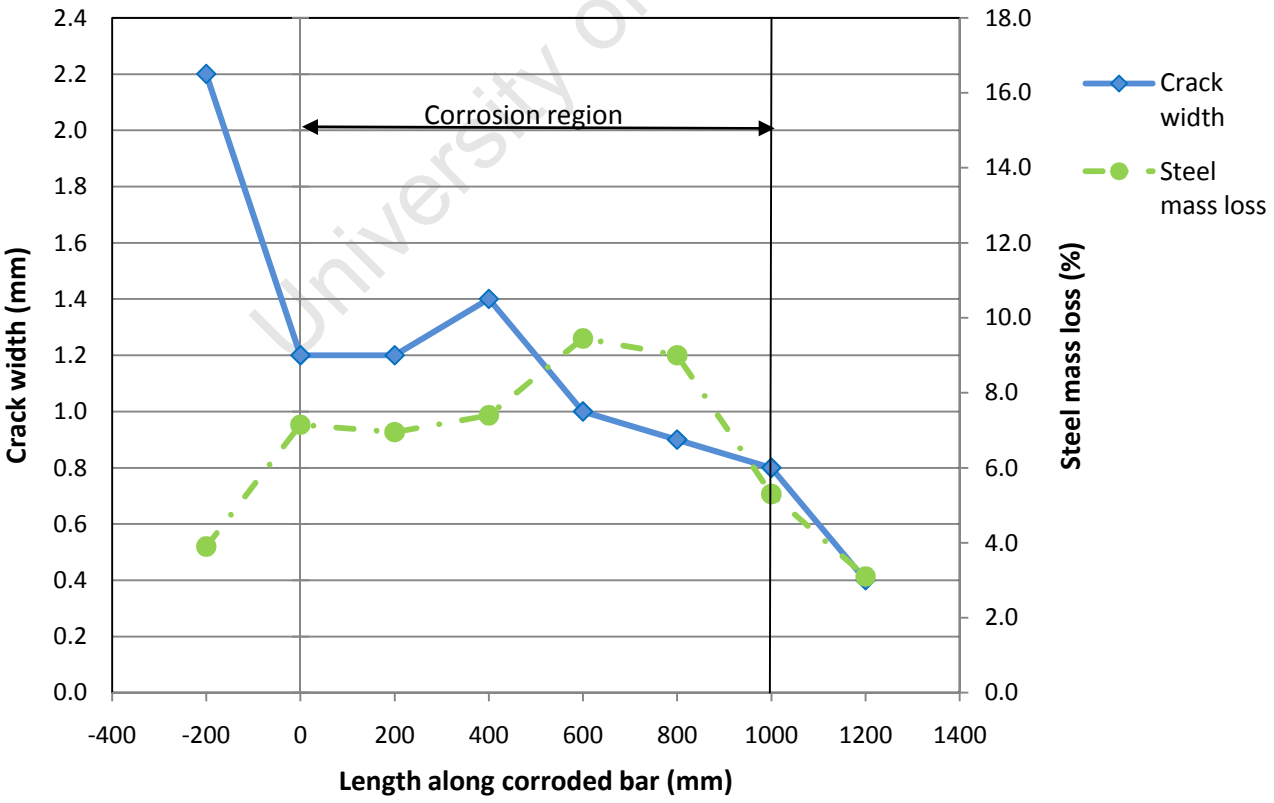

Figure 4.6b: Beam 3 crack widths corresponding to steel mass loss along beam length

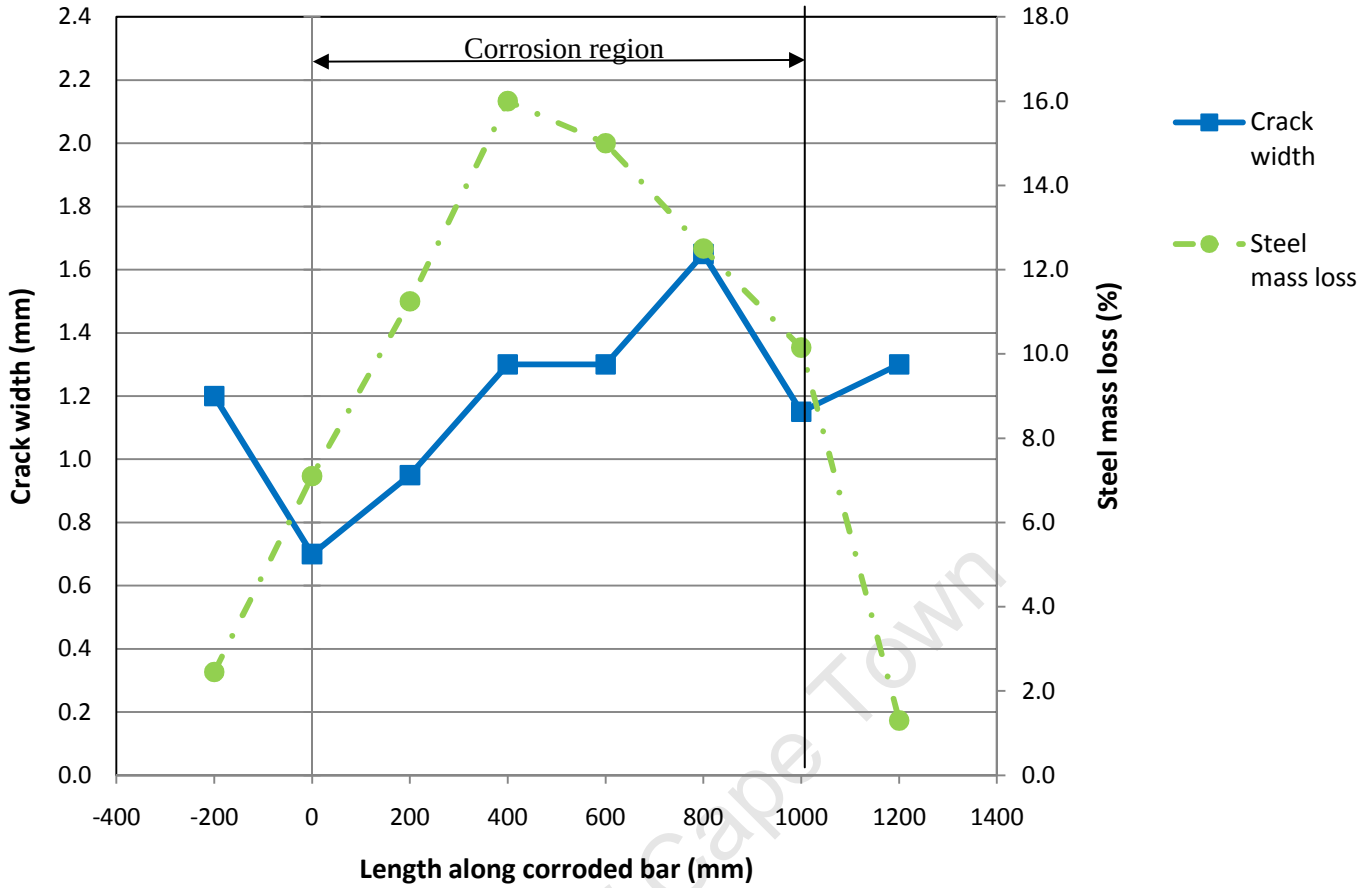

Figure 4.6c: Beam 4 crack widths corresponding to steel mass loss along beam length

The graphs show no apparent correlation between the mass loss of steel and the crack widths. There is a similar pattern observed with mass loss of steel for all beams, while the crack widths do not display any related pattern. There is no expected correlation between crack widths and steel mass loss as the crack widths can be expected to be even throughout the length of the crack, which is not the observation in this case. The crack widths do not increase with the increase in mass loss in a correlative way, but as the level of corrosion increases the crack widths also increase as shown in Figure 4.7, this has been observed from beam 4 as it was initially corroded to 10 % mass loss, and then later corroded to 15 % mass loss as indicated. The results indicate that maximum mass loss of steel does not particularly occur where the crack width is maximum.

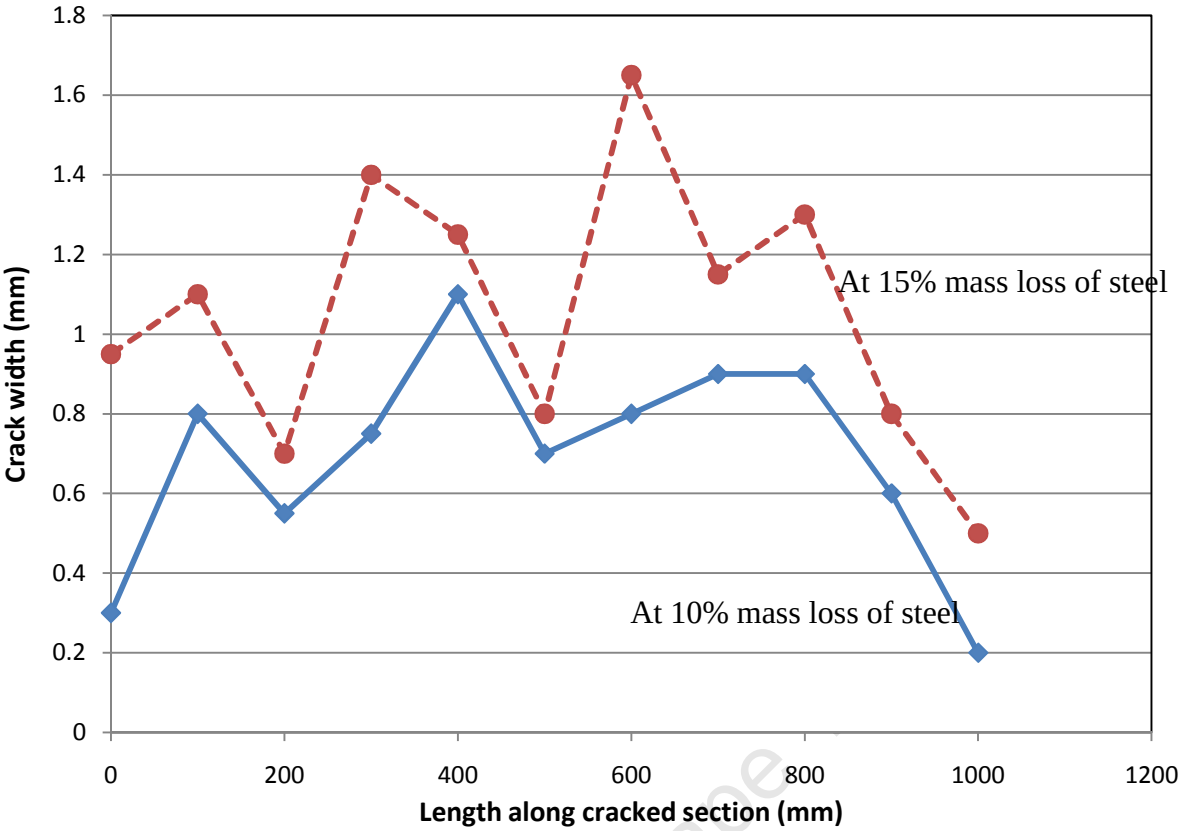

Figure 4.7: Beam 4 crack widths for different corrosion levels

Although crack widths on beam 4 increased with the increase in corrosion level as indicated in Figure 4.7, the mean crack width at 15% steel mass loss is 1.2 mm and 0.8 mm at 10 % steel mass loss, formulating Equation 4.1, where M_{loss} is the steel mass loss in % and W_{cr} is the crack width in mm. This equation can be used as an estimate for steel mass loss where corrosion cracks are visible. The graph shows no obvious pattern in the increase as it increases at different magnitudes at different points.

$$M_{loss} = 12.5W_{cr} \quad \text{---------- (4.2)}$$

Chapter 5

DYNAMIC TESTING RESULTS AND DISCUSSIONS

5.1 Modal analysis

In this research, the natural frequencies of vibration are of interest. This is the most common type of dynamic analysis. In addition to the frequencies, the mode shapes of vibration which arise at the natural frequencies are also of interest. These are the damped free vibration response of the structure caused by an initial disturbance from the static equilibrium position. During testing, not all modes were excited on different beam conditions (undamaged, corroded, exposed reinforcement, patch repaired and CFRP strengthened).

Data was collected by a dynamic program called LABVIEW Express and interpreted in another frequency program called ME ScopeVES. Acquired data was imported in a form of data blocks shown in Figure 5.1, which were later transformed to frequency-time domain shown in Figure 5.2. Frequency peaks (resonances) on the frequency-time graph were manifested into modes. Each resonance gives a certain frequency that corresponds to a particular mode shape and damping ratio.

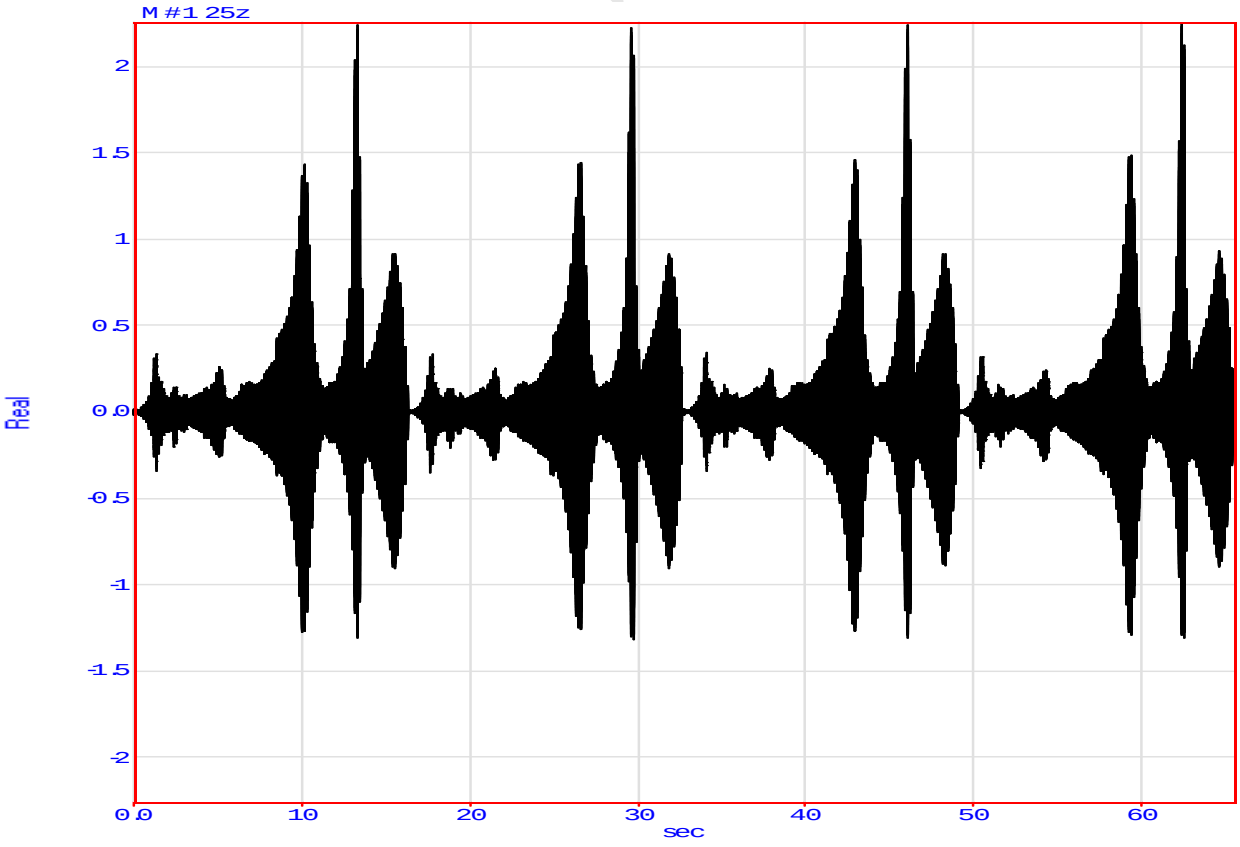

Figure 5. 1: Data block from MEScope

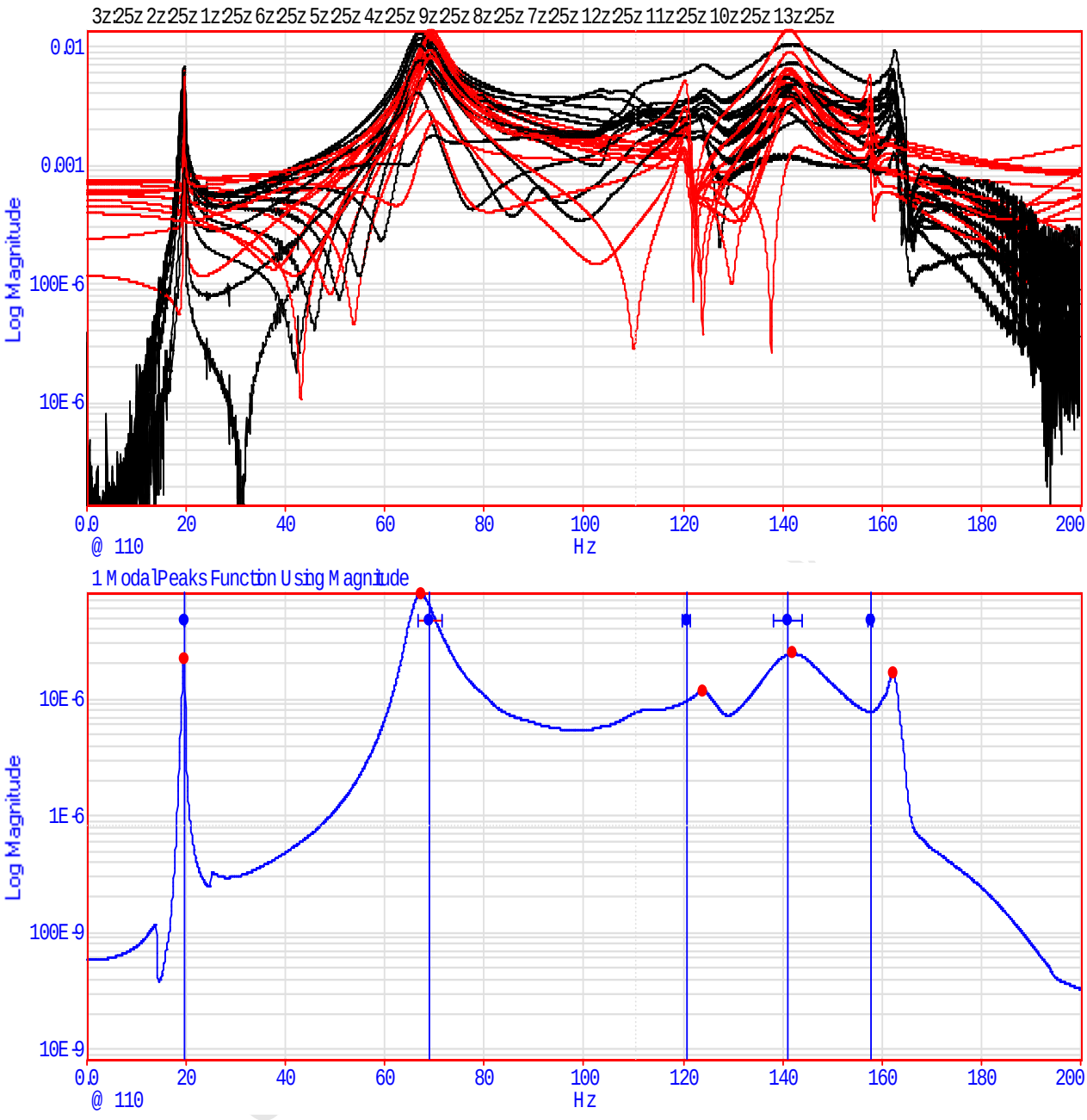

Figure 5.2: Data interpreted into frequency – time graph

The first and second bending mode shapes picked from the resonance frequency shown on the frequency-time graph are shown in Figure 5.3a and 5.3b as extracted from ME Scope. At each beam condition (undamaged, corroded, exposed reinforcement, patch repaired and CFRP strengthened) similar mode shapes were extracted.

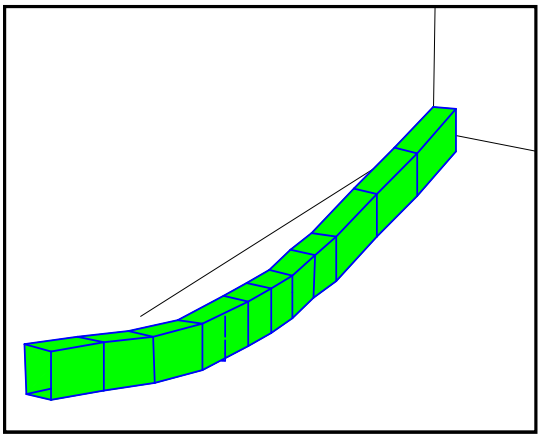

Figure 5.3a: First bending mode shape of the beam

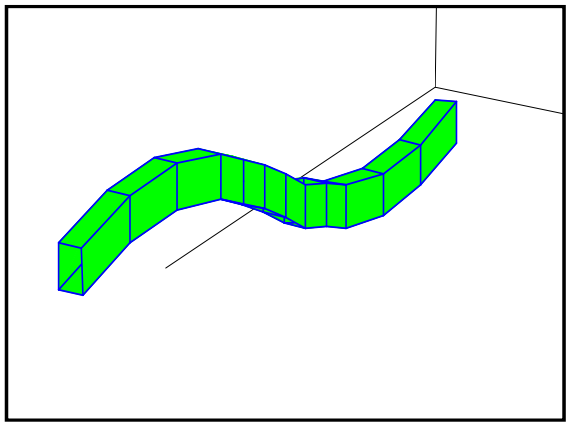

Figure 5.3b: Second bending mode shape of the beam

5.2 Natural frequency and mode shapes

The excited modes corresponding to the theoretical mode shapes are listed in Table 5.1a, b and c for beams 2, 3 and 4 respectively. Different frequencies were picked for their corresponding mode shapes in all beam conditions. From the natural frequencies obtained. The mode shapes of a beam in bending are a sine wave. The number of waves increases with the increasing mode number. Mode one (first mode shape) has a single wave, mode two is observed by two waves, mode three will have three waves.

Table 5.1 a: Mode shapes and their corresponding natural frequencies (Hz) for Beam 2

Theoretical mode shapes	Corresponding frequencies (Hz)				
	Undamaged state	10% Corroded	Corroded & cut open	Patch repaired	Patch repaired + FRP
Mode 1 	20.4	17.8	13.5	17.2	18.2
Mode 2 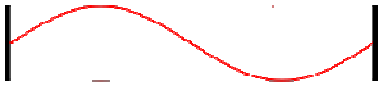	71.7	59.2	39.6	57.5	55.9
Mode 3 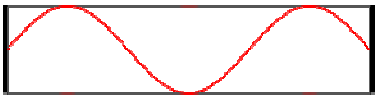	146	126	123	106	128

Table 5.1 b: Mode shapes and their corresponding natural frequencies (Hz) for Beam 3

Theoretical mode shapes	Corresponding frequencies (Hz)			
	Undamaged state	10% Corroded	Corroded & cut open	Patch repaired
Mode 1 	19.6	18.4	15.6	17.3
Mode 2 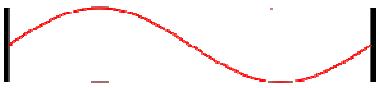	66.0	66.6	54.5	56.9
Mode 3 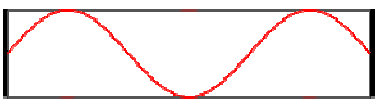	141.0	124	110	121

Table 5.1 c: Mode shapes and their corresponding natural frequencies (Hz) for Beam 4

Theoretical mode shapes	Corresponding frequencies (Hz)					
	Undamaged	10% Corroded	15% corroded	Corroded & cut open	Patch repaired	Patch repair + FRP
Mode 1 	19.5	18.2	18.0	14.9	17.8	18.8
Mode 2 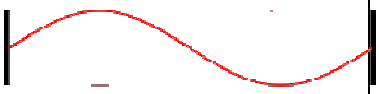	69.5	62.7	51.1	48.6	52.6	63.8
Mode 3 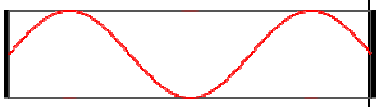	141	135	123	109.9	130	140

The damping ratios corresponding to the natural frequencies are shown in Tables 5.2a to d. At every resonance frequency, there is a mode shape and the damping ratio corresponding to it.

Table 5.2 a: Beam 1 natural frequencies with their corresponding damping ratios

Mode shape	Freq (Hz)	Damping (%)
1	19	1.5
2	64.5	2.21
3	134	4.71

Table 5.2 b: Beam 2 natural frequencies with their corresponding damping ratios

Mode shapes	Undamaged		10% corroded		Cut (Exposed bars)		Patch repaired		FRP strengthened	
	Freq (Hz)	Damping (%)	Freq (Hz)	Damping (%)	Freq (Hz)	Damping (%)	Freq (Hz)	Damping (%)	Freq (Hz)	Damping (%)
1	20.4	1.2	17.8	0.55	13.5	0.5	17.3	1.5	18.2	0.5
2	71.7	3.1	59.2	1.14	39.7	1.2	57.5	1.36	55.9	1.55
3	146	1.22	126	1.5	123	0.06	106	0.05	128	0.44

Table 5.2 c: Beam 3 natural frequencies with their corresponding damping ratios

Mode shapes	Undamaged		10% corroded		Cut (Exposed bars)		Patch repaired	
	Freq (Hz)	Damping (%)	Freq (Hz)	Damping (%)	Freq (Hz)	Damping (%)	Freq (Hz)	Damping (%)
1	19.6	0.23	18.4	0.15	15.6	0.23	17.3	0.4
2	66.0	0.79	66.6	1.7	54.5	0.11	56.9	4.89
3	141	3.25	124	0.05	110	1.35	121	1.77

Table 5.2 d: Beam 4 natural frequencies with their corresponding damping ratios

Mode shapes	Undamaged		10% corroded		15 % corroded		Cut (Exposed bars)		Patch repaired		FRP strengthened	
	Freq (Hz)	Damping (%)	Freq (Hz)	Damping (%)	Freq (Hz)	Freq (Hz)	Damping (%)	Damping (%)	Freq (Hz)	Damping (%)	Freq (Hz)	Damping (%)
1	19.5	0.15	18.2	0.013	18.0	1.5	14.9	1.5	17.8	0.5	18.8	o.46
2	69.5	3.71	62.7	3.25	51.1	1.88	48.6	2.14	52.6	3.95	63.8	2.66
3	141	3.46	135	2.97	123	1.05	109	1.52	130	0.51	140	1.02

There is no correlative pattern that existed between the damping ratios of the same mode shape and the damping ratios of the same beam condition but different modes. This proves that the damping ratios cannot be used as assessment factors on the effect of the change in beam conditions to the structure; therefore the natural frequencies and mode shapes were considered for damage assessment.

Damage was quantified as the percentage change in natural frequency of the damaged beam to the reference beam by Equation 5.1. The damage index for beams 2 to 4 are shown in Table 5.3a to c.

$$i_{damage} = \frac{\omega_o - \omega_d}{\omega_o} \text{ ---------- (5.1)}$$

Table 5.3 a: Damage Index for Beam 2

State	Mode 1	Damage Indicator
Undamaged (ω_o)	20.4	-
10% Corroded (ω_d)	17.8	12.7
10% corr + cut (ω_d)	12.1	40.7
Patch Repaired(ω_r)	17.3	15.2
Patch + FRP (ω_{rs})	18.2	10.8

Table 5.3 b: Damage Index for Beam 3

State	Mode 1	Damage Indicator
Undamaged (ω_o)	19.6	-
10% Corroded (ω_d)	18.4	6.2
10% corr + cut (ω_d)	15.6	20.4
Patch Repaired(ω_r)	17.3	11.7

Table 5.3 c: Damage Index for Beam 4

State	Mode 1	Damage Indicator
Undamaged (ω_o)	19.5	-
10% Corroded (ω_d)	18.2	6.7
15% Corroded (ω_d)	18.0	7.7
15% corr + cut (ω_d)	14.9	23.6
Patch Repaired(ω_r)	17.8	8.7
Patch + FRP (ω_{rs})	18.8	3.6

5.3 Mode shape MSF and MAC values

Different mode shapes are scaled off by using the Modal Scale Factor (MSF) in order for them to be compared. All mode shapes from different damage state are scaled with reference to the mode shape of the undamaged state using Equation 5.2, where Φ1 and Φ2 are ordinates for the first and second mode shapes. The MSF of the first and

second mode shapes of beam 2 are presented in Tables 5.4a and b and the mode shapes are presented in Figures 5.4a and b. All modes are scaled off for comparison.

$$MSF_{2\to1} = \frac{\Phi_2^{'}\Phi_1}{\Phi_2^{'}\Phi_2} = \frac{\Phi_2.\Phi_1}{\Phi_2.\Phi_2} \text{ ---------- 5.2}$$

Table 5.4 a: MSF values for the first mode of Beam 2

	10% corroded	Exposed reinforcement	Patch repaired	Patch repaired and CFRP strengthened
MSF	1.58	6.86	10.54	7.33

Table 5.4 b: MSF values for the third mode of Beam 2

	10% corroded	Exposed reinforcement	Patch repaired	Patch repaired and CFRP strengthened
MSF	37.01	144.79	4.89	7.96

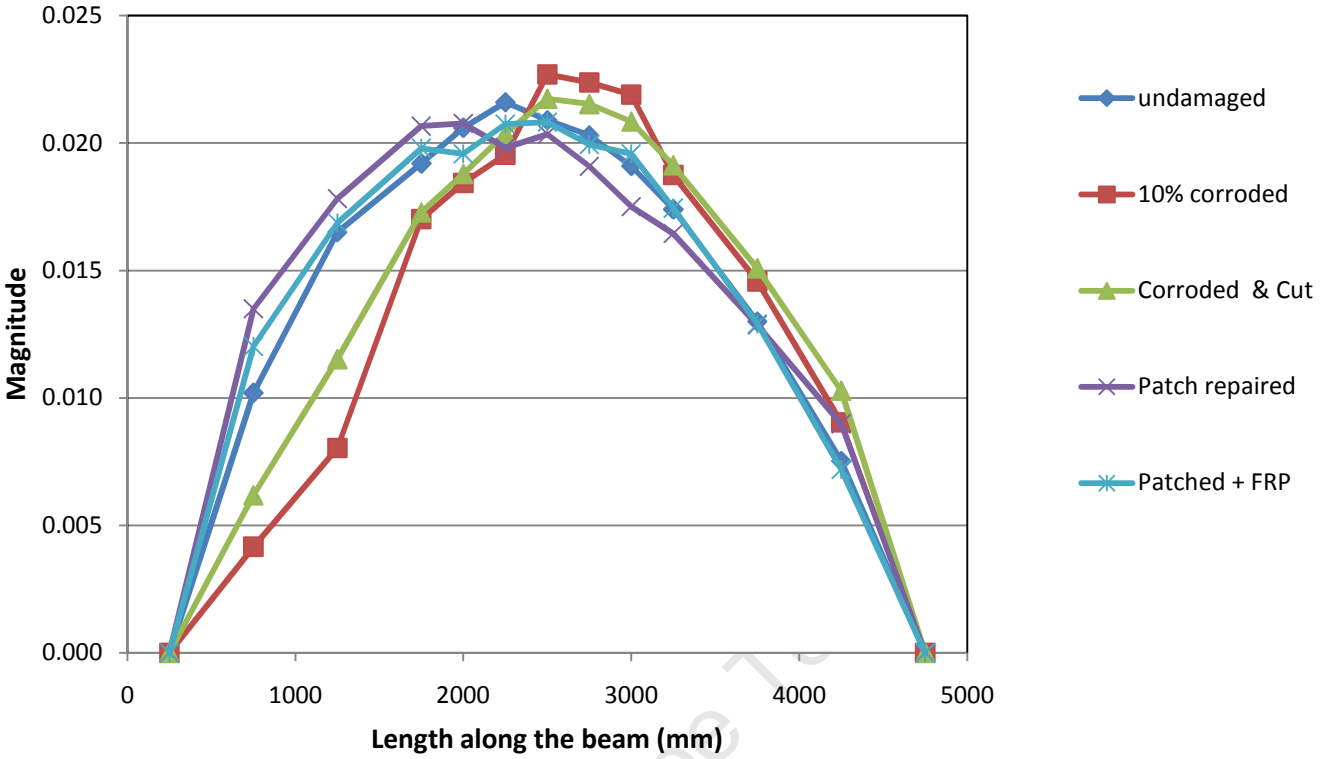

Figure 5.4a: Scaled first mode shape

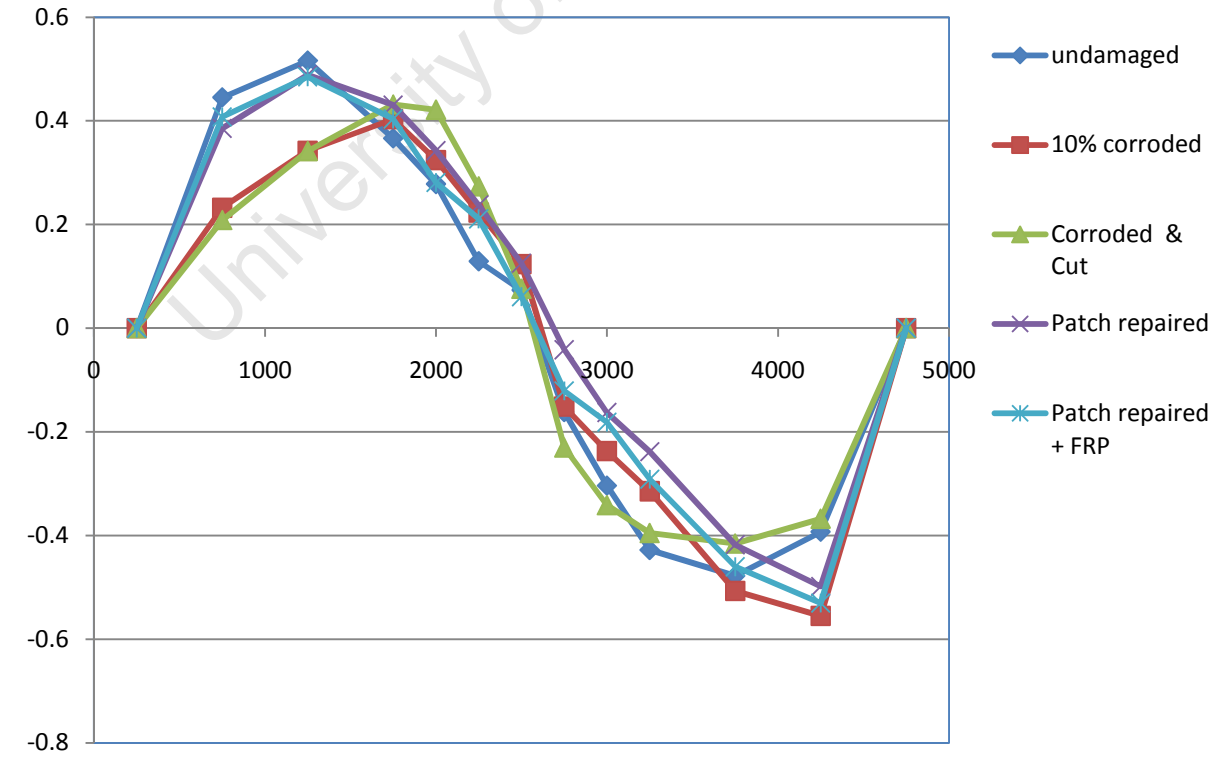

Figure 5.4b: Scaled second mode shape

In order to assess the similarity or difference in the mode shapes of different damage states, a Modal Assurance Criterion (MAC) which is a correlation coefficient of how similar the modes are regardless of size was applied and it was calculated using Equation 5.3. A change in MAC values across the different structure conditions showed damage in the structure. MAC values above 0.95 shows good correlation between the modes, while values less than 0.95 shows the difference. Tables 5.5a to c showed the change in MAC values of beams 2 to 4 respectively across different beam conditions in comparison with the undamaged state.

$$MAC_{2,1} = \frac{\left(\Phi_2^{'}\Phi_1\right)^2}{\left(\Phi_1^{'}\Phi_1\right)\left(\Phi_2^{'}\Phi_2\right)} \quad \text{---------- 5.3}$$

Table 5.5 a: MAC values for Beam 2

State	MAC values
10% Corroded	0.96
10% Corroded + cut	0.98
Patch Repaired	0.99
Patch + FRP	1.00

Table 5.5 b: MAC values for Beam 3

State	MAC values
10% Corroded	0.96
10% Corroded + cut	0.98
Patch Repaired	0.99
Patch + FRP	1.00

Table 5.5 c: MAC value for Beam 4

State	MAC values
10% Corroded	0.99
15% Corroded	0.98
15% Corroded + cut	0.97
Patch Repaired	0.99
Patch + FRP	1.00

The observed MAC values show an improvement on the mode shapes of the damaged beams due to repair and strengthening. The average MAC value of the corroded beams relative to the undamaged state is 0.98, when the beam is cut open, it drops

further to 0.97, after repair the MAC value improves and it is at 0.99 and finally after strengthening the MAC value became 1.0, showing perfect match between the undamaged beam and FRP strengthened beam. Although there s a clear trend on the MAC values, they show a negligible change on the damaged beams. The MAC values above 0.95 are considered too close, so if the decision to repair the beam relied only on the MAC vales, then there will not be a need to repair the beams as the mode shapes show close relation, meaning that the damage due to corrosion and cutting of the beams is insignificant.

Table 5.6: Natural frequency (%) damage indicator

State	Beam 1	Beam 2	Beam 3	Beam 4
Undamaged	4	0	0	0
10% Corroded	-	13	6	7
10% Corr + cut	-	41	20	-
15% Corroded	-	-	-	9
15% Corr + cut	-	-	-	24
Patch Repaired	-	9	4	9
Patch + FRP	-	5		3

Table 5.7 a: Damage indicators for higher order modes for Beam 1

State	Mode 1	Mode 2	Mode 3
Undamaged (After loading)	4	12	28

Table 5.7 b: Damage indicators for higher modes for Beam 2

State	Mode 1	Mode 2	Mode 3
10% Corroded	13	17	39
10% corr + cut	41	45	56
Patch Repaired	9	73	63
Patch + FRP	5	22	43

Table 5.7 c: Damage indicators for higher order mode for Beam 3

State	Mode 1	Mode 2	Mode 3
10% Corroded	6	-1	12
10% corr + cut	20	18	53
Patch Repaired	4	14	41

Table 5.7 d: Damage indicators for higher order modes for Beam 4

State	Mode 1	Mode 2	Mode 3
10% Corroded	7	10	-10
15% Corroded	9	26	34
15% Corr + cut	24	33	39
Patch Repaired	9	24	37
Patch + FRP	5	17	26

The general consensus in the literature (Baghiee et al, 2008, Dimarogonas, 1996 and Maeck et al, 2000) is that the natural frequencies for the undamaged beam should be higher than those of damaged beams as the frequencies decrease with the increase in damage, which in this study refers to the increase in the level of corrosion and exposed reinforcement beam. Similarly, the results from this study indicate a matching phenomenon.

From the results, the fundamental (first) mode shape was used to analyse the consequence of the changes induced by the changing beam conditions. The percentage change in the natural frequency was used as a damage indicator. As observed from all the tested beams, there was an average decrease of 8 % in the natural frequency of the beam when it was corroded to 10 % mass loss. Then it increased to 9 % when the level of corrosion increased to 15 %. Table 5.6 gives a summary of the damage indicators for different beam conditions. Tables 5.7a – d show the corresponding damage indicators for the subsequent higher order modes.

Damage reduces local stiffness and increases flexibility of a structural element. Therefore, the peak CFRF amplitudes for undamaged beam are expected to be lower

than those from corroded and cracked beams ones. The patch repaired beams and CFRP strengthened beams have the lower peaks than the damaged beams. From the damping ratios obtained, there is no clear correlation between damage states and damping ratio, therefore the damping ratios are considered ineffective as a dynamic parameter for identifying changes in the structure.

5.4 Effect of corrosion, repair and strengthening on natural frequency

5.4.1 Corroded beam

The corrosion damaged beams were all tested in their exposed reinforcement state (cut before repair). This state revealed a drastic drop in the natural frequency. It is clear that removing the damaged section before repair reduces the stiffness by up to 40%. Although the beam was cut beyond the depth of the cracks as it is difficult to determine the depth of the cracks when a beam is corroded. It is sensible to suppose the cracks opens from the corroded reinforcement bar.

5.4.2 Patch repair

Based on the results obtained from the natural frequency, it is hard to identify the improvement brought about by the application of the patch repair from the corroded condition as the natural frequency of the patch repaired beam is lower than that of a corroded beam before repair preparation. The only noticeable improvement is from the exposed reinforcement state. This could be explained by the change observed from beam 1, which was used as a control beam; where there was a drop in the natural frequency due to transverse cracks developed on the tensile face of the beam resulting from lifting and moving of the beams due to the long span of the beams.

The other reason for the drop in the natural frequency of beam 1 and the other beams could be that cracks were induced when loading the beam below their cracking moment. All beams were loaded after the initial natural frequencies were measured. Reason being to measure their local strains with the strain gauges mounted on the

reinforcement. The corroded beams developed some transverse cracks on the tensile face as they were being cut with a jack hammer for repair preparation.

5.4.3 CFRP strengthening

The CFRP laminates are not expected to increase the stiffness of the member due to their small cross-section area, but because of their high elastic modulus; using modular ratio, could have a trivial contribution. The dynamic results reflect a contradictory effect on the members as the stiffness improves due to application of CFRP laminates. This could be the result of the epoxy used to bond the CFRP laminates to the beam. The epoxy may have possibly filled the micro-cracks that resulted from loading the beams or lifting and carrying the beam around. The epoxy has a much higher tensile strength than the concrete substrate and the patch repair used.

Chapter 6

STATIC TESTING RESULTS AND DISCUSSIONS

This chapter presents the results and discussions on the static tests conducted; namely deflections, strain measurements and ultimate capacity testing.

6.1 Deflection measurements

The deflections on each beam were monitored with increasing load. Deflections were measured 30 mm away from left and right supports and at the mid-span of the beam. t

Stiffness

The stiffness of the beams is inferred from deflection measurements measured during the Ultimate Limit State (ULS). For comparison, deflections presented in Figure 6.1 are up to 60 kN loading as beams failed at different loadings. Beam 1 (control) had the least static stiffness of 2.5 kN/mm as it displayed the highest deflections, followed by a Beam 3 (patch repaired) with stiffness of 2.7kN/mm, Beams 2 and 4 with FRP strengthening presented the largest stiffness of 3.2 and 3.6 kN/mm respectively.

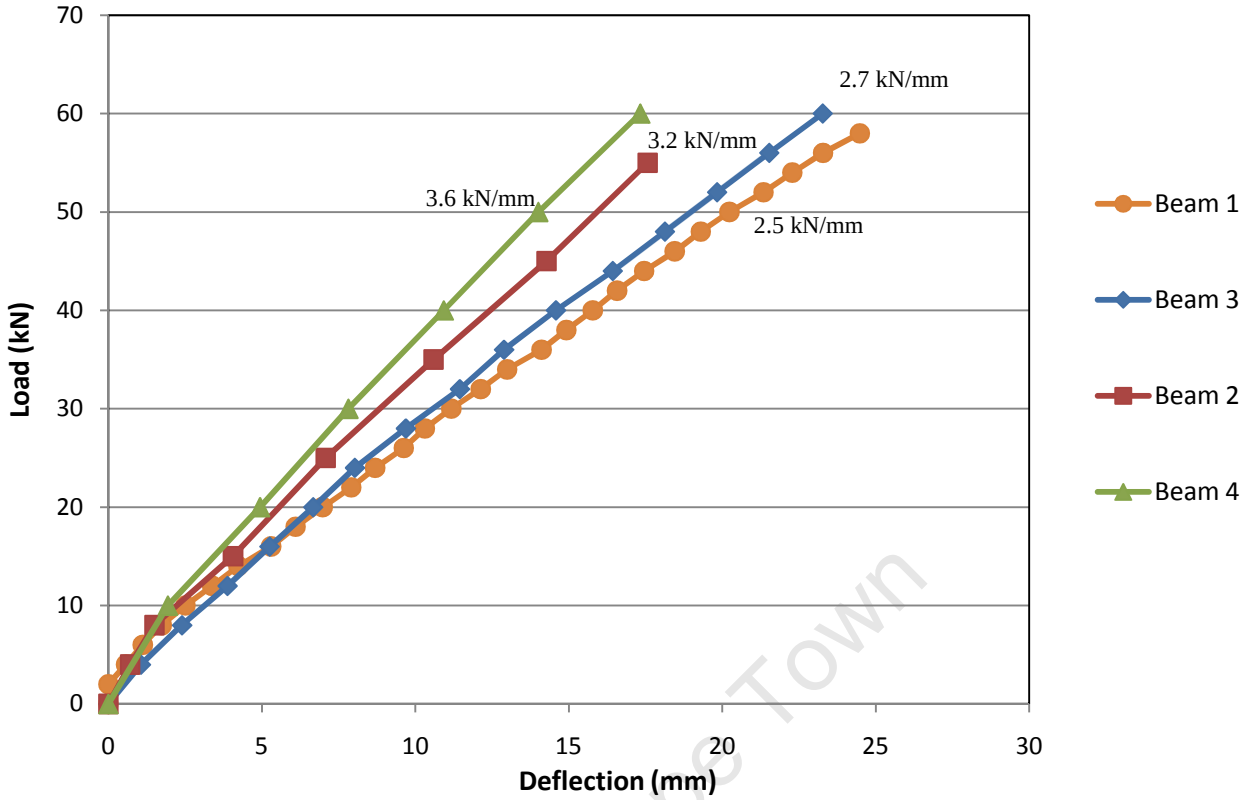

Figure 6.1: Deflection measurements of all beams

From the results presented, it can be observed that the application of both patch repair and CFRP strengthening improves the stiffness of the RC members by up to 50%. Patch repair on its own slightly improves the stiffness by less than 10 %. These results confirm the work done by Soudki et al (2003), where the CFRP strengthened beams exhibited increased stiffness over the unstrengthened specimen.

6.2 Strain measurements

The strains were measured on the compression and tension side, 30 mm away from the extreme compression face and extreme tensile face. Another set of strain targets (vertical) were placed 100 mm below the targets on the compression face to monitor debonding that might occur between the patch repair and the substrate; compressive, tensile and vertical strains were measured as shown on Figure 6.2. The average results of the compression, tensile and vertical strains are presented in Figures 6.3a to 6.3d.

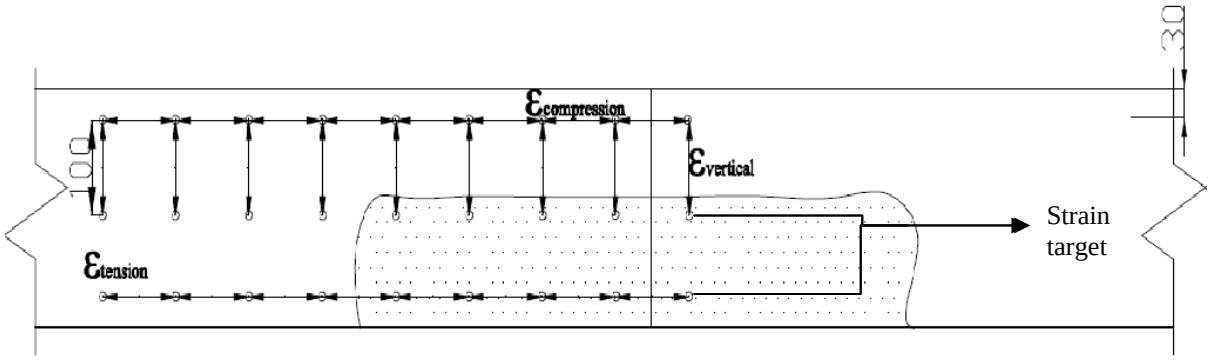

Figure 6.2: Location of strain targets for monitoring strain measurements during loading

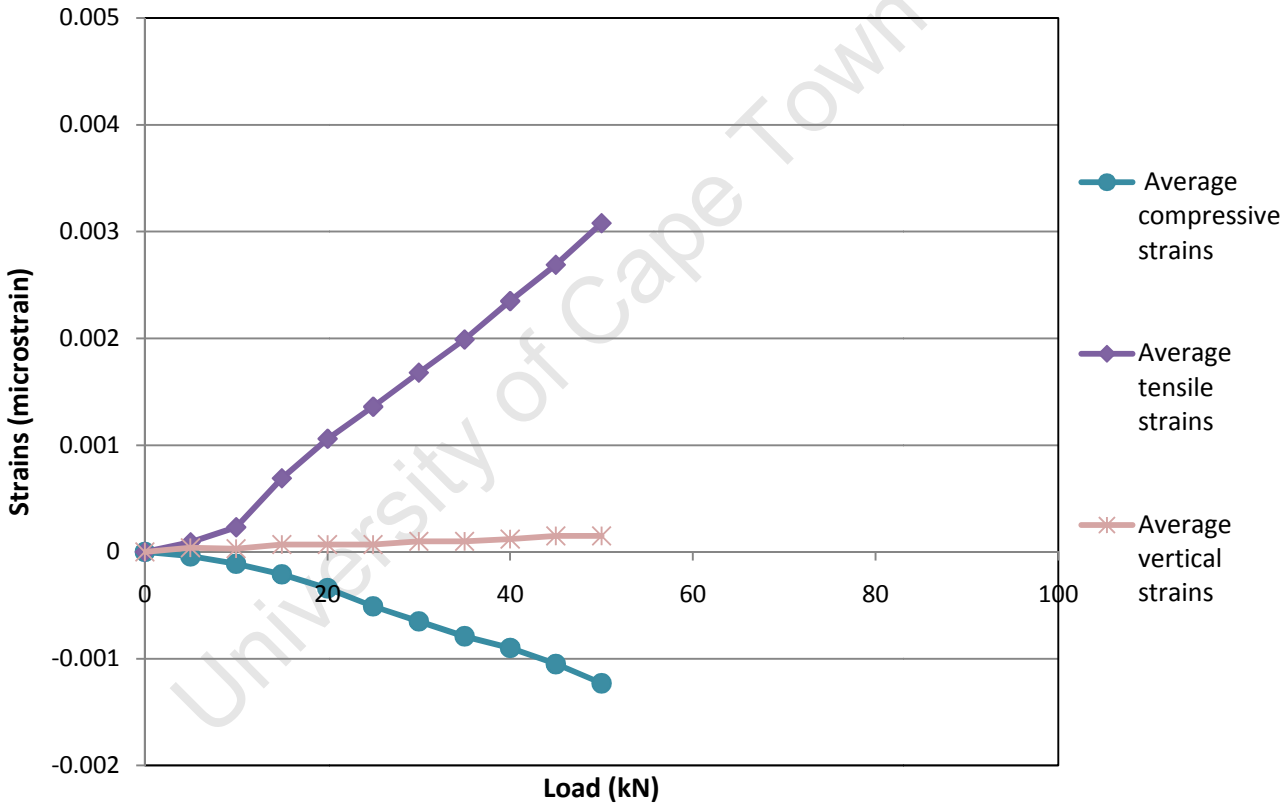

Figure 6.3 a: Strain measurements for Beam 1

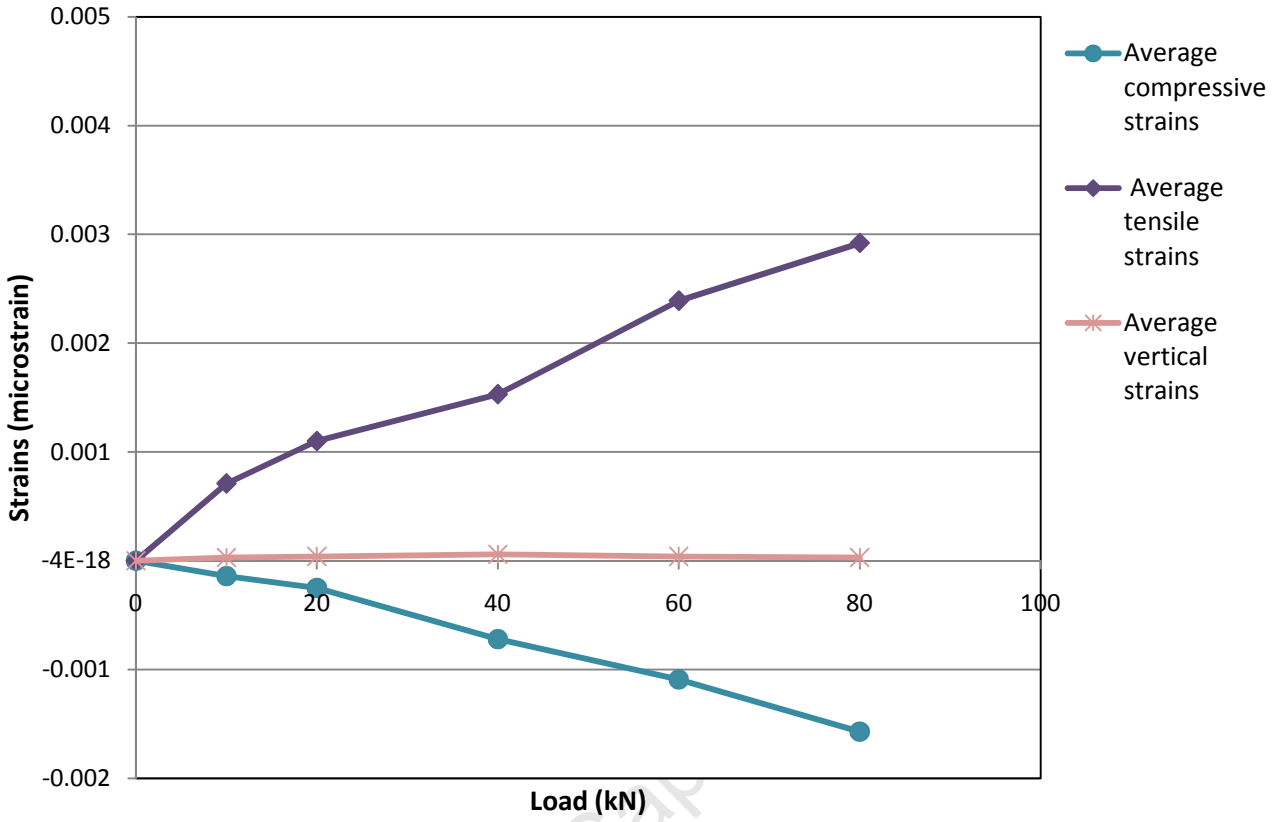

Figure 6.3 b: Strain measurements for Beam 2

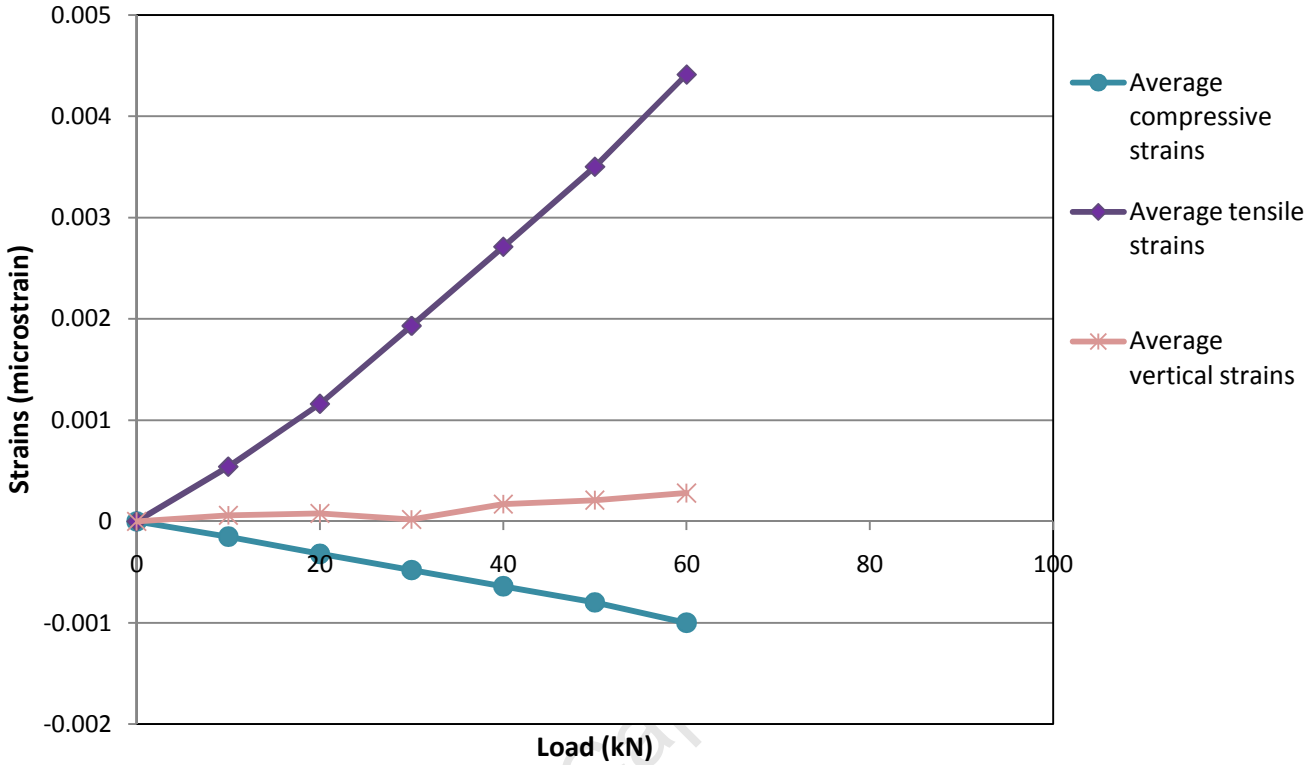

Figure 6.3 c: Strain measurements for Beam 3

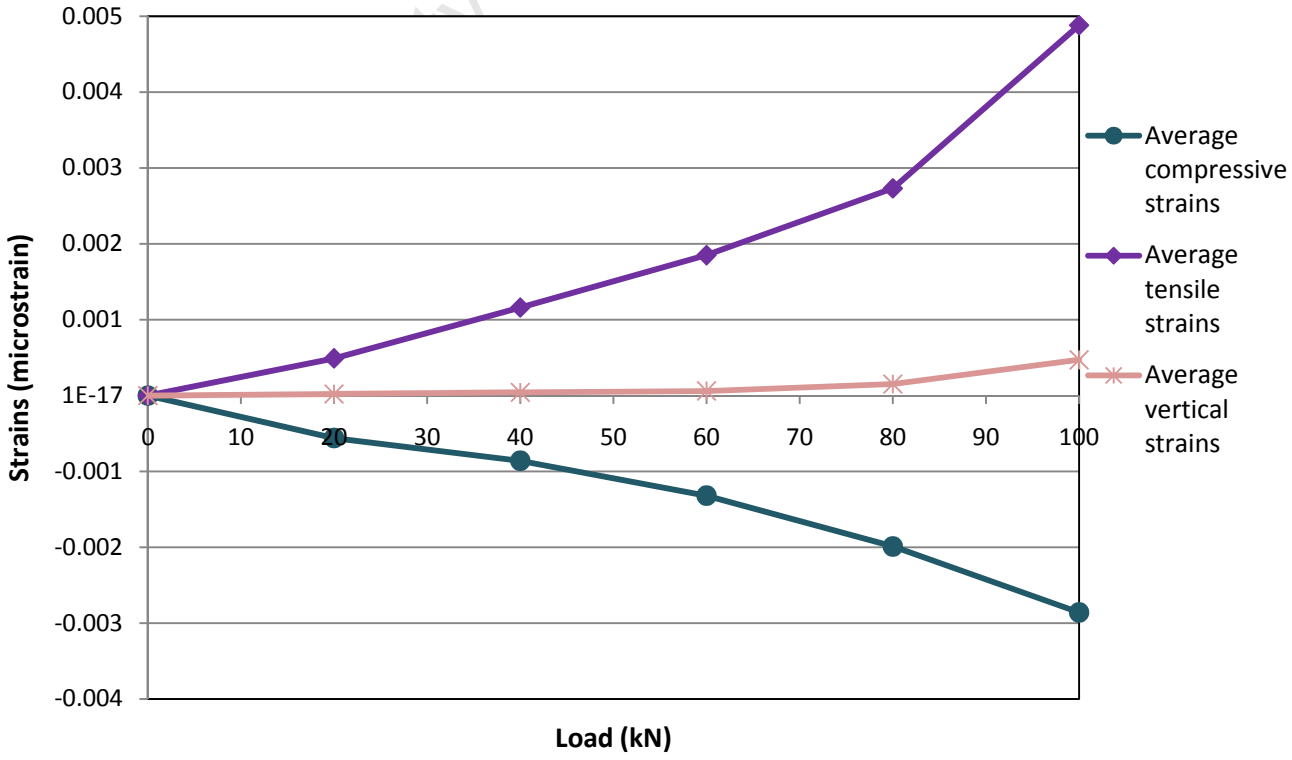

Figure 6.3 d: Strain measurements for Beam 4

Strains were measure to different loads depending on the capacity of the individual beams. At one common load (50kN), Beam 1 (control) and Beam 3 (patch repaired) had the highest tensile strains of 0.0031 and 0.0035 microstrains, while Beams 2 and 4 (patch repaired and CFRP strengthened) had the least tensile strains of 0.0019 and 0.0015. The results showed that the CFRP strengthened beams have the highest stiffness in comparison to beams which are not strengthened.

The vertical strains show that there was no debonding between the patch repair and substrate as the vertical strains for the repaired beams are comparable to the vertical strains on the control beam, therefore the member behaves as a composite.

Neutral axis

The depth of the neutral axis (NA) shifts towards the compression face as the load increased as shown in Figure 6.4. The results of beams 2, 3 and 4 reflect the shift in the NA, while the results of the control beam showed no change in NA location. This may be due to the small changes in the compressive strains that results in error when reading the strains. The depth of the NA was higher on the CFRP-strengthened beams than on the patch repaired beam, showing that stiffness is more compromised on the patch repaired beams than on the CFRP-strengthened beams.

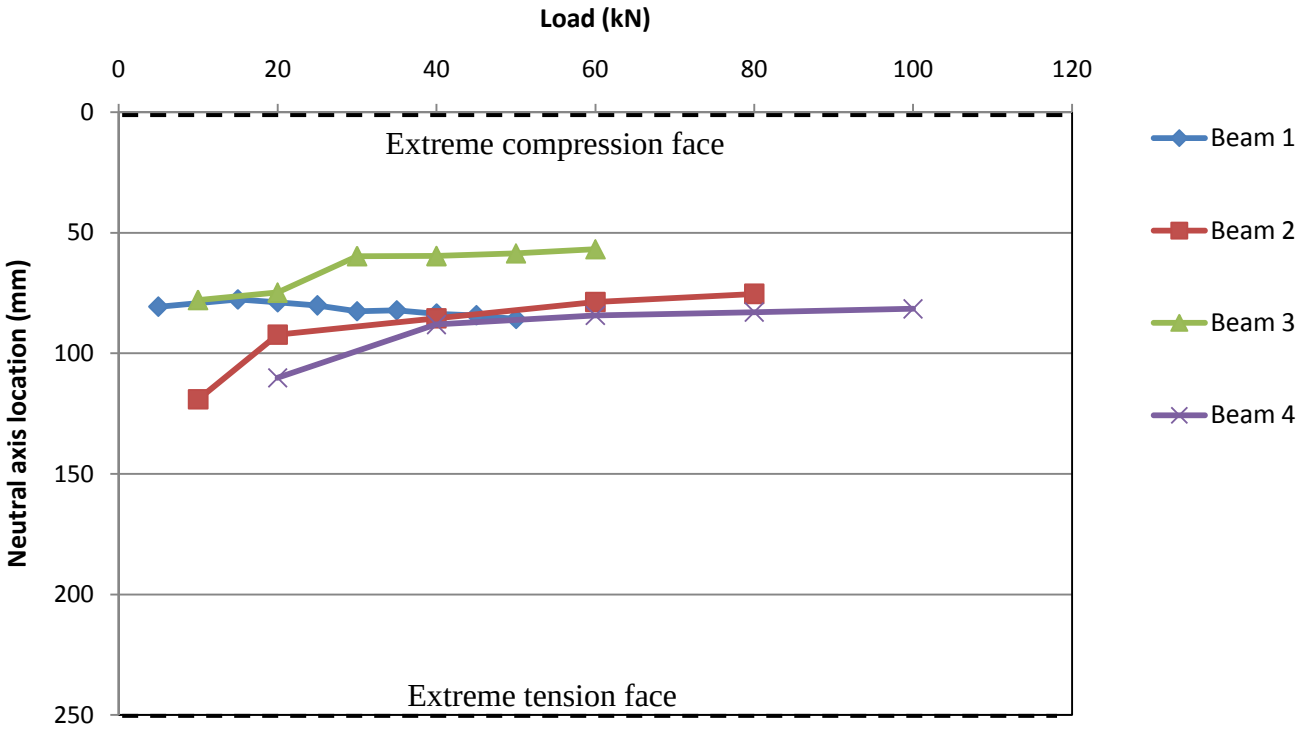

Figure 6.4: Shift in neutral axis with load

A set of five strain gauges mounted on the extreme tensile face of the beam were used to monitor debonding between the CFRP laminates and the concrete. Three gauges were located at mid-span of the beam and two were located at 1000 mm and 600 mm on opposite sides from mid-span as shown in Figure 6.5. The results of the strains measured with the increasing load are presented in Figure 6.6.

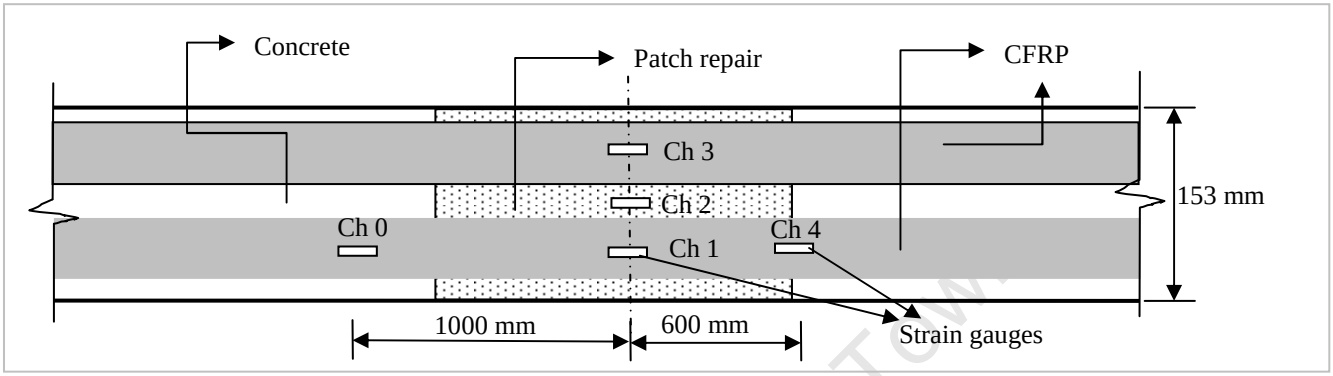

Figure 6.5: Plan view of the tension face of the beam with mounted strain gauges

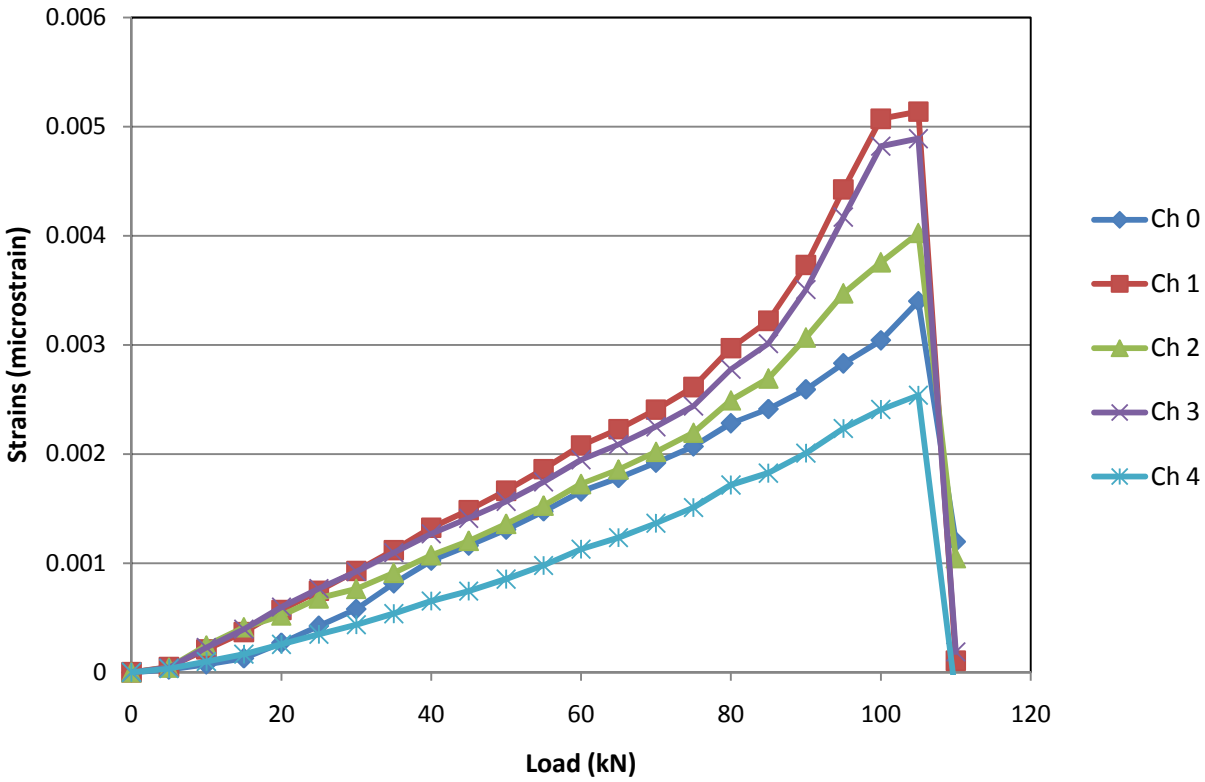

Figure 6.6: Strain measurements for assessing bond between concrete and CFRP laminates

The strains measured at the mid-span of the beam with the strain gauges are similar to the strains measure manually with the strain targets on the tension side of the beam at the mid-span as shown on Figure 6.7.

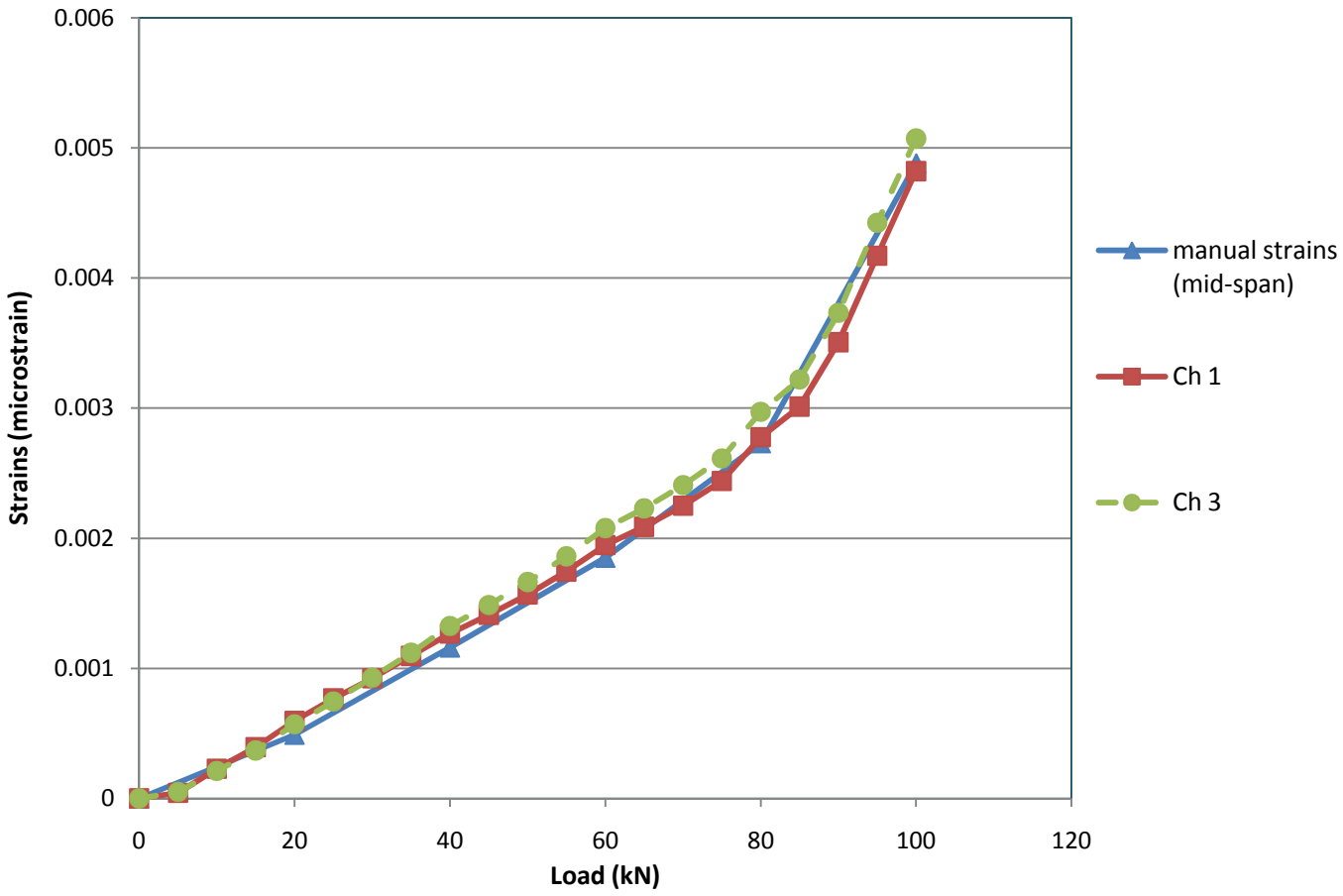

Figure 6.7: Comparison of the strain measurements to monitor debonding between CFRP laminates and concrete

The set of strains were measured from the strain targets placed on the surface of the concrete (manual strains). From the strain measurements, the change in the neutral axis (NA) of the beam due to loading has been inferred. Figure 6.4 shows a shift in NA of the beam with an increasing load. The NA is measured from the compression face of the beam.

The apparent observation form Figure 6.4 is that; as load increases, NA shifts towards the compression face. The NA is associated to stiffness through EI, which is a measure of stiffness. Shift in NA changes the moment of area (I) therefore results in a change in stiffness. These results concur with the deflection results; Beam 4 has the highest stiffness in comparison with the other beams, followed by Beams 2 and 3 showing the least stiffness. Strain measurements were used to monitor

the quality of bond between the materials in contact during ULS. The two sets of bonds were between patch repair and substrate and CFRP laminates and concrete surface. Strain targets were used to monitor bond between patch repair and substrate; from the results obtained, there was no debonding as the strains measured were the same as the strains reported for the control beam without repair. Electronic strain gauges were used to monitor the bond between the concrete and CFRP. There was no sign of debonding between CFRP and concrete; this is established from Figure 6.7 showing the strains measured on two CFRP laminates on the tensile face of the beam compared to the strain measurements from the strain targets on the tension side of the beam. The build up of tensile strains is similar on the tension face and sides.

6.3 Ultimate capacity

The four beams under review were tested for ultimate capacity. As the beams were loaded to failure under a four-point loading test, the deflections and strains were monitored. The failure loads of all beams are reported in Table 6.1.

Table 6. 1: Maximum failure load

Beam condition	Ultimate capacity (kN)
Beam 1: Undamaged	74
Beam 2: 10 % corroded + patch repair + CFRP	109
Beam 3: 10 % corroded + patch repair	70
Beam 4: 15 % corroded + patch repair + CFRP	110

The results show that the Beam 3 (patch repaired) had the least capacity, followed by Beam 1 (control). Beams 2 and 4 with CFRP strengthening had the highest ultimate capacity. The 10% corroded beam with patch repair has a 5% reduction in ultimate capacity compared to the control beam. This proves that the reduction in area of steel plays a more significant role with regards to ultimate capacity than stiffness of members. The combined effect of patch repair and FRP application improves both the stiffness and ultimate capacity of the member. The ultimate capacity increases by almost 50% as shown on Table 6.2 while deflections are improved by 25 %. Although the patch repair improves the stiffness, it has no effect on the ultimate capacity of the beam.

Table 6. 2: % Change in ultimate capacity relative to control beam

Beam #	Ultimate capacity (kN)	% change compared to Beam 1
1 (Control)	74	0.0
2 (10% Corrosion + Patch + CFRP)	109	47.3
3 (10% Corrosion + Patch)	70	-5.4
4 (15% Corrosion + Patch + CFRP)	110	48.6

The results demonstrate that the reinforcement does not play a significant role in the ultimate capacity when CFRP is used. The ultimate capacity is dependent on the bond between CFRP and concrete as it will be observed from the failure mode that failure occurred when the laminates debonded. Once the laminates debond, the steel yields and failure takes place.

6.4 Failure modes

Different failure modes were observed when the beams were loaded. Figures 6.8 a-d show the failure modes of beams 1 to 4 respectively. Beam 1(control) developed vertical cracks along the length of the beam. The cracks were equality spaced, but at failure; when steel yielded cracks between the two loading points opened wider followed by crushing of concrete at the point where the load was applied.

Figure 6.8a: Crack pattern on Beam 1 during failure

Beam 3 (patch repaired) showed a different failure mode. Vertical cracks developed along the length of the beam. Beam 3 failed first by yielding of steel then followed by opening up of cracks on the

tension side at mid-span, thereafter followed by crushing of concrete on the compression face at mid-span. There was no debonding between the patch repair and the substrate at failure, the cracks extended from the patch repair through the substrate.

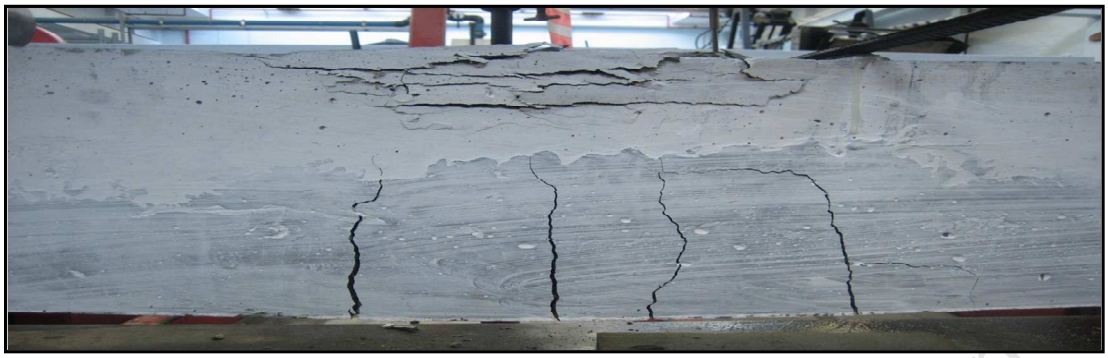

Figure 6.8b: Crack pattern on Beam 3 during failure

Beams 2 and 4 (with patch repair and CFRP) showed similar failure modes as show in Figures 6.8 c and d. The vertical cracks opened wider at the point of load application, followed by debonding of the CFRP laminates. Immediately as the laminates debonded, the beam failed. Debonding of CFRP commenced from the crack to one end of the beam where the laminates were anchored while the other side of the laminates remained intact.

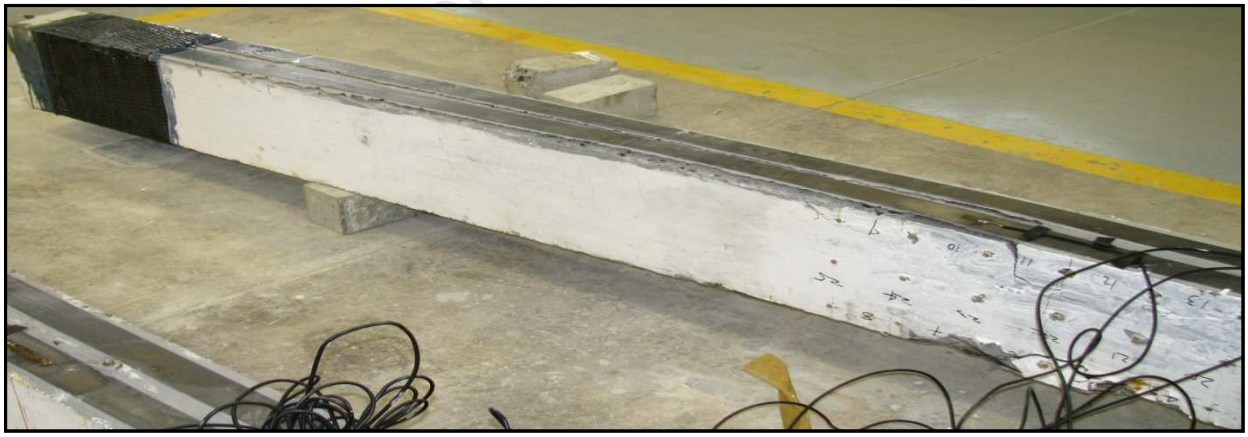

Figure 6.8c: Crack pattern on Beam 2 during failure

Figure 6.8d: Crack pattern on Beam 4 during failure

From the results presented, the application of patch repair improves the stiffness of the member as observed on the load-deflection curve presented in Figure 6.1. This may be due to the fact that cementitious grout used for repair has a higher tensile strength than that of concrete. The tensile strength of concrete and grout are 2.5 MPa and 5 MPa respectively.

The crack patterns for the tested beams are shown in Figures 6.9a to c. The propagation of cracks does not initiate at the mid span on the undamaged beam. The first crack on the undamaged beam is observed at a load of 30 kN. At failure Beam 1 opened vertical crack the widest at the point of load application as shown in Figure 6.9a. The vertical cracks on Beam 3 (patch repaired) started at a load of 25 kN, then at 40 kN the cracks developed around the mid-span where the patch repair was applied. At failure cracks opened the widest at mid-span as shown in Figure 6.9b. The two Beams 2 and 4 (patch repaired and CFRP strengthened) developed cracks at a much higher load of 40 kN. Both beams displayed similar failure modes and crack patterns, the beams had fewer cracks than other Beams 1 and 3. The initial crack was observed on the concrete substrate, and then followed by cracks on the patch repair at 45 kN. At failure, the vertical crack at the load application point widened, followed by delamination of CFRP as shown in Figure 6.9c

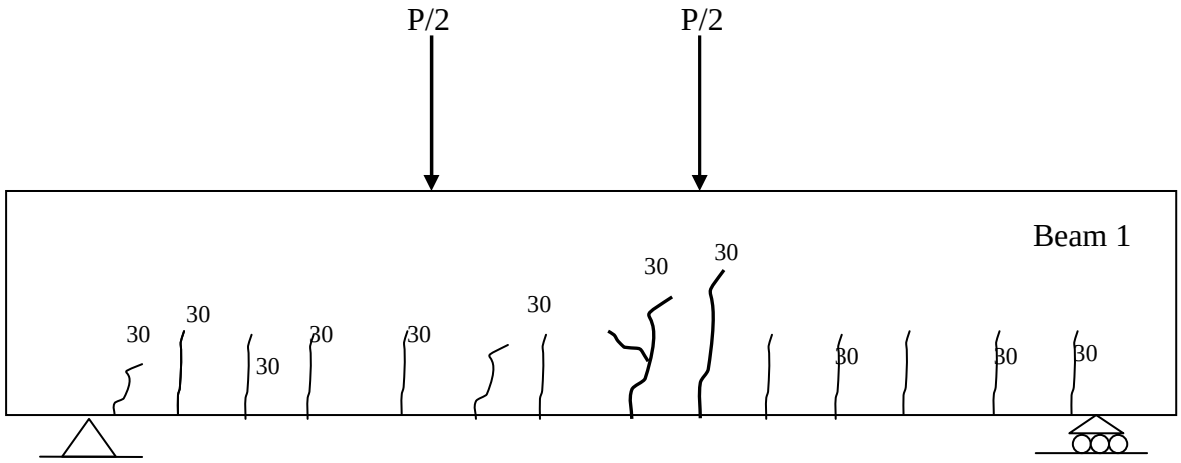

Figure 6.9a: Crack pattern on beam 1 (Undamaged)

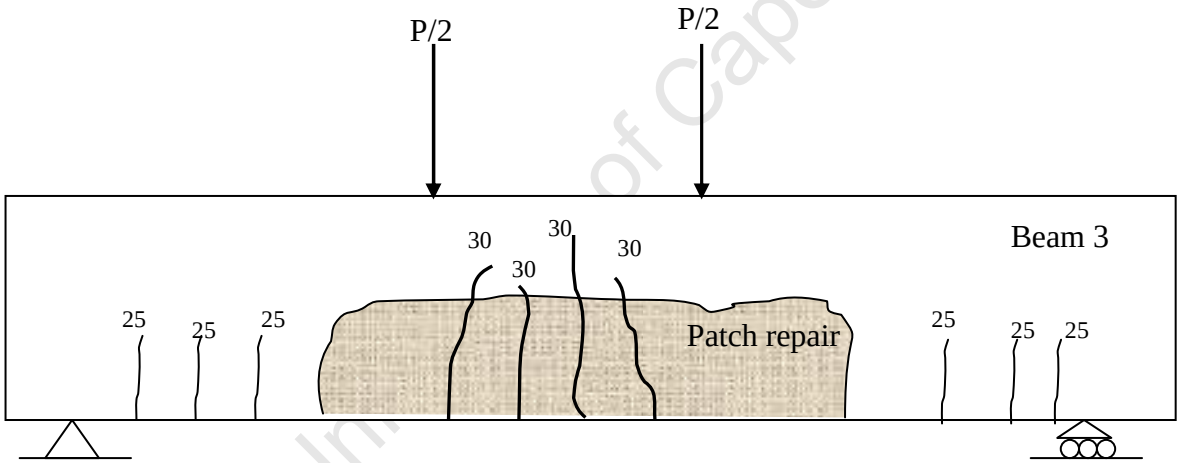

Figure 6.9b: Crack pattern on beam 3 with patch repair

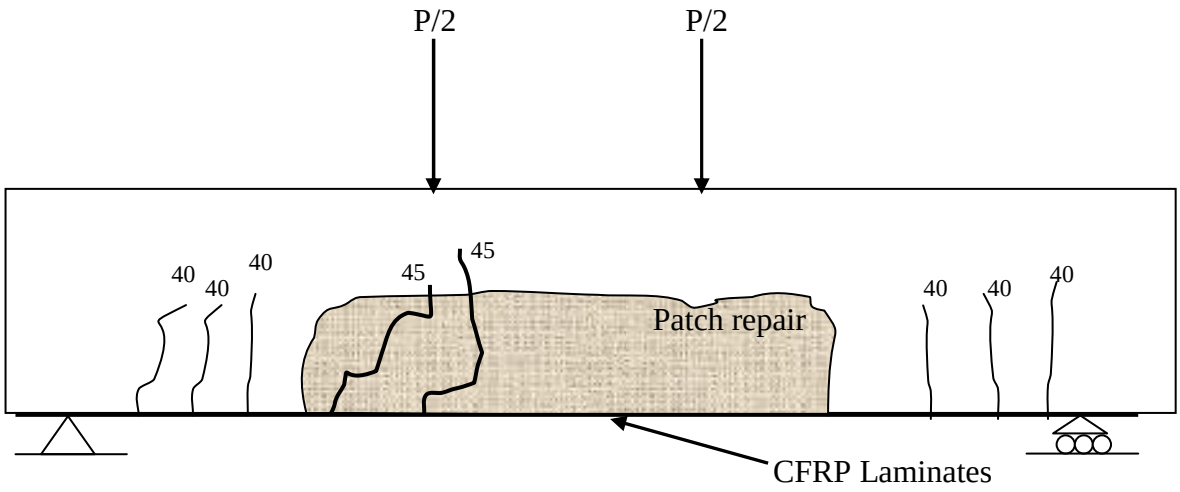

Figure 6.9c: Crack pattern on beams 2 and 4 with patch repair and CFRP strengthening

Chapter 7

CONCLUSIONS AND RECOMMENDATIONS

This research focused on non-destructive and destructive testing of RC beams to identify and quantify the effect of structural repair and strengthening on the stiffness and ultimate capacity of corrosion-damaged RC beams. The study was conducted on four beam specimens of length 5 m, cross section 153 mm x 254 mm. Three of the beams were damaged by inducing accelerated corrosion on the tension reinforcement and patch repaired with a patch repair mortar. Two of the repaired beams were further strengthened with carbon fibre reinforcing polymer (CFRP) laminates.

The experimental design was successful in acquiring the necessary data. The acquired non-destructive parameters were the natural frequencies, damping ratios and mode shapes by means of dynamic testing. The use of dynamic testing is potentially helpful for routine integrity assessment of structures. Modal parameters, such as mode shapes and natural frequencies can be used periodically for structural health monitoring (SHM) and condition assessment. The static parameters acquired are deflections, strains and ultimate capacity.

7.1 Conclusions

7.1.1 Corrosion damage

Loss of stiffness begins when corrosion cracks develop. Loss of stiffness during corrosion is observed by increase in deflection on beams subjected to corrosion under sustained load as compared to the control beam. There is an initial rapid stiffness loss which tapers off after a certain degree of corrosion. Deflections after 10% corrosion did not increase; therefore further corrosion beyond 10% did not reduce stiffness as was demonstrated by the resulting deflection at 15% corrosion. Crack development as well depends on the level of corrosion, but does not relate to the stiffness change. The deflection change from 10% corrosion to 15% corrosion was negligible, but the crack increase was noticeable from 10% to 15%, therefore the two cannot be directly interrelated.

Even though increase in corrosion level increases the crack widths, there is no correlation witnessed between the mass loss on the bar and the crack width at that particular point on the beam. Mass loss of the corroded bar was uneven along the corroded region due to a lot of pitting corrosion observed on the bars as a result of high current applied when accelerating corrosion. The use of high current

was able to approximately achieve the predicted corrosion level as the estimated mass loss of 10 % resulted in average mass loss of 7% with maximum mass loss of 12 % and the estimated mass loss of 15% resulted in an average mass loss of 10.1% with maximum mass loss of 18%. These contradict the findings by Andrade, 1996; that Faraday's constant overestimate the average mass loss. Andrade (1996) concluded that Faraday's constant overestimate the average mass loss by over 50%. This is observed mainly where low current intensities less than 100 $\mu A/cm^2$ are used and does not apply where higher current intensities above 500 $\mu A/cm^2$ are used.

Corrosion affected the efficiency of the strain gauges mounted on the reinforcement for monitoring the global stiffness of the beam. There was a short circuit resulting from the corrosion products which moved along the gauge wiring to the strain gauges. For this reason, the results of the strain measurements on the bars were neglected as they could not be measured for other following stages of corrosion.

7.1.2 Dynamic testing

The change in stiffness is also observed from measured dynamic parameters (natural frequencies and mode shapes). The natural frequency drops after corrosion initiation. The beams were tested dynamically at every stage; before damage, after corrosion, at repair preparation stage (exposed reinforcement), after patch repairing and CFRP strengthening. The average natural frequency for the undamaged beams was 19.5 Hz which dropped to 18.1 Hz after 10% corrosion and 18.0 Hz after 15% corrosion. This finding corresponds to the conclusion drawn from stiffness change during corrosion; which shows that after 10% corrosion, the stiffness drop is negligibly small. The natural frequency further dropped as the beams were tested after cutting with the reinforcement exposed. The average frequency of a cut beam was 14.2 Hz; this shows that there is a noteworthy difference between the stiffness of a corroded and cracked beam and a beam with exposed reinforcement.

Although patch repair was expected to increase the dynamic stiffness; the results revealed a contradicting effect as the average natural frequency increased to 17.5 Hz which shows an improvement from the beam with exposed reinforcement but is below the frequency of the cracked corroded beam. The probable reason for these could be another form of damage induced by initial loading and cutting of beams with a jack hammer, resulting in transverse cracks along the length of the beam. Cracks were observed after the beams were cut before repairing. Strengthening of the

beam with CFRP laminates improved the natural frequency to 18.5 Hz, which is more than the frequency of the patch repaired beams. The FRP laminates have a small cross-sectional area, for that reason, the CFRP laminates were not expected to improve the stiffness significantly. The reason for the apparent improvement could be the epoxy used to adhere the laminates to the concrete. This epoxy is believed to close the small transverse cracks on the beam developed from loading and breaking of beams for repair.

The other dynamic parameter recorded was the damping ratio; which proved to be ineffective as there is no correlation with the natural frequencies or the state of damage. Damping ratios only express the ability of the beams to absorb vibrating energy, therefore cannot be used to assess damage. Mode shapes were also reported; mode shapes were analysed by the MAC values which compares the modes to each other. The MAC values showed a good correlation with the state of the beams. The MAC values decreased due to corrosion damage and decreased further after exposing the reinforcement, then increased after repair and strengthening of the beams. Even though this is the case, the MAC values were all above 0.95 for the fundamental mode shape (mode 1); which shows no significant change due to damage. MAC values in this case are not helpful in deciding whether or not repair is required, as any value above 0.95 shows similarity between different modes.

7.1.3 Static testing

Patch repairs and CFRP strengthening have a positive effect on the structural capabilities of improving the load carrying capacity of the beam, reinstating durability and protecting reinforcement from further corrosion damage. Application of patch repair and CFRP strengthening improves the stiffness of the beams by up to 30% while patch repair on its own improves the stiffness by less than 10%. Application of both CFRP and patch repair improves the ultimate capacity by up to 50%, while patch repair on its own fails to improve the ultimate capacity as it is dependent on steel reinforcement.

The quality of bonds between patch repair and concrete substrate did not affect the performance of the composite beams as there was no sign of debonding between the substrate and patch repair during loading and at failure. There was also no sign of debonding between CFRP laminates and the substrate up to loads of 90% of the capacity. Debonding between the CFRP laminate and concrete

results in failure of the beams as the reinforcing steel is responsible for carrying all the tensile load that were carried by the CFRP laminates.

The static stiffness differs from the dynamic stiffness. In static stiffness, patch repaired beams have higher stiffness than undamaged beam contrary to dynamic stiffness behaviour. Dynamic stiffness was influenced by the repair preparation stage whereby beams were cut with a jack hammer; therefore inducing transverse cracks. These affected the dynamic stiffness considerably, as any change on the structure alters its frequency response; on the other hand static tests were carried out on the beams that were exposed to the same conditions before loading to failure.

The material configuration on the structural elements affect the failure mode of the beams as demonstrated by different failure patterns observed from an undamaged beam, patch repaired beam and CFRP strengthened beams. An undamaged beam yielded and opened cracks at the load application point while the patch repaired beam opened cracks at the mid-span of the beam. The CFRP strengthened beam did not fail by yielding of steel first, but failed when the CFRP laminates debonded.

The constituents of the beam composite showed perfect bond between each other; the bond between the substrate and the patch repair was monitored by measuring strains at the bond; which corresponded with the strains of the control beam at the same level. The bond between the CFRP laminates and the concrete proved to be good as the strains measured coincided with the strains on the concrete.

The reason for using both the patch repair and CFRP laminates was to understand the combined effect of the two. In practice, they are usually used separate and they therefore fail to fully enhance the structure stiffness and capacity.

7.2 Recommendations for future work

On the basis of the findings and conclusions, the following recommendations are made:

- Research the static behaviour of the cracked beam and beam with exposed reinforcement without patch repair to quantify the role played by the patch repair.

- Study the influence of the quality of workmanship on the bond between the CFRP laminates and concrete to determine how workmanship can influence the ultimate capacity of the CFRP strengthened beams.
- Corrode the reinforcing bars without protecting the stirrups from corrosion to understand the effect of the stirrups on the cracking pattern of the structure and influence on the dynamic properties.
- Standardise parameter tests used to characterize composite interfaces for better comparison.
- Standardise methods used for inducing accelerated corrosion for more consistent lab procedures.
- Design of a testing set up that will allow both dynamic tests and static tests to be carried out without moving the beams around to avoid damage induced by moving.

The research objective was fulfilled as the effect of corrosion on the beam stiffness could be quantified and the effect of the repair and strengthening could also be observed. The obtained results can be used to estimate stiffness depending on the type of repair system used. The work has highlighted the influence of structural repair and strengthening on the ultimate capacity of damaged structures in bending.

The work carried out emphasised how dynamic testing plays a significant role in identifying corrosion damage in structures by showing changes in their response due to damage, repair and strengthening. This work created a better understanding of modal analysis and its applications.

Corrosion damaged structures should be patch repaired before strengthening to minimize the risk of future corrosion. Appropriate patch repair steps should be followed to produce durable repairs and should be carried out by trained persons. CFRP strengthening in the same way requires specialists, therefore appropriate training is necessary.

REFERENCES

Andrade C. and Alonso C., **Corrosion Rate Monitoring in the Laboratory and on-site,** Construction and Building Materials, Vol 10, No. 5, 1996.

Azad A.K., Ahmad S. and Azher S.A, **Residual Strength of Corrosion-Damaged Reinforced Concrete Beams,** ACI Materials Journal, Vol 104, No. 1, 2007.

Baghiee N., Esfahani R.M. and Moslem K., **Studies on damage and FRP strengthening of reinforced concrete beams by vibration monitoring**, Engineering Structures Journal, Vol 31, 2008.

Bakis C. E., Banks L. C., Brown V. L., Cosenza E., Davalos J. F., Lesko J. J., Machida A., Rizkalla S. H. and Triantafillou T. C., **Fibre-Reinforced polymer composites for construction- State-of-the-art review**, American Institute of Civil Engineers, 150th anniversary paper, 2002.

Bayissa W.L and Haritos N., **Experimental Investigation into Vibration Characterization of a Cracked RC T-beam**, 2005.

Belaid F., Ariliguie, G. and Francois, R., **Corrosion Products of Galvanized Rebars Embedded in Chloride-Contaminated Concrete.** Corrosion, Vol. 56, (9), pp 960. USA, 2000.

Bentur A., Diamond S. and Berke N.S, **Steel Corrosion in Concrete – Morden Concrete Technology 6,** Fundamentals and Civil Engineering Practice, 1997.

Benyoucef S., Tounsi A., Benrahou E.A. and Bedia A., **Time-dependent behaviour of RC beams strengthened with externally bonded FRP plates: Interfacial stresses analysis**, Mech Time-Depend Materials Journal, 2007.

Blevins R.D., **Formulation for natural frequency and mode shape,** Second edition, Krieger publishing company, Malabar, Florida, 2001.

Brandon, J. A., Stephens, A. E., Lopes, E. M. O. and Kwan, A. S. K., **Spectral indicators in structural damage identification: a case study,** Proceedings of the Institution of Mechanical Engineers Part C- Journal of Mechanical Engineering Science, Vol 213, pp 411-415, 1999.

Broomfield, J.P., **Corrosion of steel in concrete, understanding, investigation and repair,** Taylar and Francis e-Library publishers, 2003.

Buyukozturk O. **Failure behaviour of FRP bonded concrete affected by interface fracture.** National Science Foundation, Massachusetts institute of Technology, 2005.

Buyokozturk O. and Au C. **Debonding of FRP plated concrete: A tri-layer fracture treatment**. Science Direct, Massachusetts Institute of Technology, Cambridge, MA 02139, United States, 2005.

Cairns J., Plizzari G. A., Du Y., Law D.W. and Franzoni C., **Mechanical Properties of Corrosion-Damaged Reinforcement**, ACI Materials Journal, 2005.

Capozucca R., **Damage to Reinforced Concrete due to Reinforcement Corrosion,** Construction and Building Material, Vol 9, No 5, pp 295 – 303, 1995.

Cerna, M. and Harvey. F, **The fundamentals of FFT-Based signal analysis and measurement,** National Instruments, Application Note 041, 2000.

Chidiac S. E. and Mailvaganam N. P., **Finite element analysis of patch repair in a concrete flat slab,** appearing in the Proc. Of the ANS symposium, Waterloo, Canada, 1997.

Cusson D. and Mailvaganam V. **Durability of repair materials**. Concrete International, A study of moisture diffusion, Vol 18, 34 – 38, 1996.

Cusson R. and Xi Y. **The behaviour of Fibre-Reinforced polymers reinforcement in low temperature environmental climate,** Department of Civil, Environmental and Architectural Engineering, University of Colorado, 2002.

Dehwah, H.A.F, Maslehuddi, M. and Austin, S.A. **Effects of sulfate ions and associated cation type on the pore solution chemistry in chloride-contaminated plain and blended cements**. Cement and Concrete Composites, Vol. 25, (4-5), pp 513 – 525.

Dimarogonas, A. D., **Vibration of cracked structures**: A state of the art review, Engineering Fracture Mechanics, Vol 55, pp 831-857, 1996.

El Maaddawy T., Soudki K. and Topper T., **Long-Term Performance of Corrosion-Damaged Reinforced Concrete Beams**, ACI Structural Journal, Vol 102, No 5, 2005.

El Maaddawy T. and Soudki K. **A Model for Prediction of time from corrosion Initiation to Corrode Crack**, Cement & Concrete Composites, Vol 29, 2007.

El Maaddawy T. and Soudki K. **Effectiveness of Impressed Current Technique to Simulate Corrosion of Steel Reinforcement in Concrete**, Journal of Materials in Civil Engineering, Vol. 15, No. 1, 2003.

Eurocode 2 Editorial Group: **Design of concrete structures**, part 1: General rules and rules for buildings. In: Eurocode No. 2, Brussels, 1991.

Gandomi, A.H., sahib, M.G., Rahaaei, A. and Safari Gorji, M., **Development in the mode shape – based structural fault identification technique**, World applied science journal, Vol. 5 (1), pp 29 – 38, 2008.

Idichandy, V.G. and Ganapathy, C., **Modal parameters for structural integrity of fixed offshore platforms**, Experimental mechanics, Vol 30 (4), pp 382 – 391, 1990.

Jendele L. and Cervenka J., **Finite element modelling of reinforcement with bond,** Computers and structures journal, Vol 84, 1780 -1791, 2006.

He J. and Fu Z., **Modal analysis**, Butterworth Heinemann publishers, Oxford, 2001.

Huang R. and Yang C.C., **Condition Assessment of Reinforced Concrete Beams Relative to Reinforced Corrosion,** Cement and Concrete Composites, Vol 19, 1997.

Li C, yang Y. and Melchers R.E, **Prediction of Reinforcement Corrosion in Concrete and Its Effects on Concrete Cracking and Strength Reduction**, ACI Materials Journal, 2008.

Lau K.T., Dutta P.K., Zhou L.M. and Hui D. **Mechanics of bonds in an FRP bonded concrete beams**. Elsevier Science, Composites: Part B 32, 491 – 502, 2001.

Lu X. and Dong Y., **Numerical simulation on local bond-slip between steel and concrete with experimental verification,** Joint international conference on computing and decision making in Civil and Building Engineering, Montreal Canada, 2006.

Maeck, J., Abdel Wahab, M., peters, B., De Roeck, G., De Visscher, J., De Wildee, W.P., Ndambi, J.M. and Vantomme, J., **damage identification in reinforced concrete structures by dynamic stiffness determination,** Engineering Structures, Vol 22, pp 1339 – 1349, 2000.

Malumbela, G., Moyo, P. and Alexander, M., **Behaviour of RC beams corroded under sustained load,** Construction and Building Materials, 2009.

Malumbela, G. Alexander, M. and Moyo, P., **Steel corrosion on RC structures under sustained service load,** Engineering structures, Vol 31, pp 2518 – 2525, 2009.

Paz M. and Leigh W., **Structural Dynamics; theory and computation**, Fifth edition, 2004.

Phaedonos F. A., **Cementitious repair of concrete structures,** GeoPave Material technology, Technical Note 72, Vic roads, 2006

Rahman K., Baluch M. H. and Al-Gadhi A. H., **Modelling of shrinkage and creep stresses in concrete repairs,** ACI Materials Journal, 1999.

Rahman K., Baluch M. H. and Al-Gadhi A. H., **Simulation of shrinkage distress and creep relief in concrete repair,** Composites: part B 31, 2000.

Razak A.H and Choi F.C., **The Effect of Corrosion on the Natural Frequency and modal damping of reinforced concrete beam**s, Engineering Structures Journal, Vol 23, 2001.

Richardson M., **Fundamentals of Durable Reinforced Concrete**, Modern Concrete Technology 11, 1995.

Simonelli G., **Finite element analysis of RC beams retrofitted with fibre reinforced polymers,** PhD thesis, Università degli Studi di Napoli Federico II. London, 2005.

Salane, H.J., Baldwin, J.W and Duffield, R.C., **Dynamic approach for monitoring bridge detection**, Transportation Research Record, 832, pp 21 – 28, 1987.

Salane, H.J. and Baldwin, J.W, **Identification of modal properties of bridges,** Journal of Structural Engineering, ASCE, 116 (7), 2 pp 2008 – 2021, 1990.

Salawu, O.S., **Detection of structural damage through changes in frequency,** Engineering structures, Vol. 19, No. 9, pp 718 – 723, 1997.

Salawu, O.S. and Williams, C., **Review of full-scale dynamic testing of bridges,** Engineering structures, Vol. 17, No. 2, pp 113 – 121, 1995.

Shwarz, B and Richardson, M., **Measuring operating deflection shapes under Non-stationary conditions**, 2000.

Soudki A.K., Sherwood T. And Masoud S., **FRP Repair of Corrosion-Damaged Reinforced Concrete Beams**, Department of Civil Engineering, University of Waterloo, Canada, 2003.

Taljsten B. **FRP strengthening of existing concrete structures.** Design guideline, fourth edition, Lulea University printing office, 2006.

Torres-Acosta A.A., Fabela-Gallegos M.J., Munoz-Noval A., Vazquez-Vega D., Hernandez-Jimenez J.R. and Martinez-Madrid M., **Influence of Corrosion on the Structural Stiffness of Reinforced Concrete Beams**, NACE International, Corrosion Engineering Section, 2004.

Tounsi A., **Improved theoretical solution for interfacial stresses in concrete beams strengthened with FRP plate,** International journal of solids and structures, vol 43, 4154 - 4174, 2006.

Tounsi A. and Benyoucef S., **Interfacial stresses in externally FRP plated concrete beams,** International Journal of adhesion and Adhesives, vol 27, 207 – 215, 2006.

Tsai, W.H. and Yang, J.C.S., **Nondestructive evaluationof composite structures using identification techniques,** Engineering material Technology ASME, Vol. 110,No. 2, pp 134 – 139, 1988.

Ueda T. and Dai J. **Interfacial bond between FRP sheets and concrete substrates – properties, numerical modelling and roles in member behaviours**. Division of Structural and Geotechnical Engineering, Hokkaido University, Sapporo, Japan, 2004.

Vaysburd M. A., **Holistic system approach to design and implementation of concrete repair.** Science Direct, Cement and & Concrete Composites, Vol 28 (2006) pgs 671 – 678.

Vandoros K.G. and Dritsos S., **Concrete jacket construction detail effectiveness when strengthening RC columns**, Construction and Building Materials, Vol 22, pgs 264 – 276, 2006.

http://irc.nrc-cnrc.gc.ca/ircpubs, **Preventing rebar corrosion in concrete structures,** Concrete On-Site, v. 1, no. 1, Sept/Oct. 2004, pp. 14-15.

http://www.cement.org/tech/faq_cracking.asp, **Concrete technology**, Portland cement association, 15/04/2009.

http://www-civ.eng.cam.ac.uk/cjb/cjbresearch1.html, **Fracture mechanics of bonded FRP plate failure – Active,** University of Cambridge, 11/08/2008.

Appendix 1: Beam Design

Tension reinforcement

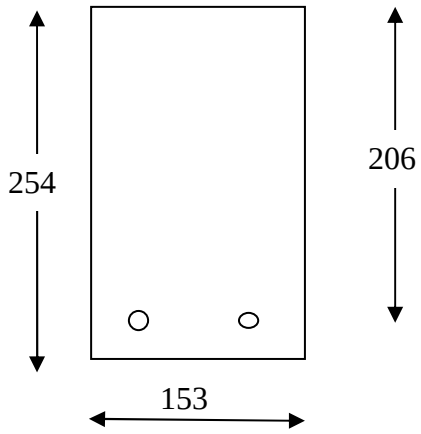

$$d = h - \text{cover} - \frac{\phi}{2} - link$$

Assume:

Bar diameter: 20 mm

Stirrups: 8 mm

Cover: 30 mm

$$d = 254 - 30 - \frac{20}{2} - 8$$

$$d = 206mm$$

Design assumptions

$$f_{cu} = 40MPa$$

$$f_y = 450MPa$$

$$k > 0.156 > \frac{M_u}{f_{cu} bd^2}$$

$$M_u = 0.156 f_{cu} bd^2$$
$$M_u = 0.156 \times 40 \times 153 \times 206^2$$
$$M_u = 40.5 KNm$$

$$Z = \left[0.5 + \sqrt{0.25 - \frac{k}{0.9}} \right]$$

$$Z = \left[0.5 + \sqrt{0.25 - \frac{0.156}{0.9}} \right]$$

Z = 160 mm

Check: Z < 0.95d =196 mm (OK)

$$A_s = \frac{M_u}{0.87 f_y Z}$$

$$A_s = 617 mm^2$$

Use 2 Y 20 (628)

Compression reinforcement

$$A_s^{'} = \frac{\left(k - k^{'}\right) f_{cu} bd^2}{f_{yc}\left(d - d^{'}\right)}$$

k = k’ = 0.156

$A_s^{'} = 0$

Minimum reinforcement for redistribution < 10%

$A_s^{'} = 0.1A_s$

$A_s^{'} = 0.1 \times 628$

= 63 mm^2

Use 2 Y 10 (157 mm^2)

Shear reinforcement

d = 206 mm

$$\upsilon = \frac{V}{bd}$$

$$\upsilon \leq \frac{V}{bd} \leq 4.75$$

$$V = 4.75bd$$
$$V = 4.75 \times 153 \times 206$$
$$V = 150kN$$

$$\upsilon_c = \frac{0.79}{\gamma_m}\left(\frac{f_{cu}}{25}\right)^{1/3}\left(\frac{100A_s}{b_v d}\right)^{1/3}\left(\frac{400}{d}\right)^{1/4}$$

$\gamma_m = 1.4$
$\therefore \upsilon_c = 0.98$

$$\frac{A_{sv}}{S_v} = \frac{b(V - \upsilon_c)}{0.87 f_{yv}}$$

$f_{yv} = 250MPa$

$V = 0.75\sqrt{f_{cu}}$
$V = 4.75$

$$\frac{A_{sv}}{S_v} = 2.65$$

Minimum link spacing ratio to area

$$\frac{A_{sv}}{S_v} = 0.002 b_t$$
$= 0.3$

Maximum spacing

$S_{v_{\max}} = 0.75d$
$S_{v_{\max}} = 155mm$

Use: R 8 @ 150 mm c/c

Maximum deflection

= 20 mm

Appendix 2: Corrosion calculations

From the literature, there formula for determining the amount of current required to achieve an estimated amount of steel lost during the accelerated corrosion process is as follows:

$$I_{corr} = \frac{\Delta mFz}{Mt}$$

Where

Δm: mass of steel consumed (g)

M: Atomic weight of steel (56 g)

I: Current (A)

t: time (s)

z: Ionic charge (2)

F: Faraday's constant (96 500 A/s)

From the specimen set up, there are two 20 mm bars on the tension zone to be corroded; the length of corrosion is 1000 mm. The mass of the steel bars to be corroded is calculated as follows:

$$V_{steel} = \frac{\pi d^2}{4} L$$

$$V_{steel} = \frac{\pi \times 2^2}{4} \times 100$$

$$V_{steel} = 314 cm^3$$

Density of steel (D_{FE}) = 7.86 g/cm^3

Mass of two steel bars of length 1 m:

$$m_{steel} = D_{FE} V_{steel}$$

$$m_{steel} = 2 \times 7.86 \times 31$$

$$m_{steel} = 4938 g$$

Based on the required mass loss of 10 and 15%, the current required to achieve the corrosion level can be assumed.

Beam No.	Mass loss (%)	Mass loss (g)	Current (mA)	Duration (Days) (Estimated wetting)
1	0	0	0	0
2	10	494	1000	20
3	10	494	1000	20
4	15	740	1000	30